



OSLO METROPOLITAN UNIVERSITY
STORBYUNIVERSITETET

Department of Civil Engineering and Energy Technology

Postadresse: Postboks 4 St. Olavs plass, 0130 Oslo

Visit address: Pilestredet 35, Oslo

CANDIDATE NUMBER

417

AVAILABILITY

Open

Telephone 67 23 50 00

www.oslomet.no

MASTER THESIS

TITLE	DATE
Performance analysis of a solar thermal system coupled with a ground source heat pump in Nordic conditions	May 25, 2022
	NUMBER OF PAGES/APPENDIX
	66/65
AUTHOR	SUPERVISOR
Sandra Fransson Wilberg	Habtamu Bayera Madessa

ABSTRACT

The main objective of this thesis is to investigate the performance of a solar assisted ground source heat pump for a school in Oslo and provide information on how such systems should be optimized. The energy system is designed in such a way that the solar collector prioritizes to provide heat to the hot water tank, and whenever there is excess heat from the solar collector it can be used to charge the ground borehole. A detailed thermodynamic analysis of the system has been carried out in Engineering Equation Solver (EES), where isobutane (R600a), propane (R290), ammonia (R717) and solstice (R1234ze(E)) have been investigated as working fluid for the heat pump. Dynamic simulations of the solar assisted ground source heat pump was also conducted in IDA ICE. The result revealed positive outcomes from using SC in a Nordic climate, and the different working fluids have affected both the COP and the exergy of the system.

3 KEYWORDS

SGSHP

EES

IDA ICE

Preface

This thesis finalizes my master's degree in Energy and Indoor Environment in Buildings at Oslo Metropolitan University. Previous to this master degree I finished a bachelors degree in Renewable Energy at the University of Agder.

I would like to extend my gratitude to my supervisor, Habtamu Bayera Madessa. He has been available for guidance and assistance through the entire semester, and I am grateful for the feedback and the knowledge he has shared. Lastly, I'd want to express my gratitude to my family and classmates for their support and encouragement during my studies.



Sandra Fransson Wilberg
24.05.2022, Oslo

Abstract

Increased insight into global warming together with the Paris Agreement and the UN climate report has sparked an interest in renewable energy associated with buildings. Utilizing renewable energy sources will help reduce the energy consumption in the building sector and minimize greenhouse gas emissions. Ground source heat pumps (GSHP) are a frequently used energy system in Norway today. Since more passive houses have been built in the last years and the need for efficient energy systems has increased, an increased interest in solar assisted ground source heat pumps (SGSHP) has been observed. There are however shortcomings in detailed performance analysis of such systems in a cold climate, and therefore uncertainties if it is beneficial to implement solar thermal energy to a GSHP.

The main objective of this thesis is to investigate the performance of a SGSHP for a school building designed according to criteria for passive houses. The performance analysis was then used to determine if solar thermal energy is suitable for use in a GSHP and how such systems should be optimized in cold climates. The energy system will provide energy both for domestic hot water production (DHW) and space heating. The SGSHP is designed in such a way that the solar collectors (SC) prioritize providing heat to the hot water tank and whenever there is excess heat from the SC it will be used to charge the ground borehole.

In the thesis, a detailed thermodynamic analysis of the system was carried out in Engineering Equation Solver (EES). As working fluid for the heat pump (HP) isobutane (R600a), propane (R290), ammonia (R717) and solstice (R1234ze(E)) have been investigated. Several sensitivity analyzes were conducted to be able to identify how different parameters influence the performance of the SGSHP and to provide important knowledge for the optimization of the system in a colder climate.

It was also conducted dynamic simulations in IDA ICE to further investigate how the configuration of the SGSHP influences the performance. Two separate plants were constructed. In the first system, the SC was solely used to heat the water tank, and in the second system the SC was only connected to the ground heat exchanger (GHX) to recharge the ground. One year energy simulations were performed to investigate the energy distribution from the systems, and the soil temperature in the boreholes was plotted over a seven year period.

The main results of the thermodynamic analysis and the dynamic simulations were as follows.

- Recharging the ground with SC will increase the Coefficient of Performance (COP) of the HP and maintain a thermal stable soil.
- Heating the hot water tank with solar thermal energy will reduce the need for delivered energy.
- R717 was found to achieve the best COP and lowest exergy destruction in the HP.
- The compressor stood for a significant part of the HP's exergy destruction, and it was discovered that subcooling the refrigerant after the condenser reduced this amount.

The investigated SGSHP appeared to be a well-suited approach for heating passive houses in cold climates. Implementing SC can help a GSHP become more efficient, increase its lifetime and reduce the overall need for delivered energy to a building.

Sammendrag

Økt innsikt i global oppvarming sammen med Parisavtalen og FN sin klima rapport har vekket interesse for fornybar energi knyttet til bygninger. Bruk av fornybare energikilder i bygninger vil bidra til å redusere energiforbruket og minimere klimagassutslippene i byggesektoren. I Norge er bergvarmepumper et mye brukt energisystem idag. Siden det har blitt bygget flere passivhus de siste årene og behovet for effektive energisystemer har økt, har man sett en økt interesse for solassisterte bergvarmepumper. Det er imidlertid mangel av detaljerte ytelses analyser av solassisterte bergvarmepumper i et kaldt klima, og derfor usikkerhet om det er fordelaktig å implementere slike systemer i Norge.

Hovedmålet med denne oppgaven var å undersøke ytelsen til en solassisterte bergvarmepumpe knyttet til et skolebygg designet etter kriterier for passivhus. Ytelses analyses ble så brukt til å undersøke om det er en fordel å benytte termisk sol energi sammen med grunn varme pumpe, og hvordan eventuelt slike system kan optimaliseres i Norge. Den solassisterte bergvarmepumpen gir energi både til varmt tappevann og romoppvarming. Systemet er utformet på en slik måte at solfangerne prioriterer å gi varme til varmtvannstanken, og når det produseres overskudds varme fra solfangerne brukes dette til å lade energibrønnene.

I oppgaven ble det utført en detaljert termodynamisk analyse av systemet er i Engineering Equation Solver (EES). Som arbeidsmedium til varmepumpen ble isobutan (R600a), propan (R290), ammoniakk (R717) og solstice (R1234ze(E)) undersøkt. Flere sensitivitetsanalyser ble utført for å kunne identifisere hvordan ulike parametere påvirket ytelsen til systemet som ga viktig kunnskap for optimalisering av systemet i et kaldt klima.

Det ble også utført dynamiske simuleringer i IDA ICE for ytterligere å undersøke hvordan konfigurasjonen av en sol assisterte bergvarmepumpe påvirket ytelsen. To separate systemer ble bygget. I det første systemet ble solfangerne utelukkende brukt til å varme opp vanntanken, mens i det andre systemet ble solfangerne kun koblet til energibrønnene for å lade opp grunnen. Ett års energi-simuleringer ble utført for å undersøke energi fordelingen i systemene, og grunntemperaturen i energibrønnene ble plottet over en syvårsperiode.

Hovedresultatene av den termodynamiske analysen og de dynamiske simuleringene viste følgende:

- Ladning av energibrønnene ved hjelp av solfangerne ga høyere COP for varmepumpen og en mer termisk stabil grunn
- Bruk av solvarme til oppvarming av varmtvannstanken ga et redusert behov for levert energi
- R717 oppnådde høyest COP og lavest eksergiødeleggelse
- Kondensatoren stod for en stor andel av eksergiødeleggelsen til varmepumpe og en underkjøling av arbeidsmediet ga en positiv effekt.

Funnene avslørte at solassisterte bergvarmepumper er lovende energisystemer for passivhus i kalde klimaer. Implementering av solfangerne hjelper en bergvarmepumpe til å bli mer effektiv, øke dens levetid og redusere behovet for levert energi til en bygning.

Contents

1	Introduction	1
1.1	Background	1
1.2	Main objective	1
1.3	Limitations	1
2	Literature review	2
2.1	Review Approach	2
2.2	General trends	3
2.2.1	Publishing year	3
2.2.2	Represented countries	3
2.2.3	Implemented method	4
2.2.4	Building category	5
2.3	Findings from literature review	6
2.3.1	Thermal imbalance in the soil	6
2.3.2	Affect of solar collector on borehole length	6
2.3.3	Energy consumption	7
2.3.4	Coefficient of performance	7
3	Theory	9
3.1	Solar assisted ground source heat pump	9
3.1.1	Solar collector	9
3.1.2	Ground heat exchanger	10
3.1.3	Heat pump	11
3.2	Thermodynamics	12
3.2.1	Enthalpy	13
3.2.2	Entropy	13
3.2.3	Exergy	13
3.3	Heat Transfer	14
3.3.1	Conduction	14
3.3.2	Convection	14
3.3.3	Radiation	15
3.4	System configuration	15
3.4.1	System 1	15
3.4.2	System 2	16
3.4.3	System 3	17
3.4.4	System 4	18
3.4.5	System 5	19
4	Method	20
4.1	Reference building	20
4.2	System solution	21
4.3	Solar collector dimensioning	21
4.4	Ground heat exchanger dimensioning	21
4.5	Heat pump dimensioning	21
4.6	Engineering Equation Solver	22
4.6.1	Assumptions	22
4.6.2	Solar collector model	23
4.6.3	Ground heat exchanger model	26

4.6.4	Heat pump model	30
4.7	IDA ICE	34
4.7.1	Energy plant	34
5	Results and discussion	37
5.1	Validation of the mathematical models	37
5.1.1	Solar collector model	37
5.1.2	Ground heat exchanger model	37
5.1.3	Heat pump model	39
5.2	Solar collector model	41
5.2.1	Area and placement	41
5.2.2	Thermal efficiency	41
5.2.3	Energy production	43
5.2.4	Exergy	44
5.3	Ground heat exchanger model	46
5.3.1	Dimensioning of the borehole field	46
5.3.2	Outlet temperature	48
5.3.3	Exergy	49
5.3.4	Recharging the ground	50
5.4	Heat pump model	52
5.4.1	T-s and P-h diagrams	52
5.4.2	Coefficient of performance	54
5.4.3	Energy from the condenser	56
5.4.4	Area evaporator	57
5.4.5	Exergy	58
5.5	Solar collector to water tank	61
5.6	Solar collector to ground heat exchanger	62
6	Conclusion	63
7	Future work	64
A	Draft of paper sent to a conferance	69
B	Literature review - Articles	77
C	Gjennestad High School	79
D	Data sheet for the solar collectors	81
E	Data sheet for the heat exchanger	82
F	Data sheet for the condenser	83
G	Data sheet for the evaporator	84
H	Formulas implemented in EES	85
H.1	Nusselt correlation for R290 and R600a	85
H.2	Nusselt correlation for R717 and R1234ze(E)	85
I	EES SC model	86

J EES GHX model	89
K EES HP model	94
K.1 R600a HP model	94
K.2 R290 HP model	101
K.3 R717 HP model	107
K.4 R1234ze(E) HP model	113
L P-h graphs	119
M EES SC results	121
N EES GHX results	122
O EES HP results	123
O.1 R600a HP results	123
O.2 R290 HP results	125
O.3 R717 HP results	127
O.4 R1234ze(E) HP results	129
P IDA ICE plant 1	131
Q IDA ICE plant 2	133

List of Figures

1	Publication year of the selected articles.	3
2	Geographical location of the studies case.	4
3	Implemented Method.	4
4	The different building categories implemented in the studies.	5
5	Flat plate solar collector [26].	9
6	A closed-loop ground heat exchanger with a vertical borehole.	10
7	Schematic of a simplified heat pump.	11
8	System configuration 1 - Indirect use of SC to heat water tank and recharge the GHX.	16
9	System configuration 2 - Direct heating of brine before evaporator and recharge the GHX.	17
10	System configuration 3 - Indirect use of SC to recharge the GHX.	17
11	System configuration 4 - Brine from the GHX pumped through SC.	18
12	System configuration 5 - SC connected to thermal storage tank used to heat the water tank, DHW directly and recharging GHX.	19
13	Boundary condition for the solar system implemented in EES.	23
14	Boundary condition for the ground heat exchanger implemented in EES.	26
15	Boundary condition for the heat pump implemented in EES	30
16	Energy system in IDA ICE where the SC is connected to the water tank.	34
17	Energy system in IDA ICE where the SC is connected to the GHX.	35
18	The variation of the outlet temperature of the ground heat exchanger due to the mass flow rate of the brine.	38
19	The total area of needed SC when the heat demand increase.	41
20	The variation in thermal efficiency with fixed fluid temperatures and varying solar flux and ambient temperature.	42
21	The impact of solar flux on the produced thermal energy from the SC.	43
22	Relation between second law efficiency of the SC and the ambient temperature.	44
23	Relation between the second law efficiency and the inlet temperature of the SC with different working fluids.	45
24	Relation between the length of each borehole and the needed number of boreholes to achieve the energy demand with different types of grout materials.	46
25	Relation between the length of each borehole and the needed number of boreholes to achieve the energy demand with different mass flow rate of the brine.	47
26	The effect of recharging the ground with SC on the needed length of each borehole.	47
27	The impact of the soil temperature on the outlet temperature of the borehole with different types of grout materials.	48
28	The impact of the temperature of the brine from the HP on the outlet temperature of the GHX.	49
29	The influence of the inlet and outlet temperature on the exergy destruction of the borehole field.	50
30	The impact of the hot inlet temperature to the HX on both the cold outlet temperature and the exergy destruction of the HX.	51
31	Effect of the energy from the SC on the outlet temperature of the brine from the borehole.	51
32	T-s diagram for R600a.	52
33	T-s diagram for R290.	53
34	T-s diagram for R717.	53

35	T-s diagram for R1234ze(E).	54
36	The COP of the HP with the different refrigerants when the mass flow rate is altered.	55
37	The impact of the brine temperature out of the evaporator on COP for the R290 HP.	56
38	How an increase of the outlet temperature of the GHX impacts the produced energy of the HP.	57
39	Area of the evaporator with different mass flow rates of the refrigerant with the variation of the inlet temperature of the brine for the R290 HP.	58
40	How subcooling the refrigerant after the condenser affects the second law efficiency of the condenser in the R717 HP.	59
41	How subcooling the refrigerant after the condenser affects the total exergy destruction for the HP.	60
42	The soil temperature at 140 meters over a seven-year period without SC recharging the ground.	61
43	The soil temperature at 140 meters over a seven-year period with SC connected to the GHX.	62
44	Gjennestad High School	79
45	1. floor of Gjennestad High School	79
46	2. floor of Gjennestad High School	80
47	P-h diagram for R600a	119
48	P-h diagram for R290	119
49	P-h diagram for R717	120
50	P-h diagram for R1234ze(E)	120
51	Used energy for plant 1 in IDA ICE - Diagram collected from IDA ICE.	131
52	Used energy for plant 2 in IDA ICE - Diagram collected from IDA ICE.	133

List of Tables

1	Properties of R600a, R290, R717 and R1234ze(E) [34].	12
2	Building details	20
3	Energy demand of the building.	20
4	Effect demand of the building.	21
5	Heat pump dimensions. *The energy demand for ventilation is included in the space heating.	22
6	Input data in the solar system.	24
7	Input data in the GHX model.	26
8	Identified parameters of the HP based on the state and prerequisites.	30
9	Pierre's constants for the different refrigerants [57][58].	31
10	Input values for the plants in IDA ICE.	35
11	Input values from the study of Gurracino et al. [67].	37
12	Results of the validation of the SC model [67].	37
13	The different input parameters from the study of Madessa et al.[52].	37
14	Results of the validation of the GHX model [52].	38
15	Input values for HP model from Esen et al. [69].	39
16	Results of the validation of the HP model[69].	39
17	The different input parameters from the study of Kjellsvik et al. [70].	40
18	Validation of the area of the evaporator [70].	40

19	The calculated exergy of the GHX.	49
20	Calculated COP for all the refrigerants.	54
21	Calculated area of the evaporator area for the different refrigerants.	57
22	Calculated exergy destruction in each component of the HP for the different refrigerants.	58
23	Calculated second law efficiency in each component of the HP for the different refrigerants.	59
24	Articles gathered in the literature review from Science Direct, Scopus and Web of Science	77
25	Used energy for plant 1 in IDA ICE - Table collected from IDA ICE.	131
26	Utilized free heat for plant 1 in IDA ICE - Table collected from IDA ICE.	132
27	Energy required from the top heater in plant 1 when the mass flow rate in the solar system is set to $2e^{-8}$ kg/s - Table collected from IDA ICE.	132
28	Used energy for plant 2 in IDA ICE - Table collected from IDA ICE.	133
29	Utilized free heat for plant 2 in IDA ICE - Table collected from IDA ICE.	134
30	Energy required from the top heater in plant 2 - Table collected from IDA ICE.	134

Nomenclature

Abbreviation	Explanation
AHU	Air handling unit
Comp	Compressor
Cond	Condenser
COP	Coefficient of performance
Des	Destruction
DHW	Domestic hot water
o	Out of the system
EES	Engineering equation solver
ESBO	Early stage building optimization
Evap	Evaporator
Exp	Expansion valve
f	Fluid
g	Gas
GHX	Ground heat exchanger
GSHP	Ground source heat pump
GWP	Global warming potential
HP	Heat pump
HX	Heat exchanger
i	Into the system
IDA ICE	IDA Indoor Climate and Energy
Iso	Isentropic
LMTD	Log mean temperature difference
m	Mean value
ODP	Ozone depletion potential
PV	Photovoltaic
Refrg	Refrigerant
Sat	Saturated
SC	Solar collector
SGSHP	Solar assisted ground source heat pump
TRNSYS	Transient System Simulation Tool
UA	Useful area
Vol	Volumetric

Symbols	Description	Unit
A	Area	[m^2]
c_p	Heat capacity	[J/kgK]
D	Diameter	[m]
G	Solar irradiance	[W/m^2]
g	Gravity of earth	[m/s^2]
h	Heat transfer coefficient	[W/m^2K]
h	Specific enthalpy	[J/kg]
I	Solar flux	[kWh/m^2]
J_g	Dimensionless vapor velocity	[-]
k	Thermal conductivity	[W/mK]
L	Length	[m]
\dot{m}	Mass flow rate	[kg/s]
Nu	Nusselt number	[-]
P	Pressure	[Pa]
Pr	Prantl number	[-]
\dot{Q}	Rate of heat	[W]
R	Thermal resistance	[mK/W]
R_f	Fouling factor	[m^2K/W]
Re	Reynolds number	[-]
s	Specific entropy	[J/kgK]
Su	Suratman number	[-]
T	Temperature	[K]
U	Overall heat transfer coefficient	[W/m^2K]
v	Velocity	[m/s]
\dot{W}	Work	[W]
X	Lockhart-Martinelli	[-]
x	Quality of the fluid	[-]
\dot{X}	Exergy	[W]
Greek letters		
α	Absorption coefficient	[%]
β	Tilt angle from the horizontal surface	[°]
ϵ	Roughness of wall	[m]
τ	Transmission coefficient	[%]
ρ	Density	[kg/m^3]
ϵ	Emissivity	[-]
η	Efficiency	[%]
μ	Viscosity	[kg/ms]
ψ	Specific flow exergy	[J/kg]
δ	Depletion rate	[-]
ϕ	Latitude of location	[°]
v	Volumetric flow rate	[m^3/s]
Δ	Interval	[-]

1 Introduction

1.1 Background

The building sector's energy demand has been rising for the last decades and is now accounting for 30% of the final global energy consumption, making it one of the largest energy consumption sectors [1]. The Paris Agreement, adopted by 196 countries in 2016, and the UN climate report published in 2021 are expressing a deep concern for the environment, which has heightened the focus on reducing the energy usage [2] [3]. It is, therefore, vital to minimize greenhouse gas emissions in the building sector and enhance energy efficiency in order to meet the Paris Agreement's target of limiting global warming to 1.5 °C compared to the prediction. Therefore, a considerable percentage of energy production should come from renewable sources proven to be energy efficient and durable.

As more passive houses and low-energy buildings have been built in recent years, the need for efficient energy systems has grown. As well, due to the change in the weather pattern and cold climate in the north, there is still some uncertainty about how some types of energy sources can best be utilized for the building sector, like solar systems. Ground source heat pumps (GSHP) are a well-established technology in Norway today. Solar energy is, however, less used, particularly solar thermal energy systems. If the purpose is to use solar energy for heating, it is advantageous to convert the sun's rays directly into heat rather than go the way through electricity [4]. There has been an increase in interest in combining these two technologies to improve the energy system's operating conditions and minimize the need for delivered energy. Several studies have compared the performance of a solar assisted ground source heat pump (SGSHP) to a conventional GSHP, and the results showed benefits of having solar thermal energy combined with a GSHP. The configurations of SGSHP can be done in a variety of ways. The heat generated by the solar collectors (SC) can be utilized to raise the evaporation temperature, recharge the ground, produce the building's domestic hot water, or a combination of these methods. In recent years, there has been an increase in the number of published research works examining how system solutions for SGSHP affect the performance, and different positive outcomes from each configuration have been observed. However, the performance of these systems in Norway is a gap in this field, and will therefore be conducted in this thesis.

1.2 Main objective

The main objective of this thesis is to look into the energy and exergy performance of a SGSHP and investigate if it is beneficial to assist a GSHP with solar thermal energy in a cold climate. Different parameters will be analyzed in order to understand how they affect the performance of the energy system and provide important information for the optimization of a SGSHP. This was accomplished by performing a comprehensive thermodynamic analysis of the selected energy system in Engineering Equation Solver (EES) and through dynamics simulations in IDA ICE (IDA Indoor Climate and Energy). The SGSHP is connected to a school building in Oslo, Norway, which is designed according to the Norwegian passive house standard. The SGSHP under consideration will provide energy both for domestic hot water production (DHW) and space heating. The configuration of the system will be designed in such a way that the flat plate SC prioritizes providing heat to the hot water tank, and any excess heat from the SC will be used to charge the ground heat exchanger (GHX). In the thermodynamic analysis of the system, four different potential working fluids have been investigated for the heat pump (HP): isobutane (R600a), propane (R290), ammonia (R717), and solstice (R1234ze(E)).

1.3 Limitations

For this master thesis, only one system configuration for the SGSHP is considered due to time limitations. For the same reason, neither cost profitability nor environmental impact is taken into account.

2 Literature review

2.1 Review Approach

A scoping review was carried out to map the relevant literature in the field of SGSHP. An overview of the study design and available evidence in this field, regardless of quality, might indicate specific questions and methods that should be implemented in new research and in this thesis to further advance the research field. The scoping review follows the framework given by Arksey and O'Malley in their seminal paper on Scoping review [5].

1. Identifying the research question
2. Identifying relevant studies
3. Study selection
4. Charting the data
5. Collating, summarizing and reporting the result

The research question for this literature review was defined as: *What is known from existing literature on the performance of a ground source heat pump coupled with solar collectors?*

The next stage was to compile a list of relevant studies. This was accomplished by identifying relevant keywords and terms connected to the research subject. The used search was: "Performance analysis" AND "solar thermal system" OR "solar collector" AND "ground source heat pump". Only articles written in English and Norwegian were considered. It is worthy to mention that Web of Science, Scopus and Science Direct are the only databases utilized in this literature review. The databases were chosen based on their accessibility through the university as well as their capacity to do advanced searches. To limit the quantity of studies and improve the quality of the articles while maintaining a defined scope, review papers, conference reviews, conference papers, and books were removed.

An abstract review process was carried out next, in which the abstract was read to eliminate publications that were not relevant. These were articles that didn't include the keywords, gave the keywords a different meaning, or used the keywords differently. The keyword "solar collector" is an example of this, which can be used in conjunction with a photovoltaic panel (PV) in many circumstances, but this literature analysis focuses solely on SC as a source of solar thermal energy. Articles that were not accessible through the university were likewise left out. When the relevancy of an article was questioned, the conclusion was read and the remainder of the article was examined more extensively to see whether it should be included or not. Finally, articles that were repeated in the three databases were removed. As a result, the literature review consists of a total of 33 studies. Appendix B provides a list of the articles retrieved from the databases.

The framework's next step was to extract and chart the data. The articles were carefully examined and classified into various properties. Excel and NVivo were both used to neatly organize the data. The aim of the study and the important results were identified by the the authors own words. This step is critical for providing an overview of existing literature, as well as identifying research gaps and key discoveries.

2.2 General trends

General data for the 33 articles was gathered to examine if there were any general trends in the data that might be used to identify study gaps. This master's thesis will address some of the gaps that have been noticed.

2.2.1 Publishing year

The number of publications on this topic is growing, but it is still a modest amount with a small increase, as seen in figure 1. The use of HPs has risen in recent years, particularly water-to-water HP [6]. A growing awareness of buildings' environmental implications could potentially be a motivating element behind this small rise. We want to improve the heating and cooling system's efficiency and lifetime while reducing the use of fossil fuels, and coupling a GSHP with SC could be a good solution, which still needs to be optimized. The coronavirus may have made it difficult to operate experimentally and together with others, which could explain why the amount of new research from 2020 until now has remained constant and did not increase as one could expect.

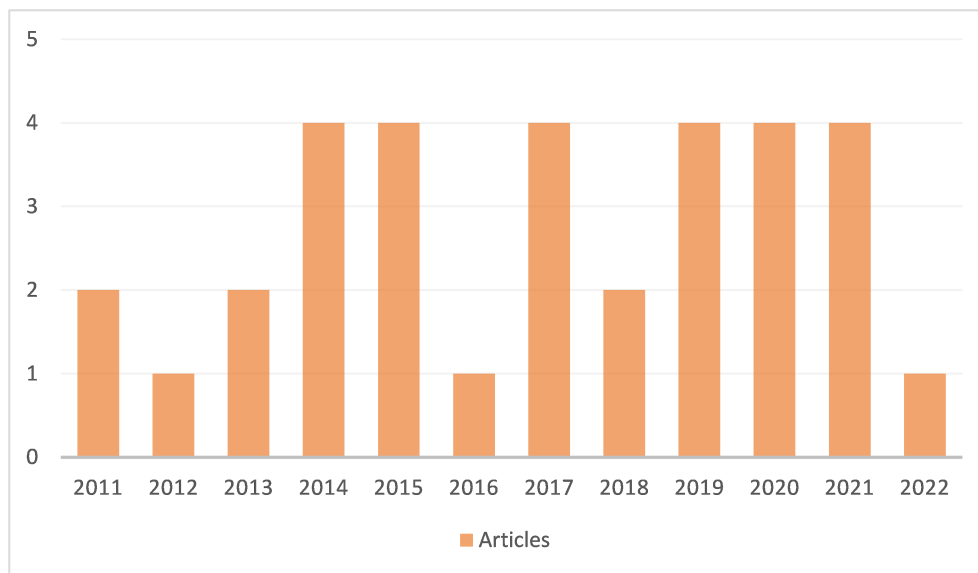


Figure 1: Publication year of the selected articles.

2.2.2 Represented countries

The geographical location of the analyzed SGSHP is presented in figure 2, and it shows that 15 distinct countries are represented. This representation can also predict which climates have been studied the most. In 24% of the cases, the investigation took place in China. China has developed a considerable solar manufacturing industry, and the cost of a solar collector in China is significantly lower than in other countries [7]. This makes it more cost-effective to utilize and, as a result, more desirable to investigate. The countries represented make up 8% of the United Nations' membership. The low proportion shows that the subject is still developing.

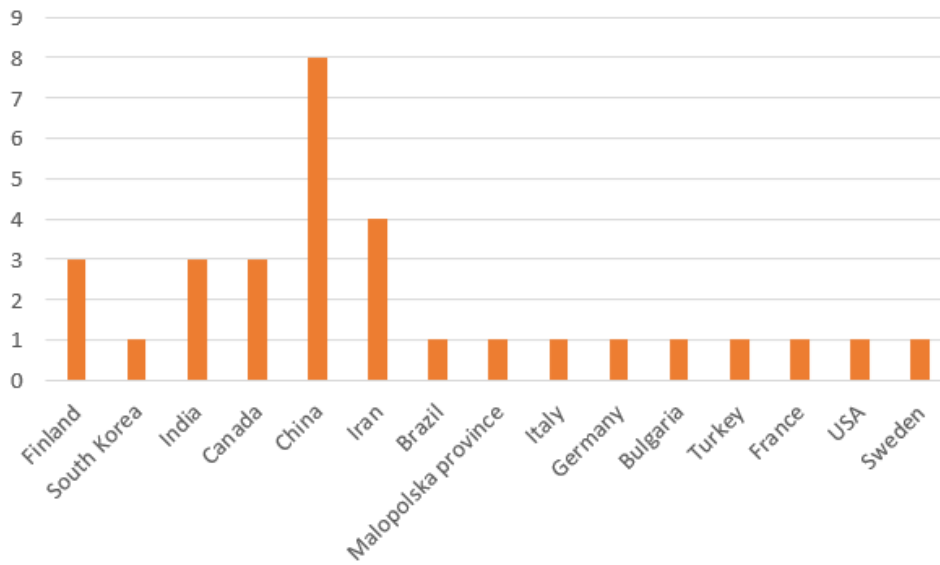


Figure 2: Geographical location of the studies case.

2.2.3 Implemented method

In this section, the different methods used in the gathered articles have been investigated and charted. Figure 3 illustrates the distribution of 3 different methods: simulation tool, experimental and mathematical modeling. One article used both a simulation tool and an experimental method, and the baseline is therefore 34.

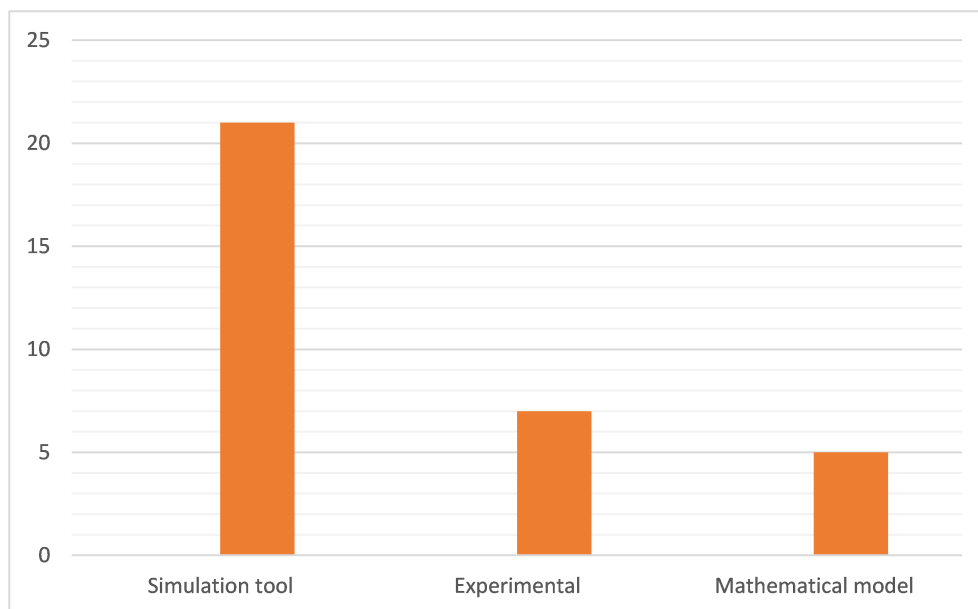


Figure 3: Implemented Method.

The most frequently used method is, by far, simulation. Simulating the energy system can be an efficient and low-cost way to indicate if the studied method is useful and should be further implemented in a real environment. The software programs today also have high accuracy and are easy to access. The most popular software was TRNSYS (Transient System Simulation Tool), which 86 % of the studies performed

simulations used. Other simulation tools used were IDA-ICE, Polysun, and Dymola.

Many of the studies used mathematical modeling, which has several of the same advantages as simulation. The fundamental distinction between these two methods is that with a mathematical model, you may use general equations and mathematical expressions to represent the relationships between variables and outcomes. As a result, you have an explicit expression of the behavior pattern. The downside is that unrealistic assumptions must be made, but this can be overcome via simulation.

Experimental studies account for only 20% of the total. This low percentage may be because of the complexity of these kinds of systems and the cost thereof. An experimental study also has limitations on the study period and varying the input.

To further advance this research field, more studies should implement the developed SGSHP in real buildings to test their actual performance. This implementation will increase the possibility of using SGSHP on more buildings today, lowering total energy consumption in the building sector.

2.2.4 Building category

The researched energy systems were tested on a variety of buildings in order to verify their utility and performance. The various building categories are classified into four groups based on the functional use: residential, educational, commercial and other building types. Yan et al. and Vikas and Murugesan are under other building types since they used a test room and did not specify other than "heating for a room" [8] [9].

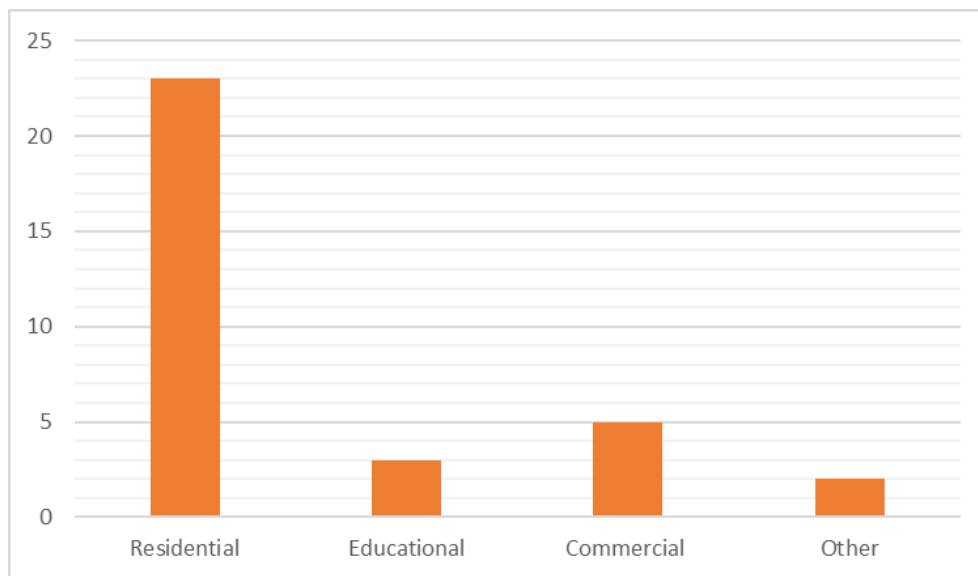


Figure 4: The different building categories implemented in the studies.

Figure 4 shows that the SGSHP is mostly investigated based on the energy demand of a residential building, 70% of the studies. This was mainly found to be in small houses. The popularity of using this building type may be because of the available data and accessibility. Even though commercial and residential buildings have enormous potential in energy reduction, because of the high consumption, these buildings are a bit more complex and not as easy to access or simulate [10]. More research on SGSHP tied to educational and commercial buildings is needed to develop this topic of study further.

2.3 Findings from literature review

The gathered findings from the selected articles will be summarized and compared in the next section based on a specific evaluated outcome of using SGSHP.

2.3.1 Thermal imbalance in the soil

With the use of GSHP, a thermal imbalance in the soil occurs when the heating and cooling loads are not equal over time. As a result, the soil temperature, the efficiency of the system and the lifetime will decrease. Additional research have investigated how the GHX and the operation mode should be modified, and other studies have tried to integrate other applicants to the system, such as a boiler, waste heat and solar energy, to resolve this problem. This review will look at how combining GSHP with SC can help with the soil's thermal imbalance.

Shamsabadi et al. developed a mathematical model of a small hybrid system to investigate the effect of using flat plate solar collectors for recharging the ground in Tehran [11]. The temperature of the soil climbed 1-2°C with SC during the course of a month in the summer. Without SC, the soil temperature dropped by 1.25–1.85°C, demonstrating the importance of ground charging to avoid ground thermal depletion. Ji et al. and Gao et al. achieved a similar result, but used TRNSYS to simulate a GSHP and a SGSHP, and studied for a longer period, 10 years [12] [13]. Ji et al. plotted the average ground temperature over a 10-year period, and a GSHP was compared to a SGSHP with 1212 m^2 of SC and 2424 m^2 of SC. The temperature dropped by 8.65°C without SC, but only by 1.07°C with a SC area of 1212 m^2 . The soil temperature increased by 4.87°C as the area of SC was doubled. Gau et al. studied the system in 3 different locations, introducing climate as a factor. The three different locations were Beijing, Harbin and Shengzhou, a cold climate, a severe cold climate and a hot summer and cold winter climate, respectively. For all three SGSHP the average soil temperature remained stable over the 10 years. For the GSHP in Beijing, Harbin and Shengzhou the average soil temperature dropped by 7.3°C, 7.5°C and 4.2°C respectively. Regardless of the climate, the injected heat to the ground from SC will help balance the ground, but the study proves that it is more important to do so in a colder climate where the temperature will drop drastically over time with the use of GSHP.

Lee et al. compared the ground temperature of two SGSHP systems, one with a serial configuration and the other with a parallel configuration [14]. If the temperature in the buffer tank is high enough, heat collected from the SC is pumped into the GHX in the first system. The heat from the SC was used directly as a secondary heat source in the HP in the second system, which could not inject heat into the ground. When compared to a conventional GSHP, the soil temperature of the first and second systems increased by 20.7% and 7.2%, respectively. Lee et al. therefore proves that using SC to recharge the ground or as a secondary heat source helps balance the ground temperature, but also concluded that by recharging solar heat into the ground, the SGSHP raised the soil temperature significantly.

It has been demonstrated that combining GSHP with SC prevents drastically temperature drops in the soil, hence reduces depletion over time. The majority of research focused on recharging, stating that it reduces the temperature drop over time and that these steps are more important to implement in colder areas. Few studies have looked at the effect of utilizing the SC directly to limit heat extraction from boreholes, but Lee et al. demonstrate that this is a measurement that can be implemented, thus it's worth doing more research to determine how this measure differs in different climates.

2.3.2 Affect of solar collector on borehole length

One issue with GSHP is the cost and complexity of constructing the GHX. Several studies therefore aimed to see if using SC with a GSHP can reduce the length of the borehole.

Duarte et al. simulated a solar hybrid GSHP in Milton, Canada [15]. During the heating season, the relationship between the SC area and the GHX length was investigated. The best relationship was discovered with a SC area of 6.81 m^2 , which reduced the GHX length by 15% compared to excluding the SC. After a sensitivity analysis was carried out for four different cities in Canada, they concluded that the proposed solar hybrid GSHP system was most suitable for Vancouver, which has the mildest climate.

The ratio of GHX length reduction to SC area was determined to be 7.64 m/m^2 .

Cimmino and Eslami-Nejad simulated a SGSHP system over a 30-year period, with various GHX network arrangements under different values of minimum fluid temperature returning to the heat pump, total solar collector area, and borehole spacing [16]. All cases are compared against a one borehole configuration with and without solar heat injection. The results revealed a considerable difference in the reduction of borehole length. When heat is injected into a single borehole, the required borehole length is lowered by 10%. With a SC area of 10 m^2 , the required borehole length for a shallow bore field might be reduced by up to 29%. Finally, they concluded that the minimum temperature returned to the HP also has a significant impact on the necessary borehole length in both single and shallow bore field setups.

Eslami-Nejad and Bernier compared the performance of two distinct SGSHP systems, consisting of a single borehole, over a 20-year period to a traditional GSHP system [17]. In case 1, the SC recharged the boreholes, but in case 2, the SC heated the working fluid before it entered the evaporator. In comparison to the conventional system, the simulations revealed borehole length reductions of 17.6% and 33.1% for case 1 and 2, respectively. They believe that the first result is primarily due to solar energy injected and stored into the ground over the heating season, which raises the ground temperature in the borehole's proximity. They also looked into how the ground's thermal conduction affects borehole length. By increasing the thermal conductivity from 1.5 to 3 W/mK, the borehole length could be reduced by 27%.

Overall, these studies concluded that implementing SC to the GSHP would reduce of needed borehole length regardless of the system configuration.

2.3.3 Energy consumption

The great efficiency and low energy consumption of GSHP is one of the reasons why it is becoming more widely employed. One of the key goals of combining GSHP with a solar system is to utilize more renewable energy over electricity or fossil energy.

In Zahedan, Iran, different system scenarios were simulated by Razavi et al. over a ten-year period [18]. The direct solar-assisted GSHP, in which the fluid from the GHX passes through the SC to help raise the temperature before the evaporator, uses the least amount of energy and saves 8.4% over the stand-alone GSHP. The scenario in which the SC directly supported the GSHP, by heating the ground working fluid before it enters the HP or by heating the water tank when the ground fluid temperature reaches the maximum, only resulted in a 0.3% energy decrease. Eslami-Nejad and Bernier simulated a similar SGSHP system, case 2 as mentioned earlier, and reported an energy consumption reduction of 6.3% compared to a GSHP [19]. For case 1, where the solar energy was injected into the ground, the reduction was lower; only 3.5% less energy consumption. Thygesen and Karlsson simulated a SGSHP in which the SC was solely utilized to heat the water tank [20]. Due to the difficulty of coupling HP with systems that compete with heat pump operation, such as DHW or space heating, this study indicated that the SC only saved a little amount of energy. Hwang et al. came to a conclusion that differed from the other studies in their experimental analysis of a GSHP and an SGSHP [21]. Their SC heated a low temperature storage tank which increases the temperature before the evaporator or recharges the ground. When compared to the GSHP, the SGSHP experienced a much higher energy reduction of 20%.

These findings suggest that coupling SC to a GSHP can lower energy consumption when compared to a stand-alone GSHP, although the amount of savings varies depending on the system solution and control strategies. The variance in the results highlights the need for further research in this field.

2.3.4 Coefficient of performance

One other way to evaluate the performance of a SGSHP is to compute the Coefficient of Performance (COP). An increase in COP leads to a reduction of the need for an auxiliary unit and an increase in the life span of the system.

Vikas and Murugesan concluded that charging the ground with the use of SC can increase the COP of the system, and in their studied case the COP increased by 23% for space heating in the nighttime [22].

Razavi et al. explain the increase of the COP as a result of the increase in the evaporator temperature due to the higher temperature in the ground caused by the charging [18]. This gives a lower temperature difference between the evaporator and condenser. Chen et al. investigated a novel numerical model of a SGSHP system [23]. The SC was used to heat DHW, and the excess heat was utilized to heat rooms or recharge the ground. On a typical winter day in Shanghai, China, the system with the SC achieved a SCOP of 4.2, while the system without them only achieved 3.5; a 20% difference.

The study by Gao et al., as mentioned earlier, also studies the performance of the system in the three different locations in China over a period of 10 years [13]. The COP of the SGSHP systems in Beijing, Harbin, and Shengzhou remained constant over the years, 3.9, 2.6 and 3.8, but for the GSHP systems the COP decreased by 23%, 46%, and 11% respectively. The COP with the SC remains constant over time, whereas the COP with the conventional GSHP drops, with the decrease being greater in colder locations. Varma and Murugesan get a similar result and find that their SGSHP system has the highest COP during the day and the lowest during the night in the wintertime [24]. They concluded that colder areas have a lower COP because more heat is lost to the environment. Girard et al. also underline this finding and points out that the increase of COP is higher in mild climates with high solar radiation [19].

It was found that several configurations of a SGSHP will increase the COP compared to a conventional GSHP. The increase was found to be marginal in the colder climates of the north, and suggests that more research should be done to see if coupling SC to GSHP is optimal here.

3 Theory

3.1 Solar assisted ground source heat pump

3.1.1 Solar collector

A solar collector converts radiation from the sun into heat [25]. The heat from the sun is collected in a working fluid which can be transferred and used to heat water or space. This heat is then transferred to the working fluid that can heat water or space. Evacuated tube and flat plate collectors are the most common types of solar collectors for buildings. The evacuated tube collector is made up of a series of parallel transparent glass tubes that are connected to a header pipe. The shape of these glass tubes is cylindrical. As a result, the angle of the sun is always perpendicular to the heat absorbing tubes, allowing these collectors to function well even when the sun is low. A flat plate collector has a box on top with a glass or plastic cover and a dark absorber plate on the bottom, these collectors are well insulated, see figure 5.

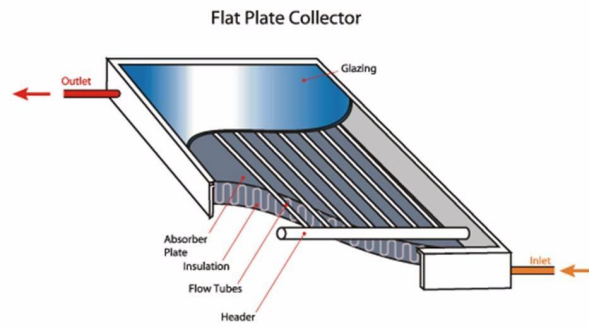


Figure 5: Flat plate solar collector [26].

Despite the fact that the module is well-built, the collector suffers some losses. Some of the sun's radiation is reflected back to the sky, while others are absorbed by the materials before the backplate. As a result, the amount of radiation at the backplate can be calculated :

$$Q_i = G(\tau\alpha)A \quad (1)$$

Where G is solar irradiance [W/m^2], A is the area of the collector [m^2] and τ and α represent the transmission and absorption coefficients respectively.

When the heat is absorbed, the temperature of the collector rises above the ambient temperature, causing heat loss to the surroundings. This heat loss can be determined by the following equation.

$$Q_o = U_L A (T_c - T_a) \quad (2)$$

U_L is the overall heat loss coefficient [W/m^2K], T_c and T_a is the temperature of the collector and is the ambient temperature [K]. As a result of the equation 1 and 2, together with a heat removal factor, the actual useful energy absorbed by the collector is given The Hottel-Whiller-Bliss equation.

$$\begin{aligned} Q_u &= Q_i - Q_o \\ &= F_R A (I(\tau\alpha) - U_L(T_c - T_a)) \end{aligned} \quad (3)$$

The thermal efficiency of the SC expresses the useful energy gain over the incident solar energy, and can be obtained from equation 4 [27].

$$\eta_{th} = \eta_0 - \frac{a_1(T_m - T_a)}{G} - \frac{a_2(T_m - T_a)^2}{G} \quad (4)$$

The optical efficiency, η_0 , and first and second order heat loss coefficient, a_1 and a_2 , are information given by the solar collector manufacturer.

3.1.2 Ground heat exchanger

A ground source heat pump is a system that utilizes the ground as a heat source or sink through a ground heat exchanger [28]. This type of HP is very efficient, with a COP around 4. The heat comes from solar energy that has been stored below the ground down to 300 meters, plus a small amount of contribution from the earth's core [28] [29]. The temperature at the upper 10-20 m depends greatly on the season, but deeper down the temperature is more stable through the year at 2-10 degrees. In the winter, the ground temperature is greater than the ambient air temperature, and in the summer, the ground temperature is lower than the ambient air temperature, resulting in higher efficiency than traditional air conditioning. The stored energy can be extracted by horizontal or vertical collectors. The horizontal collectors are placed on a wide ground area, about 1-3 m deep, whereas the vertical collectors are installed in 80-300 m deep boreholes. The depth of the borehole should be determined by the grounds' heat conductivity and groundwater flow [30]. If the amount of energy required exceeds the capacity of a single borehole, multiple boreholes working together in a system will increase the overall amount of energy produced.

A GHX can be divided into two categories: closed-loop and open-loop [30]. An open-loop system uses the groundwater directly. The heat is extracted from the groundwater by pumping it up to the HP. After that, the chilled water will be pumped into a return well or, if permission is granted, into a nearby river [31]. This system is reliant on a large capacity and high quality of groundwater. A closed-loop system will not use the groundwater directly so the pipe will contain a brine, often a frost proof fluid. See an illustration of a closed-loop GHX in figure 6. It is critical that the brine in the pipe is non-toxic, because of the risk of leakage. The brine will collect heat at the bottom of the borehole, circulate it to the HP, and the heat will be recovered in the building's heating system. This approach is less likely to pollute groundwater, but it is less efficient than an open-loop system because it involves two heat exchange operations.

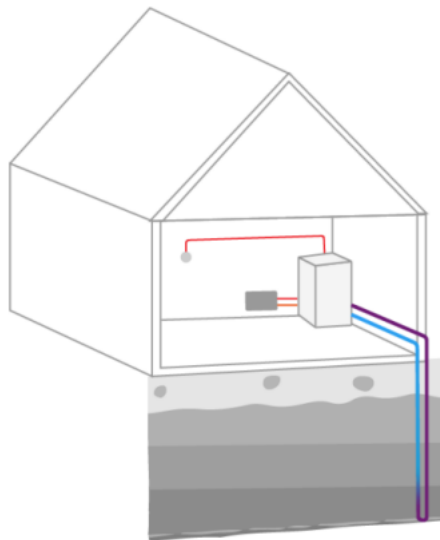


Figure 6: A closed-loop ground heat exchanger with a vertical borehole.

Hot fluid can be cooled in the borehole throughout the summer. This procedure is known as freecooling and it is a direct way of cooling a building using a ground source heat pump. This method also helps to maintain the energy balance, allowing the borehole to expand its capacity and lifespan. If the borehole is not utilized for cooling, the heat extracted can be replaced by water movement in the ground for deep boreholes or solar energy for more shallow boreholes [32].

3.1.3 Heat pump

A heat pump is able to move thermal energy from a lower to a higher temperature source, which allows it to heat a hot reservoir or cool a cold reservoir. A HP consists of four main components, as seen in figure 7:

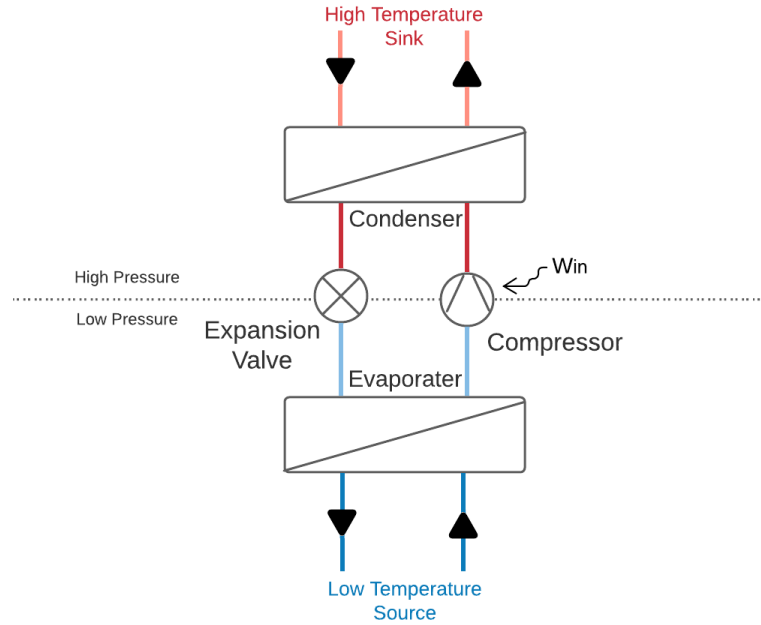


Figure 7: Schematic of a simplified heat pump.

- **Evaporator** - heat from the source is collected in the refrigerants as it evaporates
- **Compressor** - the pressure and temperature of the refrigerant is increased
- **Condenser** - heat transfers from the refrigerant to the building when the refrigerator condenses
- **Expansion valve** - the pressure is reduced, resulting in lower temperature and boiling point for the refrigerant

The amount of energy required for the process is less than the amount of produced heat, making the heat pump an efficient and economical product. This relation is known as the coefficient of performance of heat pumps, an important factor describing the efficiency of a HP.

$$COP_{HP} = \frac{Q_H}{W_{net,in}} = \frac{Q_C + W_{net,in}}{W_{net,in}} \quad (5)$$

Q_H represent the heat transferred to the building from the HP, Q_C is the heat collected from the cold source, [W], and $W_{net,in}$ [W] is the needed energy input to the compressor.

A theoretical ideal thermodynamic cycle only consist of reversible processes. The best known is a Carnot cycle and for a heat engine it consists of isothermal expansion, adiabatic expansion, isothermal compression and adiabatic compression. A Carnot cycle presents the upper limit on the efficiency of any heat engine.

$$COP_{carnot} = \frac{T_H}{T_H - T_C} \quad (6)$$

From this equation it is clear that the COP is greatly depended on the temperature in the hot and cold reservoirs, T_H and T_C [K].

The condenser and evaporator are types of heat exchangers (HX) and the energy transfer can be calculated by the log mean temperature difference method (LMTD).

$$\dot{Q} = UA\Delta T_{lm} \quad (7)$$

ΔT_{lm} represent the logarithmic mean of the difference between the inlet and outlets temperatures for the hot and cold fluid.

The working fluid employed as the heat carrier inside the HP is called a refrigerant. The refrigerant can remove heat from the source and supply heat to the sink during phase changes. The chemical, physical, and thermodynamic properties of the refrigerant are consequently critical in ensuring that the operating and performance requirements are met. In the event of a leak, there should be no risk of fire, injury, or property damage caused by the fluid. The environmental impact of a refrigerant is an essential factor to consider, and different measurements are used to assess this. The global warming potential (GWP) is a measure of how much a refrigerant contributes to global warming over time when compared to carbon dioxide [33]. The Ozone Depletion Potential (ODP) is the ratio of the refrigerant's ozone damage to that of CFC-11 (R11), where the range varies from 0 to 1. A higher value for both measurements implies greater environmental impact. Thermodynamic properties and environmental impacts of the four refrigerants studied in this thesis are listed in table 1.

Table 1: Properties of R600a, R290, R717 and R1234ze(E) [34].

	R600a	R290	R717	R1234ze(E)
Class	Isobutane	Propane	Ammonia	Solstice ze
Classification	Hydrocarbon	Natural	Natural	Hydrofluoroolefins
Boiling point at 1 atm [°C]	-11.7	-42.0	-33.3	-18.95
Freezing point at 1 atm [°C]	-159.6	-187.28	-77.7	-156.0
Critical temperature [°C]	135.0	96.7	132.4	109.37
Critical pressure [MPa]	3.6	4.3	11.3	3.6
Flammability	Higher flammable	Higher flammable	Lower flammable	Lower flammable
GWP	5	4	0	<1
ODP	0	0	0	0

3.2 Thermodynamics

Thermodynamics can be defined as the science of energy; the ability to cause changes [35]. Because thermodynamics is such an important aspect of many engineering processes, various laws and concepts will be discussed in this paper.

According to the Law of Conservation of Energy, energy can not be created or destroyed, it can only be transferred to another thermodynamic system or converted to another form [35]. This is often known as the 1. Law of thermodynamics and the following equation illustrate this principle.

$$\dot{E}_{in} - \dot{E}_{out} = \Delta \dot{E}_{system} \quad (8)$$

3.2.1 Enthalpy

Enthalpy is a state function describing how much heat is present inside a system [36]. Enthalpy, H [J], is the sum of the internal energy, U [J], and the product of the pressure, P [Pa] and volume, V [m^3] of the thermodynamic system.

$$H = U + PV \quad (9)$$

3.2.2 Entropy

A process will only proceed in a certain direction naturally, and the 1. law does not account for this [35]. The second 2. does, and introduces entropy, S [J/K], as a property of thermodynamic systems. Over time, this property will only increase, but the quality may decrease. This law can assist in determining the theoretical limits of a process. In an internally reversible process, the change in entropy can be described as equation 10.

$$dS = \left(\frac{\delta Q}{T}\right)_{int,rev} \quad (10)$$

If the system is real, and therefore not irreversible, the change of entropy can be described as follows.

$$\Delta S_{system} = S_2 - S_1 = \int_1^2 \frac{dQ}{T} + S_{gen} \quad (11)$$

A process where the entropy remains constant is an ideal adiabatic and reversible process, often referred to as an isentropic process. When comparing the isentropic process to a real process under steady flow, the efficiency of a specific device can be evaluated.

3.2.3 Exergy

Exergy is the term for the available or useable energy inside a system, often expressed in watt [35]. This can be described as the maximum useful work that can be obtained from a system at a given state, and an exergy analysis of a system provides a measure of how close real performance is to ideal performance. Exergy is often described through exergy destruction, which indicates inefficiency, addressing the source of the malfunction in a thermal system [37]. An exergy analysis can therefore assist in the improvement and optimization of the system design. The general exergy balance is as follows.

$$\begin{aligned} \Sigma \dot{X}_{des} &= \Sigma \dot{X}_{in} - \Sigma \dot{X}_{out} - \Sigma \dot{X}_s \\ &= \Sigma \dot{X}_{heat} - \Sigma \dot{X}_{work} + \Sigma \dot{X}_{mass,in} - \Sigma \dot{X}_{mass,out} \end{aligned} \quad (12)$$

Where

$$\Sigma \dot{X}_{heat} = \Sigma \left(1 - \frac{T_0}{T_k}\right) \dot{Q}_k \quad (13)$$

$$\Sigma \dot{X}_{work} = \dot{W} \quad (14)$$

$$\Sigma \dot{X}_{mass,in} = \Sigma \dot{m}_{out} \psi_{in} \quad (15)$$

$$\Sigma \dot{X}_{mass,out} = \Sigma \dot{m}_{out} \psi_{out} \quad (16)$$

The specific flow exergy, ψ [J/kg], depends on the enthalpy and entropy, and the difference can be given by equation 17 when kinetic and potential energy is neglected.

$$(\psi_{in} - \psi_{out}) = (h_{in} - h_{out}) - T_0(s_{in} - s_{out}) \quad (17)$$

T_0 represents the dead state temperature of the system.

The second law efficiency, also known as exergy efficiency, can be used to determine how close a system is to its optimal performance [35]. This efficiency can be calculated as follows during a process.

$$\eta_{II} = 1 - \frac{\text{Exergy destroyed}}{\text{Exergy expand}} \quad (18)$$

3.3 Heat Transfer

Heat transfer concerns the thermal energy which transfers between substances [38]. This discipline is commonly divided into different modes depending on the process:

- Conduction
- Convection
- Radiation

3.3.1 Conduction

Heat diffuses between materials that are in contact with one another. This is due to the collisions and diffusion of molecules in gases and liquids, and the vibrations of the particles in solids. The heat moves from high to low temperature, and the rate of heat conduction can be expressed by Fourier's law.

$$\dot{Q}_{cd} = -kA \frac{dT}{dx} \quad (19)$$

The formula implements thermal conductivity, k [W/mK], and the length of the material, x [m]. The heat conduction can also be expressed with the thermal resistance of the object.

$$\dot{Q}_{cd} = \frac{T_1 - T_2}{R_{cd}} \quad (20)$$

3.3.2 Convection

The convective heat transfer is due to fluid motion because of the temperature difference. Natural convection occurs when a temperature difference creates a density gradient, causing motion. The process is known as forced convection when the motion is caused by the impact of a blower or pump. The rate of convection heat transfer is given by log Newtons law of cooling.

$$\dot{Q}_{cv} = hA\Delta T \quad (21)$$

Other parameters, such as the Nusselt number, also influence forced convection. The Nusselt number is the ratio of convection heat transfer to conduction heat transfer under the same conditions. A high value indicates efficient heat transfer due to convection.

$$Nu = \frac{hD}{k} \quad (22)$$

In the above equations, h is the heat transfer [W/m²K] and D is the inner diameter of the pipe [m]. Nusselt number can also be described as a function of Reynolds and Prandtl number.

$$Nu = C(Re)^m(Pr)^n \quad (23)$$

The Reynolds number is a dimensionless value which describes the ratio of internal forces to viscous forces to the fluid. This value can be used to determine whether the fluid is laminar or turbulent. If the Reynolds number is less than the critical Reynolds number, the fluid is laminar. The critical Reynolds number varies depending on the properties of the fluid, but is typically around 2300, where the transition flow occurs inside of pipes up to Reynolds number 4000 [38]. For Reynolds number higher than this, the flow is turbulent. At around 4000, the largest heat transfer coefficient occurs, followed by a gradual decline as the Reynolds number increases. Reynolds number's mathematical definition is as follows:

$$Re = \frac{\rho v D}{\mu} \quad (24)$$

The Prandtl number is also dimensionless and correlates the fluid's viscosity, μ [kg/ms], and heat capacity, c_p [J/kgK], with its thermal conductivity.

$$Pr = \frac{\mu c_p}{k} \quad (25)$$

3.3.3 Radiation

Thermal radiation, unlike conduction and convection, does not require a medium to transport heat. At the speed of light, electromagnetic waves are emitted from a source. Thermal radiation is based on Stefan Boltzmann law; energy flux from a blackbody.

$$\dot{Q}_{emit,max} = \sigma T^4 \quad (26)$$

Where the constant of proportionality is $\sigma = 5,668 * 10^{-8} \frac{W}{m^2 K^4}$.

For real surfaces, the law is modified with the emissivity of the surface.

$$\dot{Q}_{emit} = \epsilon \sigma T^4 \quad (27)$$

The rate of radiation heat transfer between two surfaces is given by:

$$\dot{Q}_{rad} = \epsilon \sigma A (T_s^4 - T_{surr}^4) \quad (28)$$

3.4 System configuration

Five separate system configurations for a SGSHP will be presented in this part. In every solution, the SGSHP will provide space heating and DHW to a school that has a low-temperature heating system, but how the collected energy from the SC will be utilized differ for each system. To ensure the possibility of maintenance, all systems have gate valves. A check valve is included after the circulation pump for the SC to prevent reversed circulation at night with consequent heat loss from the SC. A volume expansion tank is also provided to protect the system against volume variations caused by temperature changes near the SC. The water tank is always heated up indirectly through coils. The distribution from the hot water tank remains the same for the five different system solutions. A controller monitors the temperature of the school's heating system and adjusts the cold water input through valves 3 and 4 to keep the provided DHW temperature at 65 °C and the space heating temperature at 35 °C. The hot water tank and HP is inside the school, but for illustration purposes they are placed outside in the following figures.

3.4.1 System 1

The first system configuration is illustrated in figure 8. The SC is used indirectly to heat the water tank and recharge the ground trough a coil and a plate heat exchanger. The circulation pump before the SC will start when the temperature in the SC is 10°C or higher, below this temperature, the SC will not be able to provide significant temperature rise in the water tank or HX [4]. The pump will shut off when the temperature rises above 100°C to avoid boiling of the fluid. If the temperature in the SC is more than 5 °C greater than the water tank temperature, Controller 1 will direct the working fluid through valve V_1 to the water tank. If this isn't the case, the controller will send the working fluid to the HC, which will heat the brine from the HP. If the SC produces a high enough temperature, the fluid will be divided, heating the water tank and recharge the boreholes simultaneously. Since the recharge takes place in a HX, the temperature down to the boreholes is kept from becoming too high [4]. When the SC is unable to heat the water tank to 70 °C alone, the HP will start, and begin extracting heat from the GHX. If neither the GSHP nor the SC can maintain the set temperature in the tank, an electrical heater will be activated. Which scenario the SC should work is determined by a controller which examines and compares the temperature at specified places and based on this adjust the flow through valve V_1 . Heating of the DHW will be prioritized.

The water tank is split into three sections. The SC heats the low-temperature water at the bottom, where the cold water from the school returns. In the middle, the HP connected to the GHX heats the tank further and the space heating is extracted. The electrical heater is placed on the top section as an auxiliary unit, which will turn on when the water temperature falls below the set point. The domestic hot water will also be distributed to the building from the top section. This sectioning is beneficial for the SC's efficiency, which is better at low temperatures, as well as ensuring that it doesn't compete with the electric energy and increases the lifetime of the HP and the electrical heater.

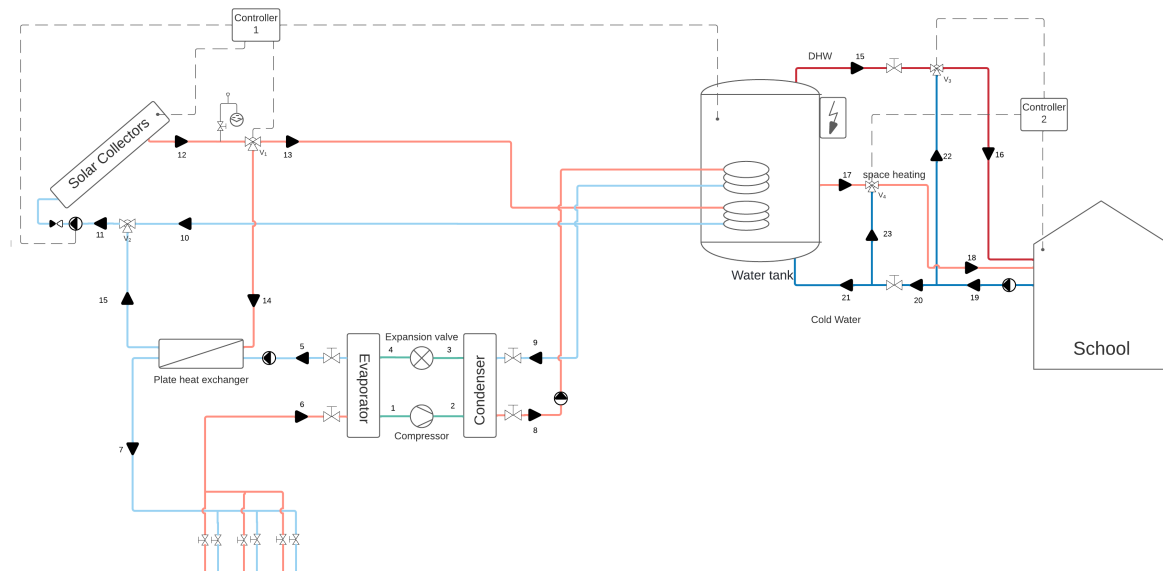


Figure 8: System configuration 1 - Indirect use of SC to heat water tank and recharge the GHX.

3.4.2 System 2

The second configuration is quite similar to the first, except that if the temperature in the SC is too low, the working fluid will not recharge the borehole, but instead raise the temperature before the evaporator directly. The brine into the evaporator should not extend 25°C , so the controller 1 must ensure this. The circulation pump before the SC will start when the temperatures in the collector is above 3°C . Because there is just one HX in this system, it suffers less heat loss, so the SC will be more efficient to use at lower temperature, and hence more efficient than the first system presented. As for the first system, the solar working fluid will be directed to the water tank when its temperature is 5K greater or more than the water and the circulation pump will shut off when the temperature reaches 100°C . The SC and GHX must use the same working fluid in this solution. The section of the water tank is the same as in system 1.

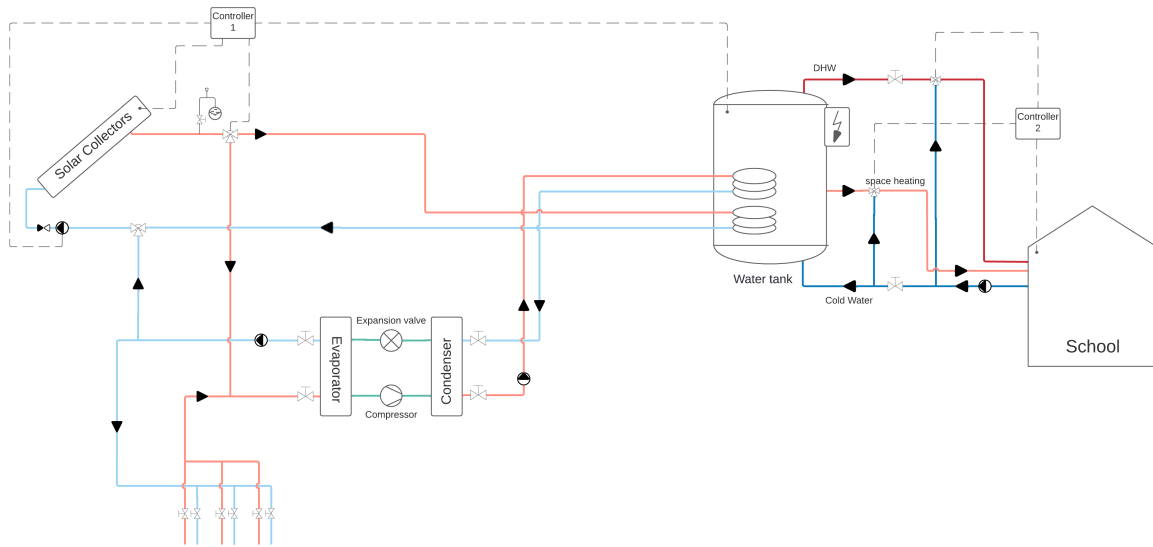


Figure 9: System configuration 2 - Direct heating of brine before evaporator and recharge the GHX.

3.4.3 System 3

The third system solution is more simple than the other two. The SC is exclusively used to recharge the boreholes through a HX if the temperature in the SC is higher than 3°C . The water tank is only heated up by the GSHP and with the help of the electrical heater if necessary. In this configuration, it is important to know what the maximum temperature down to the boreholes can be when the SC produce high temperatures, and ensure that the pipes in the boreholes withstand this temperature. Otherwise, the temperature from the SC should be monitored and control the circulation pump to avoid such high temperatures.

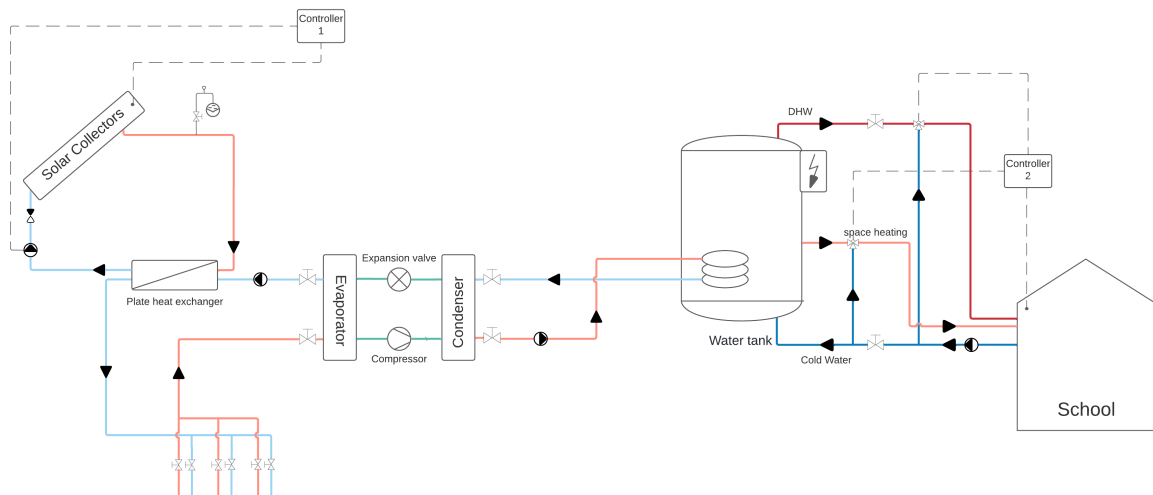


Figure 10: System configuration 3 - Indirect use of SC to recharge the GHX.

3.4.4 System 4

The GHX and the SC are directly coupled in the fourth system solution. The extracted heat from the GHX is pumped through the SC. If the environmental conditions allow it, the brine absorbs the heat of the sun and raises its temperature; otherwise, it only passes from the collector and flows toward the evaporator of the HP, causing the HP to start working and raise the water temperature in the water tank. As for system 2, the controller must shut off the SC when the temperatures get too high and can rise the brine above 25 °C. If the HP is unable to provide sufficient heat, the electrical boiler located on top of the water tank will be activated. Similar to system two, the GHX and SC must use the same working fluid.

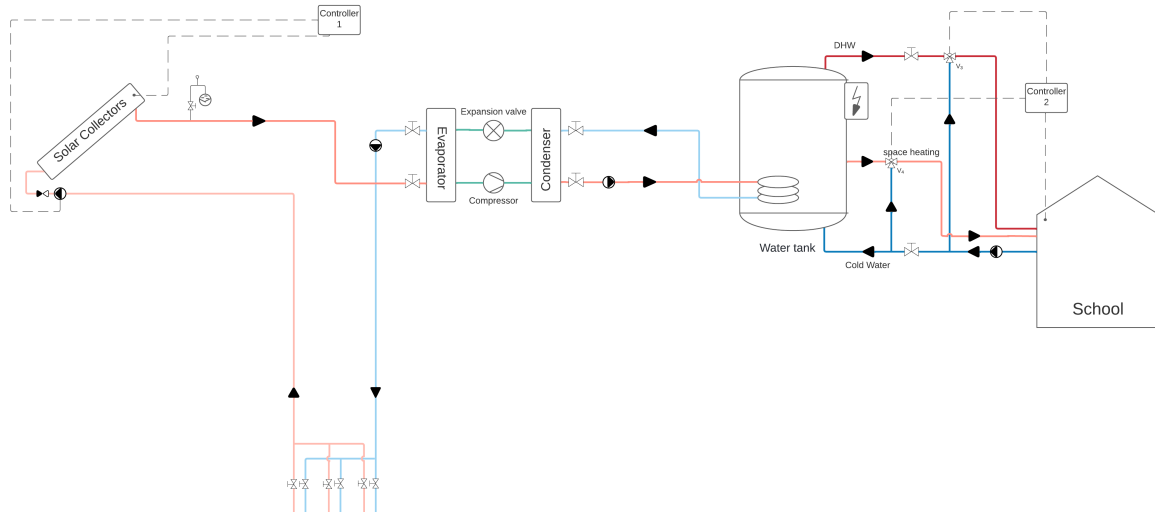


Figure 11: System configuration 4 - Brine from the GHX pumped through SC.

3.4.5 System 5

The final system solution is the most complex one and contains more applications. The SC is used to heat a thermal water storage tank continuously if the temperature is above 10°C . Controller 1 will send the thermal water straight to the DHW if the water in the storage tank is warm enough, otherwise it will heat the water tank indirectly. The boreholes will be recharged by excess heat or if the temperature in the storage tank is very low. When the SC is exposed to severe temperatures, the thermal storage tank will also function as a safety mechanism to avoid overheating in the SC. When the temperature in the SC rises above 100°C , the circulation pump in the solar system will stop.

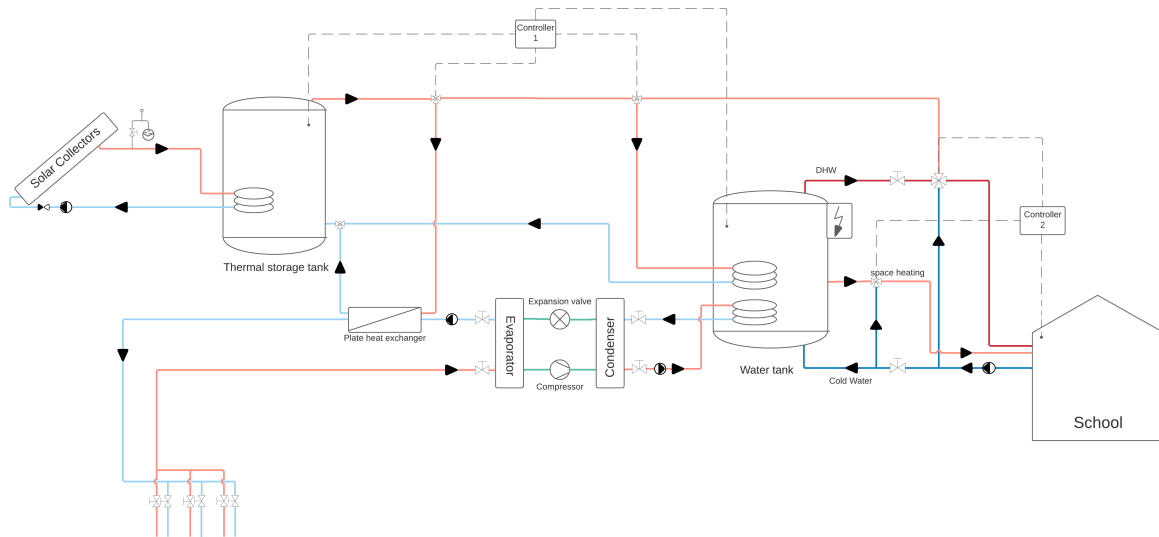


Figure 12: System configuration 5 - SC connected to thermal storage tank used to heat the water tank, DHW directly and recharging GHX.

4 Method

4.1 Reference building

The SGSHP is dimensioned and analyzed based on an imaginary building located in Oslo, Norway. Table 2 shows the central data of this building which is modified values based on Gjennestad High School. Pictures of this school are provided in appendix C.

Table 2: Building details

Building type	School
Width	10 m
Length	45 m
Floor height	3 m
Number of floors	2
Useful area, A_{UA}	900 m^2

This building is figured to be used for educational purposes, and will therefore be categorized as a school. It will also be classified as a passive house and should therefore satisfy Criteria for passive houses and low energy buildings - Non-residential buildings [39].

The climate in Oslo is cold and temperate. The mean temperature is 6.3 °C and the DUT during the winter is -19.8°C [40]. According to NSEPK 2021 [41], the set point for heating a school building is 21°C. As a result, ΔT in the energy calculations will be $21 - (-19.8) = 40.8$ °C.

The energy and effect demand of the building is 23 670 $kWh/year$ and 26 626 W , respectively. See the calculations in tables 3 and 4.

Table 3: Energy demand of the building.

Energy post	Energy demand [$kWh/m^2 * year$]	Total energy demand [$kWh/year$]	Comment
Space heating and ventilation	$EP_{H,0} + X * \frac{(1000 - A_{UA})}{100}$ $20 + 1.3 * \frac{(1000 - 900)}{100} = 21.3$	$21.3 * 900 = 19170$	[39]
Hot water	5	$5 * 900 = 4500$	[41]
Total	26	23 670	

Table 4: Effect demand of the building.

Effect post	Effect demand [W]	Comment
Space heating	$H''_{tr,inf} * BRA * \Delta T$ $0.413 * 900 * 40.8 = 15165$	[39]
	$H''_{tr,inf} = H''_{tr,inf,0} + W \frac{(1000 - A_{UA})}{100}$ $0.4 + 0.013 * \frac{1000 - 900}{100} = 0.413 W/m^2 K$	
Ventilation	$0.33 * \dot{V} * (1 - \eta_{heatrecovery}) * \Delta T$ $0.33 * 3940 * (1 - 0.8) * 40.8 = 10610$ $\dot{V} = \frac{t_{on} * \dot{V}_{on} + t_{red} * \dot{V}_{red}}{t_{on} + t_{red}}$ $\frac{214 * 9000 + 506 * 1800}{214 + 506} = 3940 m^3/h$	Presume rotary heat recovery and CAV ventilation [41]
DHW	$\frac{22.7 * 900}{24} = 851$	Tabel A.2 [41]

4.2 System solution

The chosen system solution for the SGSHP in this thesis is system 1, described in chapter 3.4.1. System 1 is able to achieve good exploitation of the SC since it can run on different scenarios based on measured temperatures in the system, unlike systems 2 and 4. Through the literature review, it was proven that implementing recharging of the GHX was a critical step to include in systems located in cold climates to avoid depletion of the soil over time, which system 3 does not do. Another benefit of recharging is the reduced chance of overheating [4]. The last system presented, system 5, is considered too complex for the modest school building and will not be analyzed due to time limitations in this study.

4.3 Solar collector dimensioning

The SC will prioritize heating the water tank to the desired temperature. If the SC produces excessive heat or too low a temperature for the water tank, the mass flow rate from the SC will be directed to the HX and recharge the ground. As a result of this prioritization, the SC will be sized based on the school's DHW demand. The SC is dimensioned to cover 60% of the DHW demand, 510.6 W/year, based on statement from Enova [42]. The performance analysis of the SC will be based on properties of the De Dietrich entry lever solar collector CH 250 which can be delivered by SGP ARMATEC AS in Norway, the data sheet is presented in appendix D [43]. The working fluid inside the solar system is an Ethylene Glycol-water mixture with a concentration of 35%, a frost proof solution to avoid freezing when the temperature is low.

4.4 Ground heat exchanger dimensioning

The GHX is made of single U-tube collectors, high-density polyethylene pipes with thermal conductivity of 0.35 W/mK, connected in parallel [44]. The depth of the boreholes is selected to be 130 meters with an internal diameter of 0.11 meters. The brine inside the pipes will be the same as the working fluid in the solar system and water will be used as the grout inside the boreholes.

4.5 Heat pump dimensioning

According to Zijdemands [45], a HP should be sized for 50-60% of the maximum building heating rate demand and 80-95% of the energy load. This will lower the overall electricity use because the use of the auxiliary unit will be reduced, as well as optimize the COP due to reducing the number of on-off times for the operation of a HP. The HP in this study will therefore be dimensioned for 55% of the heating rate demand and 90% of the energy demand. The dimension of the HP is calculated in table 5. Since this

school is a passive house and only uses DHW for toilets and sinks, the energy demand for space heating and DHW is relatively low. The HP is therefore also able to cover the preheating of the DHW which will account for 50% of the total effect for the heating of the DHW [46]. This helps optimize the system and reduce the need for delivered energy.

Table 5: Heat pump dimensions.

*The energy demand for ventilation is included in the space heating.

Effect post	Energy demand [kWh/year]	Effect demand [W]
Space heating	$19170 * 0.9 = 17253$	$15165 * 0.55 = 8341$
Ventilation	-*	$10610 * 0,55 = 5836$
DHW	$(4500 - (4500 * 0.6)) * 0.34 = 612$	$851 * 0.5 = 426$
Total	21 303	14 603

The heat pump is dimensioned for 15 kW. This gives $21303/15=1420$ hours of operation with maximum power for the HP.

The calculations for the condenser and evaporator in the HP are based on values collected from the data sheets from Danfoss, these are presented in appendix F and G. Both applicants will be micro plate heat exchangers.

4.6 Engineering Equation Solver

EES is an equation-solving program that can efficiently solve thousands of coupled non-linear algebraic and differential equations [47]. F-Chart Software developed the program, and version 10.832 is employed in the mathematical models developed in this thesis. The many built-in mathematical and thermophysical property functions with great accuracy that EES provides distinguishes it from other equation-solving tools. EES was therefore used to acquire most of the thermodynamic parameters in this work.

The mathematical models were created using equations acquired during the literature review and additional research. To simplify the script's complexity and make it easier to discover faults along the way, the system was broken down into three logical boundary conditions:

- Solar collector
- Ground heat exchanger
- Heat pump

After the models were completed, parametric tables were used to change some of the predetermined and calculated parameters to see how they affected the system's performance.

4.6.1 Assumptions

Several prerequisites were established in order to reduce the mathematical model's overall complexity. The preconditions were determined using information gathered throughout the literature review on what it is usual to presume in these thermodynamic systems. As a result, the prerequisites listed below will have no significant impact on the obtained results.

- The system operates under steady state conditions and steady flow.
- The changes in kinetic and potential energy are negligible.
- The pressure drop is negligible in the entire system.
- The pressure conditions for the systems are assumed values.

- The temperature drop in the pipes is negligible.
- The system is adiabatic; heat loss to the environment for each component in the system is negligible.
- The pinch temperature in the evaporator and condenser is 5 K.
- The evaporator and condenser are heat exchangers with counterflow.
- The thermal properties of the soil are constant.
- The water in the boreholes is considered stagnant.
- The circulation pumps in the solar and heat pump system are considered negligible.

4.6.2 Solar collector model

The first thermodynamic system implemented in EES was the flat plate solar collector system, see appendix I for the EES model. Due to the system design, the SC will heat the water tank and recharge the ground. Because of the priority, the SC's performance will be determined by its ability to provide heat to the water tank. See the boundary condition of the solar collector model in figure 13. According to the Norwegian Institute of Public Health, the temperature in the tank should be over 60 °C to eliminate the risk of legionella [48]. To achieve the set point in the water tank, the input and outflow temperatures of the SC will be set to 40 and 70 °C, respectively, based on possible temperatures in Norway [4]. The weather in Oslo changes greatly throughout the year, and some months are too cold for the SC to generate heat. The operation period will therefore be from Mars to September, based on recent temperature data from yr.no and the photovoltaic geographical information tool from the European commission [49][50]. The optimal slope and azimuth angle of the SC in Oslo based on the sun irradiation was also found from the European commission tool. Characteristics of the SC are provided in table 6.

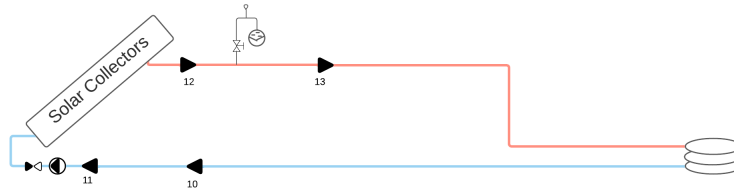


Figure 13: Boundary condition for the solar system implemented in EES.

Table 6: Input data in the solar system.

Parameter	Value
Working fluid	35% Ethylene glycol
Operation pressure, P	250 000 Pa
Heat removal factor, F_R	0.8
Heat loss coefficient, U_L	7 W/m ² K
Absorbance of the cover, α	80%
Transmittance of the cover, τ	80%
Area, A	2.51 m ²
Net aperture area, A_{sc}	2.35 m ²
Optical efficiency, η_0	76.5%
First order heat loss coefficient, a_1	3.653 W/m ² K
Second order heat loss coefficient, a_2	0.012 W/m ² K ²
Pipe diameter, $D_{pipe,SC}$	0.022 m
Ambient air temperature, T_a	293 K
Solar irradiance, G	700 W/m ²
Surface temperature of the sun, T_{sun}	4 333 K
Mass flow rate, \dot{m}_{SC}	0.02 kg/s
Surface tilt angle, β_{SC}	35°
Latitude of the location, ϕ	60°

MASS BALANCE

Due to the previously-mentioned prerequisites of steady state conditions and steady flow, the mass balance in the solar system can be expressed as follows.

$$\dot{m}_{11} = \dot{m}_{12} = \dot{m}_{solar,f} \quad (29)$$

The total mass flow rate in the solar collector system is then determined by the number of collectors.

$$\dot{m}_{solar,f} = \dot{m}_{SC} N_{SC} \quad (30)$$

THERMAL EFFICIENCY

The thermal efficiency of the SC can be determined by equation 4 where the mean temperature is calculated by the following equation.

$$T_m = \frac{T_{11} + T_{12}}{2} \quad (31)$$

TOTAL AREA OF THE SOLAR COLLECTORS

The calculation of the total aperture area needed for the SC was based on equation 3, where the total energy collected is set to 510.6 W. Further, the number of collectors needed can be determined by the ratio of the total SC area and the area of one SC.

$$N_{SC} = \frac{A_{aa}}{A_{SC}} \quad (32)$$

ENERGY FROM SC TO WATER TANK

The SC heats the water tank indirectly using a coil. The energy balance based on the 1. Law of thermodynamics regarding heat transfer is used to calculate the amount of energy transferred to the water tank.

$$\dot{Q}_{wt} = \dot{m}_{coil}(h_{13} - h_{10}) \quad (33)$$

Where \dot{m}_{coil} has the same value as $\dot{m}_{solar,f}$.

EXERGY OF THE SOLAR COLLECTORS

For the exergy analysis of the SC system, the general exergy balance from equation 12 is employed. The stored energy is $\Sigma \dot{X}_s = 0$ since the system is under steady-state conditions. According to García-Menéndez et al., exergy into a solar thermal system is separated into two parts: the working fluid at the inlet and the solar radiation [51]. The following formulae are used to compute them when the pressure drop in the solar system is set to zero.

$$\dot{X}_{i,f} = \dot{m}_{solar,f} c_{p,solar} (T_{11} - T_a - T_a \ln \frac{T_{11}}{T_a}) \quad (34)$$

$$\dot{X}_{i,sr} = \dot{Q}_i \left(1 - \frac{4}{3} \frac{T_a}{T_{sun}} + \frac{1}{3} \left(\frac{T_a}{T_{sun}} \right)^4 \right) \quad (35)$$

The exergy out of the system is only from the working fluid at the outlet of the SC.

$$\dot{X}_{o,f} = \dot{m}_{solar,f} c_{p,solar} (T_{12} - T_a - T_a \ln \frac{T_{12}}{T_a}) \quad (36)$$

The second law efficiency is calculated using the next equation, which is also based on the general exergy balance.

$$\eta_{II,sun} = \frac{\dot{X}_{o,f} - \dot{X}_{i,f}}{\dot{X}_{i,sr}} \quad (37)$$

4.6.3 Ground heat exchanger model

The mathematical model of the GHX is described in this section, where the HX between the solar system and the ground system is included. The data sheet for the chosen HX is presented in appendix E, and the EES model in appendix J. The boundary condition for the GHX model is illustrated in figure 14 and the related input data are listed in table 7.

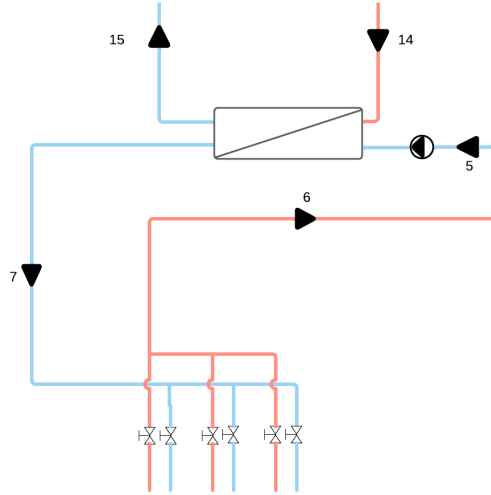


Figure 14: Boundary condition for the ground heat exchanger implemented in EES.

Table 7: Input data in the GHX model.

Parameter	Value
Working fluid	35% Ethylene-Glycol
Grout material	Water
Length of the boreholes, $L_{pipe,GHX}$	130 m
Number of tubes in one boreholes, N_{tube}	2
Borehole diameter, D_b	0.11 m
Pipe outer diameter, $D_{pipe,o}$	0.04 m
Dead state temperature, T_0	279.3 K
Grout temperature, T_g	282.3 K
Temperature out of the HP, T_5	275 K
Mass flow rate, \dot{m}_{GHX}	0.5 kg/s
Boreholes pressure, $P_{borehole}$	200 000 Pa
HX inner diameter, $D_{pipe,HX}$	0.01576 m
Thermal conductivity of the HX pipe, $\lambda_{HX,wall}$	386 W/mK
Plate thickness of the HX, d_{plate}	0.00198 m

MASS BALANCE

As for the SC, the mass balance of the GHX is determined through the following equation.

$$\dot{m}_5 = \dot{m}_6 = \dot{m}_7 = \dot{m}_{brine} \quad (38)$$

The total mass flow rate of the brine depends on the number of boreholes.

$$\dot{m}_{brine} = \dot{m}_{GHX} N_{borehole} \quad (39)$$

TEMPERATURE OUT OF THE GHX

The hot fluid in the evaporator is the brine out of the GHX, T_6 . The temperature of the brine at this point is determined with the following equation [38].

$$T_6 = T_s - (T_s - T_7) \exp\left(\frac{-1}{\dot{m}_{brine} C_{p,brine} \frac{R_{tot}}{L_{pipe,GHX}}}\right) \quad (40)$$

The temperature in the ground was set to be 283.3 K in table 7, based on the length of the boreholes, dead state temperature and assumptions made by Madessa et al [52].

The conductive resistance of the grout, the conductive resistance of the pipe wall, and the convective resistance of the brine inside the pipe make up the borehole thermal resistance, R_{tot} [53]. These are calculated by the following equations.

$$R_{tot} = R_{grout} + R_{pipe} + R_{brine} \quad (41)$$

Since the water is considered stagnant, the effect of the convection is ignored and thermal resistance of the grout can be calculated as follows.

$$R_{grout} = \frac{\ln \frac{D_b}{D_{ed,o}}}{2\pi k_g} \quad (42)$$

$$R_{pipe} = \frac{\ln \frac{D_{ed,o}}{D_{ed,i}}}{2\pi k_p} \quad (43)$$

$$R_{brine} = \frac{1}{\pi D_{ed,i} h_{GHX}} \quad (44)$$

The equivalent diameter composed by O'Neal and Gu is used in the computation of R_{brine} due to the unsymmetrical boundary condition the U-tube creates [54]. For the sake of simplicity, it is assumed that the two pipes in the single U-tube are in touch.

$$D_{ed} = \sqrt{2}D \quad (45)$$

To calculate the heat transfer coefficient, h , for fluids, equation 22 and Nusselt number correlations from recent studies were utilized. For the brine in the GHX, the Nusselt number for single-phase non-laminar flow in tubes conducted by Sándhez-Escalona et al. was chosen [55]. Sándhez-Escalona et al. used Gnielinski's and Taler's correlations as benchmarks and was found to coincide with other well-known correlations in the technical literature, such as Camaraza-Medina et al. and Skupinski et al.

$$Nu_{wf} = \frac{z_1(f/8)(Re_{wf} - z_2)Pr_{wf}}{1 - z_3\sqrt{f/8}(Pr_{wf}^{2/3} - 1)} \quad (46)$$

The Prantl number was first computed in EES and was found to be between 3 - 1000, and the constants z_1 , z_2 and z_3 are therefore 0.8761, 147.3 and 10.3 respectively.

The model of Filonenko was used for the calculation of the friction factor.

$$f = (1.82 \log Re_{brine} - 1.64)^{-2} \quad (47)$$

The Reynolds number is calculated with equation 24 and the average velocity of a fluid inside a circular tube is calculated as follows.

$$v_{avg} = \frac{\dot{m}}{\frac{\rho}{4} \pi D_i^2} \quad (48)$$

EXTRACTED HEAT

Equation 20 and 49 were used to calculate the total heat extracted from one borehole, where the temperature difference in the equation consists of the temperature of the soil and the brine.

$$\dot{Q}_{ghx} = \dot{q}_{ghx} L_{pipe,ghx} \quad (49)$$

The energy demand of the HP's evaporator must be met by the GHX. Assuming that the pipe heat loss between the borehole and evaporator is negligible, the heat extracted from the borehole field is equal to the heat transfer to the working fluid in the evaporator.

$$\dot{Q}_{ground} = \dot{Q}_{evap} \quad (50)$$

The value of the heat extracted in the evaporator is collected from the HP model and will vary for the four different refrigerants. When this value is known, the number of boreholes needed to meet this demand can be calculated.

$$\dot{Q}_{ground} = \dot{Q}_{ghx} N_{boreholes} \quad (51)$$

CIRCULATION PUMP

The work done by the circulation pump in the GHX is determined by the pressure difference between the evaporator and the borehole, together with the volumetric flow rate of the brine.

$$W_{pump} = \Delta P v \quad (52)$$

Since the density of the brine is assumed constant for the process, the volumetric flow rate can be defined by the following equation.

$$v = \frac{\dot{m}_{brine}}{\rho_{GHX}} \quad (53)$$

EXERGY

The exergy and second law efficiency formula utilized for the working fluid in the SC were also employed in the exergy analysis of the GHX [51].

$$\dot{X}_{i,ghx} = \dot{m}_{brine} c_{p,ghx} (T_7 - T_s - T_s \ln \frac{T_7}{T_s}) \quad (54)$$

$$\dot{X}_{o,ghx} = \dot{m}_{brine} c_{p,ghx} (T_6 - T_s - T_s \ln \frac{T_6}{T_s}) \quad (55)$$

$$\eta_{II,ghx} = \frac{\dot{X}_{o,ghx}}{\dot{X}_{i,ghx}} \quad (56)$$

Lastly, the exergy destruction for the borehole field was determined.

$$\dot{X}_{des,ghx} = \dot{m}_{brine} (\psi_7 - \psi_6) + \dot{Q}_{ground} (1 - \frac{T_0}{T_g}) \quad (57)$$

Equation 17 is implemented to calculate the flow specific heat differens. Entropy of brines is not available in EES, so an approximation of the entropy change for pure substances will be applied [35].

$$\Delta s = c_p \ln(\frac{T_i}{T_o}) \quad (58)$$

RECHARGING OF THE GROUND

The ability of the SC to recharge the ground was evaluated based on the energy balance in the HX. From the following equation, the temperature of the brine after the HX can be calculated.

$$\dot{Q}_{HX} = \dot{m}_{HX} c_{p,hx} (T_{14} - T_{15}) = \dot{m}_{brine} c_{p,brine} (T_7 - T_6) \quad (59)$$

HEAT EXCHANGER AREA

The calculation of the area of the HX distributing heat from the SC to the ground is determined by the LMTD method shown in equation 7. The logarithmic mean temperature difference is an approximation expressed as equation 60, where ΔT_1 and ΔT_2 for a counter flow is specified where the specific temperatures for this HX is shown in equation 61 and 62.

$$\Delta T_{lm} = \frac{\Delta T_1 - \Delta T_2}{\ln \frac{\Delta T_1}{\Delta T_2}} \quad (60)$$

$$\Delta T_1 = (T_{hot,in} - T_{cold,out}) = T_{14} - T_7 \quad (61)$$

$$\Delta T_2 = (T_{hot,out} - T_{cold,in}) = T_{15} - T_5 \quad (62)$$

The overall heat transfer, U_{HX} , in the heat exchanger is given by equation 63.

$$U_{HX} = \frac{1}{\frac{1}{h_{sun}} + R_{f,sun} + \frac{d_{wall}}{\lambda_{wall}} + R_{f,brine} + \frac{1}{h_{brine}}} \quad (63)$$

The brine in the HX and the fluid inside the SC loop are both 35% ethylene-glycol, the same Nusselt number employed for the GHX was therefor employed for the solar working fluid. Since the brine is under different conditions by the HX than down in the borehole, a new heat transfer coefficient for the brine will be calculated as well. The Prantl number for the solar working fluid and the brine by the heat exchanger are also between 3 - 1000, and the same constants presented earlier are used.

EXERGY OF THE HEAT EXCHANGER

The exergy balance of the HX also follows equation 12 and is formulated as follows under steady state conditions.

$$\dot{X}_{14} + \dot{X}_5 = \dot{X}_{15} + \dot{X}_7 + \dot{X}_{dot,HX} \quad (64)$$

The exergy at the different locations is calculated by the next equation.

$$\dot{X}_k = (h_k - h_0) - T_0(s_k - s_0) \quad (65)$$

K denotes the state of the fluid. The entropy for pure substances will also be applied for every state in the equation over.

For the second law efficiency of the HX, the general equation by Wu et al. for a HX operation below the surrounding temperature with zero pressure drop was implemented [56].

$$\eta_{II,HX} = \frac{T_0 \ln \frac{T_{14}}{T_{15}} - (T_{14} - T_{15})}{T_0 \ln \frac{T_{14}}{T_7} - (T_{14} - T_7)} \quad (66)$$

4.6.4 Heat pump model

The thermodynamic model of the HP were divided into four different models in EES due to the different refrigerants employed in the analysis. All the known or presumed parameters were first identified and organized based on the states in table 8. The temperature of the water at the inlet and outlet of the condenser were set to 30 and 50°C. Then the mathematical model was developed in order to calculate the COP, the area of the condenser and evaporator and exergy, see appendix K for the EES models. Figure 15 illustrates the boundary condition of the HP.

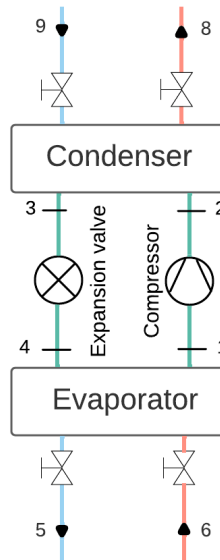


Figure 15: Boundary condition for the heat pump implemented in EES

Table 8: Identified parameters of the HP based on the state and prerequisites.

1	2	3	4
Superheated		Subcooled	Saturated
$T_1 = T_{sat, evp} + 5K$		$T_3 = T_{sat, cond} - 5K$ $T_{sat, cond} = T_8 + \Delta T_{pinch}$	$T_4 = T_5 - \Delta T_{pinch}$ $T_4 = T_{sat, evp}$
$P_1 = P_4$	$P_2 = P_3$	$P_2 = P_3$	$P_4 = P_{sat}$
$s_1 = s_{2s}$	$s_{2s} = s_1$		
		$h_3 = h_4$	$h_4 = h_3$

MASS BALANCE

As for the SC and GHX, the mass balance in the HP can be expressed as follows:

$$\dot{m}_{refg} = \dot{m}_1 = \dot{m}_2 = \dot{m}_3 = \dot{m}_4 \quad (67)$$

ISENTROPIC EFFICIENCY

The isentropic efficiency of the compressor is calculated by using Pierre's correlations shown in equation 68 and 69.

$$\frac{\eta_{vol}}{\eta_{iso}} = \left(1 + k_e \frac{(T_1 - 273) - 18}{100}\right) \exp\left(a \frac{T_{m, cond}}{T_{m, evap}} + b\right) \quad (68)$$

$$\eta_{vol} = \left(1 + k_s \frac{(T_1 - 273) - 18}{100}\right) \exp\left(k_z \frac{P_{sat, cond}}{P_{sat, evap}}\right) \quad (69)$$

The constants in the two equations differ for ammonia and the other refrigerant [57][58]. The values are listed in table 9.

Table 9: Pierre's constants for the different refrigerants [57][58].

	R717	R600a, R290, R1234ze(E)
k_1	1.02	1.04
k_2	-0.063	-0.07
k_s	0	0.15
k_e	0	-0.1
a	-1.69	-2.4
b	1.97	2.88

COP

The COP of the HP is calculated with equation 5 and evaluated against the COP_{carnot} . The useful heat obtained by the condenser, \dot{Q}_{cond} , is 15 W since this is the selected HP size. When this value is known, the mass flow rate of the refrigerant can be calculated.

$$\dot{m}_{refg} = \frac{\dot{Q}_{cond}}{h_{2a} - h_3} \quad (70)$$

The work done on the compressor is calculated by equation 71.

$$\dot{W}_{comp} = \dot{m}_{refg}(h_{2a} - h_1) \quad (71)$$

The correlation between the isentropic efficiency for the compressor and the enthalpy before the condenser in a Carnot cycle shown in equation 72 will determine h_{2a} .

$$\eta_{iso} = \frac{h_{2s} - h_1}{h_{sa} - h_1} \quad (72)$$

AREA OF THE CONDENSER AND EVAPORATOR

Since the condenser and evaporator are heat exchangers, equation 7 is employed to calculate their area as well. Equation 60 for the logarithmic mean temperature difference is also implemented here, where the temperature differences in the condenser and evaporator are as follows.

$$\Delta T_{1,cond} = (T_2 - T_8) \quad (73)$$

$$\Delta T_{2,cond} = (T_3 - T_9) \quad (74)$$

$$\Delta T_{1,evap} = (T_6 - T_1) \quad (75)$$

$$\Delta T_{2,evap} = (T_5 - T_4) \quad (76)$$

The useful heat obtained by the evaporator is given by the following energy balance.

$$\dot{Q}_{evap} = \dot{m}_{brine} c_p (T_6 - T_5) = \dot{m}_{refg} (h_1 - h_4) \quad (77)$$

The overall heat transfer coefficient for the condenser and evaporator is defined by equation 78 and 79.

$$U_{cond} = \frac{1}{\frac{1}{h_{refg}} + R_{f,refg} + \frac{d_{wall}}{\lambda_{wall}} + R_{f,water} + \frac{1}{h_{water}}} \quad (78)$$

$$U_{evap} = \frac{1}{\frac{1}{h_{refg}} + R_{f,refg} + \frac{d_{wall}}{\lambda_{wall}} + R_{f,brine} + \frac{1}{h_{brine}}} \quad (79)$$

As for the recharging of the boreholes, different Nusselt correlations were used to calculate the heat transfer coefficients of the refrigerants. The general correlation for condensation in mini/microchannels by Kim and Mudawar is used for both propane and isobutane [59]. This correlation is validated with wide-ranging data from many sources, and Morrow et al. recently recommended this correlation for the chosen refrigerants [60].

$$Nu = 0.04Re_k^{0.69}Pr_{refg}^{0.34}\frac{\phi_g}{X_{tt}} \quad (80)$$

For the condenser, the superficial liquid Reynolds number is used for the equation above, Re_f , and for the evaporator, the superficial vapor Reynolds number is used, Re_g . X_{tt} is the conventional turbulent-turbulent Lockhart-Martinelli parameter and ϕ_g is the two-phase multiplier for gas.

$$X_{tt} = \left(\frac{\mu_f}{\mu_g}\right)^{0.1} \left(\frac{1-x}{x}\right)^{0.9} \left(\frac{\rho_g}{\rho_f}\right)^{0.1} \quad (81)$$

$$\phi_g = 1 + CX + X^2 \quad (82)$$

The refrigerants are assumed to go from 100% vapor to 100% liquid in the condenser, the quality, x , is therefore set to 0.5.

Equation 82 employs the Lockhart-Martinelli parameter's general definition, X , which is based on frictional pressure gradients depending on the actual flow rates for the two phases. This definition is expressed in equation 95-103 in appendix H.1.

Shah's correlation from 2019 was used for solstice and ammonia, which has proven to achieve acceptable accuracy [61]. Firstly, the dimensionless vapor velocity, J_g , and the correlation parameter, Z , were employed to determine which of the three conducted regimes should be applied to calculate the heat transfer coefficient. These calculations are shown in appendix H.2, equation 104-107. Since equation 107 is correct, regime I is employed.

$$h_{refg} = h_I \quad (83)$$

Because the HP uses microchannels, correlation 2 was employed to determine h_I .

$$h_I = h_{LT} \left(1 + 1.128x^{0.817} \left(\frac{\rho_f}{\rho_g}\right)^{0.3635} \left(\frac{\mu_f}{\mu_g}\right)^{0.2363} \left(1 - \frac{\mu_g}{\mu_f}\right)^{2.144} Pr_f^{-0.1}\right) \quad (84)$$

The heat transfer coefficient with total mass flowing as liquid, h_{LT} , is calculated by the following equation.

$$h_{LT} = 0.023Re_{fo}^{0.8}Pr_f^{0.4}\frac{k_l}{D_{HP}} \quad (85)$$

For the water in the condenser, the Nusselt correlation for single-phase water conducted by Zhang et al. was employed [62].

$$Nu = 0.4225Re^{0.733}Pr^{1/3}\left(\frac{\mu}{\mu_{wall}}\right)^{0.14} \quad (86)$$

EXERGY

In the exergy analysis of the system, the second law efficiency was employed.

$$\eta_{IIcomp} = 1 - \frac{\dot{X}_{des,comp}}{\dot{W}_{comp}} \quad (87)$$

$$\eta_{IIcond} = 1 - \frac{\dot{X}_{des,cond}}{\dot{m}_{refg}(\psi_2 - \psi_3)} \quad (88)$$

$$\eta_{IIexp} = 1 - \frac{\dot{X}_{des,exp}}{\dot{m}_{refg}(\psi_3 - \psi_4)} \quad (89)$$

$$\eta_{IIevap} = 1 - \frac{\dot{X}_{des,evap}}{\dot{m}_{refg}(\psi_4 - \psi_1)} \quad (90)$$

The exergy flow difference due to mass transfer, when the kinetic and potential energy is neglected, is calculated by equation 17. Since h_3 is equal to h_4 , the exergy efficiency of the expansions valve will be zero.

The exergy destruction, \dot{X}_{des} , is based on equation 13-16 and calculated by the following equations for the different components of the HP.

$$\dot{X}_{des,comp} = T_0 \dot{m}_{refg}(s_2 - s_1) \quad (91)$$

$$\dot{X}_{des,cond} = T_0 \dot{m}_{refg}(s_3 - s_2) + \frac{\dot{Q}_{cond}}{T_{m,water}} \quad (92)$$

$$\dot{X}_{des,exp} = T_0 \dot{m}_{refg}(s_2 - s_1) \quad (93)$$

$$\dot{X}_{des,evap} = T_0 \dot{m}_{refg}(s_1 - s_4) - \frac{\dot{Q}_{evap}}{T_{m,brine}} \quad (94)$$

Since the HP is placed inside the school building, the dead state temperature, T_0 , is set to 21°C.

4.7 IDA ICE

For the next part of the performance analysis of the SGSHP, IDA ICE has been used. IDA ICE is a detailed and dynamic simulation tool developed by EQUA Simulation AB, and the expert version has been implemented in this thesis [63]. Parametric runs can be used to be able to evaluate how the variations of different values affect the performance of the energy system.

4.7.1 Energy plant

The ESBO plant (early stage building optimization) was used in order to build the energy system in IDA ICE. The first step was to add SC, HP and GHX. Based on these components, a standard energy system will be created after one press "build plant model". The borehole extension was implemented. Then the next step was to make some changes to the system, so it is comparable to system solution 1. A macro must be made in order for the plant to run on different scenarios in the same simulation. Due to time limitations, two separate energy systems were made instead in order to investigate how the different scenarios affect the performance of the SGSHP. For the first plant, the SC is only connected to the water tank, while the SC is only connected to the GHX through a heat exchanger in the second system. The two systems are presented in figure 16 and 17.

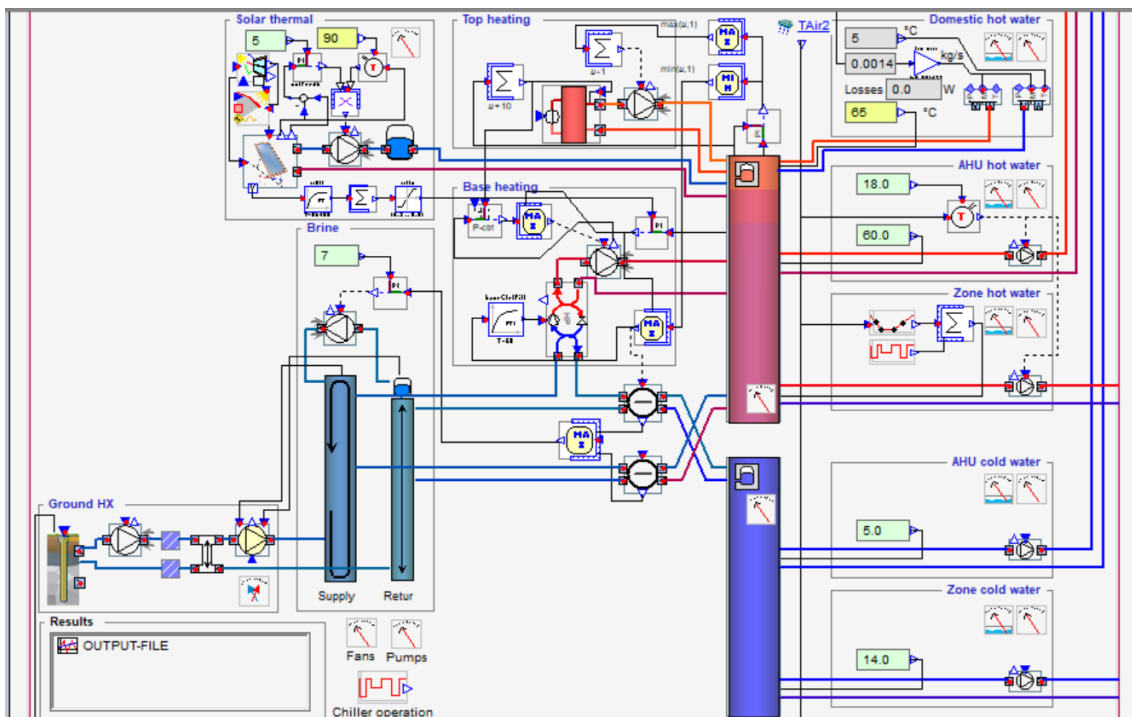


Figure 16: Energy system in IDA ICE where the SC is connected to the water tank.

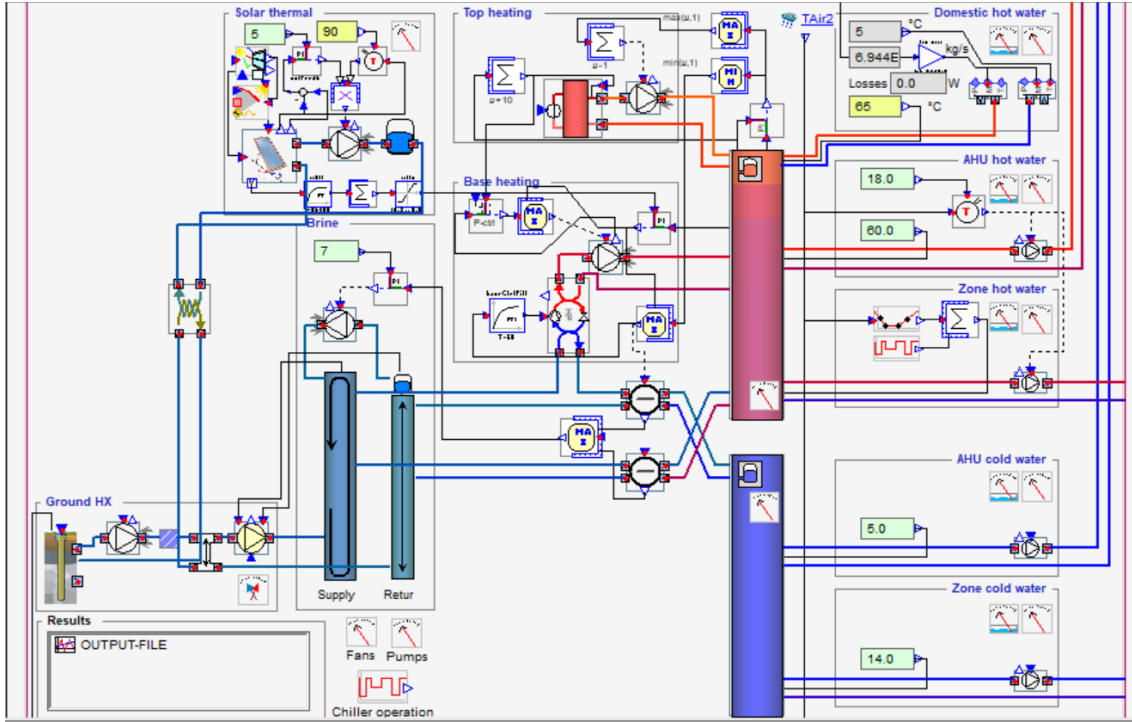


Figure 17: Energy system in IDA ICE where the SC is connected to the GHX.

To neglect zone cooling and the air handling unit (AHU), the unused EMeters and the efficiency of the HX in the AHU were set to 0. The previously determined input data for the mathematical models together with results gathered from EES was implemented in IDA ICE. A solar collector area of 5.02 m^2 , which is equivalent to two CH 250 collectors and four boreholes with 140 meters were implemented. The building connected to the plant was constructed based on table 2. For the climate profile, Oslo-Gardemoen was chosen. Some of the remaining parameters have not been defined before, and are presented in table 10, where a share of these values was found using EES. It is assumed Gneiss in the ground. For the rest of the input values not presented, the default value was utilized.

Table 10: Input values for the plants in IDA ICE.

Parameter	Value	Source
R_{PIPE}	0.016 m	EES
$THICK_{PIPE}$	0.004 m	EES
T_{MEAN}	10.3 °C	[52]
ρ_{GRD}	2880 kg/m^3	[64]
c_{PPIPE}	2000 J/kgK	[65]
ϵ_{PIPE}	$1.52 \cdot 10^{-6} \text{ m}$	[66]
c_{PGROUT}	4196 J/kgK	EES
λ_{GROUT}	0.5575 W/mK	EES

It is important to know that the conditions in IDA ICE differ from some of the assumptions implemented in the thermodynamic analysis and that some values must be fixed under the simulations. These will affect the results and are listed below:

- Freecooling is taken into account for the GHX
- The mass flow rate of the working fluid in the solar system in the second plant can not be changed and is fixed at $2.5e^{-8} \text{ kg}/\text{s}$

- Pressure loss in the system is included
- First order heat loss coefficient for the SC, $a_1 = 19.2\text{W}/\text{m}^2\text{K}$
- Second order heat loss coefficient for the SC, $a_2 = 0.0235\text{W}/\text{m}^2\text{K}^2$
- The COP of the HP is fixed to 4

5 Results and discussion

5.1 Validation of the mathematical models

The developed thermodynamics models were verified against other models to check the level of their accuracy. Using input data from the published articles, the findings were compared and evaluated.

5.1.1 Solar collector model

For the solar system, the thermal efficiency was validated against Guarracino et al. [67]. The input values for this validation are presented in table 11.

Table 11: Input values from the study of Guarracino et al. [67].

Parameter	Value
η_0	42 %
a_1	4.96 W/m^2K^2
a_2	0.003 W/m^2K^2
T_{11}	299.6 K
T_{12}	304.0 K
T_a	299.5 K
G	1053.0 W/m^2

The results from this study and Guarracino et al., together with the deviation, are shown in table 12.

Table 12: Results of the validation of the SC model [67].

Parameter	This study	Guarracino et al.	Deviation
η_{th}	41 %	42 %	2.4%

The low deviation shows that this study is accurate in calculating the thermal efficiency of the SC. The obtained result of the thermal efficiency for this study gave 56%, which corresponds to the information given by DieTrich for their flat plate solar collectors, emphasizing the accuracy of this calculation [43].

5.1.2 Ground heat exchanger model

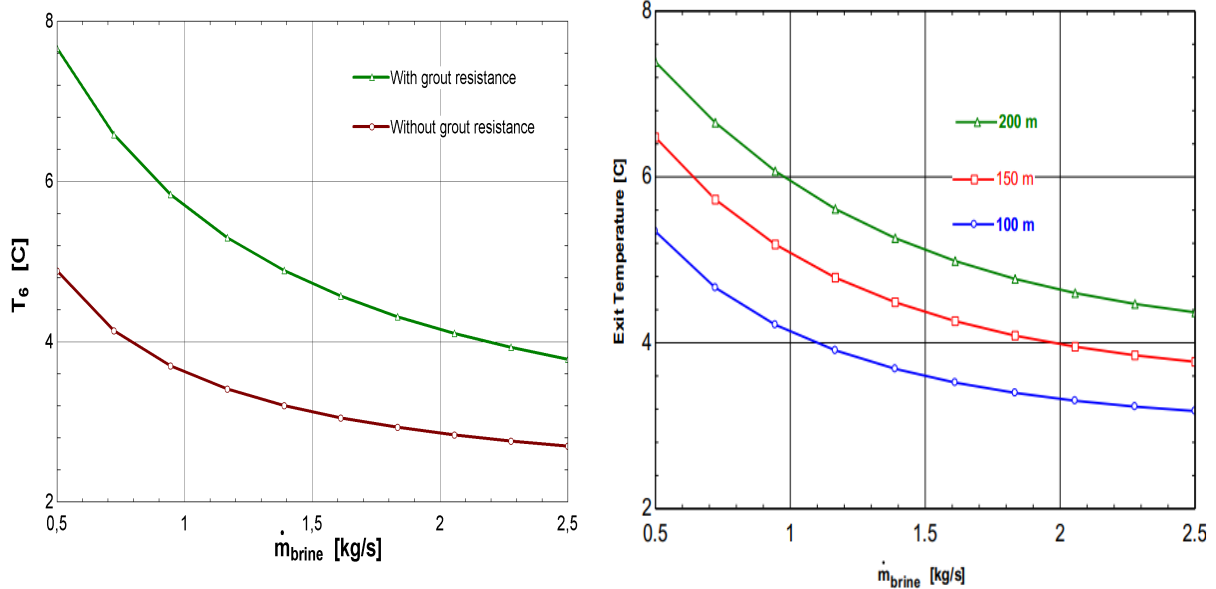
To evaluate the GHX model, the relation between the temperature of the brine into the evaporator and the mass flow rate are compared with the study from Madessa et al [52]. The difference in input data collected from this study is shown in table 13 .

Table 13: The different input parameters from the study of Madessa et al.[52].

Parameter	Value
Brine	35% ethyl-ethanol
L_{pipe}	200 m
$D_{pipe,o}$	0.04 m
$D_{pipe,i}$	0.032 m
T_s	ca. 11.3 $^{\circ}C$

This study includes the convective resistance of the grout in the calculation of the total borehole resistance, which Madessa et al. disregard. This poses a great impact on the outlet temperature of the ground heat

exchanger. The outlet temperature is therefore computed with and without the grout resistance to be able to compare the results. The computed graphs of the outlet temperature variation with the mass flow rate of the brine are shown in figure 18, where only 200 meter deep boreholes are considered for this study.



(a) This study; the brown line is with the thermal resistance of the grout and the green is without.

(b) Madessa et al [52]

Figure 18: The variation of the outlet temperature of the ground heat exchanger due to the mass flow rate of the brine.

As can be seen from the graphs, this study's temperature is lower than Madessa et al., and decreases more rapidly with the increase of the mass flow rate. This is a consequence of the use of equivalent diameter in this thesis. The exact soil temperature is not mentioned in Madessa et al's study and an assumption made from their statement was taken, and can therefore also contribute to differences. In table 14, the deviation is presented.

Table 14: Results of the validation of the GHX model [52].

Mass flow rate [kg/s]	Outlet temperature This study [°C]	Outlet temperature Madessa et al. [°C]	Deviation [%]
0.5	7.6	7.4	2.7
1	5.6	5.9	5.4
1.5	4.7	5.3	12.8
2	4.1	4.8	17.1
2.5	3.8	4.4	15.8

The total heat flux from the borehole calculated in this study is found to be 21.19 [W/m]. This value is consistent with the findings of Norges geologisk undersøkelse, which found that the thermal conductivity of the earth in Oslo is roughly 3 W/mK [68]. When this is multiplied by the difference between the soil temperature and T_6 , a heat flux of 18.6 [W/m] is obtained. This emphasizes how integrating the grout's conductive resistance leads in a more realistic result.

5.1.3 Heat pump model

The validation of the HP models is split into two parts. The study by Esen et al. was used in the first phase to validate the isentropic efficiency and COP estimations [69]. In their study, uncertainty analysis was performed on some reported parameters, which were taken into account in this validation. Table 15 displays the various input data.

Table 15: Input values for HP model from Esen et al. [69].

Parameter	Value
Refrigerant	R22
h_1	402 030 J/kg
s_3	1 163.7 J/kgK
T_1	264.21 K
T_2	348.88 K
T_3	312.80 K
T_4	266.10 K
\dot{Q}_{cond}	4 279 W
\dot{Q}_{cfan}	145 W

Because of the significant uncertainty of P_1 and P_2 , h_1 and s_3 were used as input parameters instead. Esen et al. have included \dot{Q}_{cfan} as a work input to calculate the COP, which is not included in this thesis. For this validation, this was implemented in order to compare the COP values. The model for R717 was used to calculate the isentropic efficiency of the compressor.

The obtained results are plotted in table 16. The uncertainties for the numbers from Esen et al. have been calculated in order to more precisely analyze the deviation.

Table 16: Results of the validation of the HP model[69].

Parameter	This study	Esen et al.	Deviation
η_i	68%	70%	2.8%
COP	2.88	2.5-2.77	3.8%

The low deviation shown in the table above, demonstrates that the HP model is able to provide satisfactory results for the isentropic efficiency and COP. The obtained values of the COP in this study are around 4 for all four of the refrigerants, which is consistent with the mentioned theory in chapter 3.1.2.

In the second part of the HP validation, the area of the evaporator was compared to the study from Kjellsvik et al. [70]. They made a mathematical model of the area of the evaporator at Frydenlynd school and compared it to the real evaporator. The input values which differed from the study are presented in table 17.

Table 17: The different input parameters from the study of Kjellsvik et al. [70].

Parameter	Value
T_1	274 K
T_4	268 K
T_6	279 K
Brine	10% ethanol glycol
\dot{m}_{brine}	9 kg/s
\dot{m}_{refg}	1 kg/s
$d_{plate, evap}$	0.005 m
$\lambda_{plate, evap}$	398.7 W/mK

In the real HP inside Frydenlund school uses CO_2 as the working fluid. Since this thesis does include a nusselt correlation for CO_2 , both correlation from Kim and Mudawar and Shah were evaluated. These results were then compared to the real measurement of the evaporator in table 18.

Table 18: Validation of the area of the evaporator [70].

	This study - Kim and Mudawar	This study - Shah	Real measurements	Deviation
A_{evap}	21.4 m ²	19.8 m ²	14.34 m ²	33/28 %

As seen from the table, both mathematical calculations gave a bigger evaporator area. As Kjellsvik et al. explained, this is due to a liquid separator in the real system. This increases the heat transfer rate in the real evaporator, since the fraction of vapor in the refrigerant is lower when entering the evaporator.

5.2 Solar collector model

The results from the thermodynamic analysis of the SC are given and discussed in this section. Appendix M contains the output from the EES model.

5.2.1 Area and placement

When providing 60% of the DHW to the school, the total aperture solar collector area needs to be 3.14 m^2 . This gave 1.3 SC, resulting in the need of in total 2 collectors. These can be put side by side on the rooftop and therefore avoid shading.

How the total area of the SC should increase when the need for thermal energy increases is evaluated in figure 19.

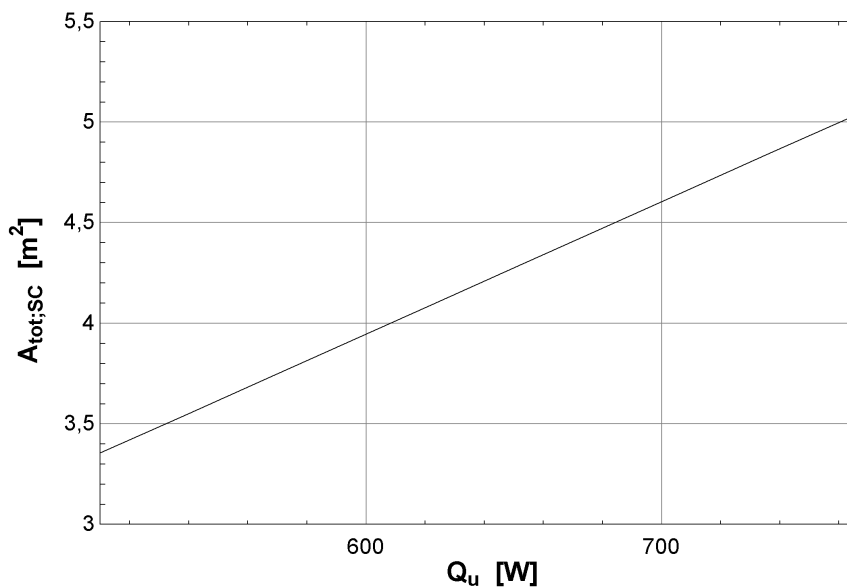


Figure 19: The total area of needed SC when the heat demand increase.

If the total energy produced from the solar system increases from 510 to 750 W, 1/3 of the heat can be used to recharge the ground simultaneously as 60% of the DHW gets covered. To produce this amount of energy, the total SC area need to be 5 m^2 , which is still two SC from DieTrich.

5.2.2 Thermal efficiency

The thermal efficiency of a SC is used to assess its performance. For the chosen type of SC, ambient temperature at 293 K and solar irradiance at $700 \text{ W}/m^2$, the thermal efficiency of the solar collectors is 56%. As can be seen from equation 4, the ambient temperature and solar flux have an impact on the efficiency of the collector. This impact is shown i figure 20.

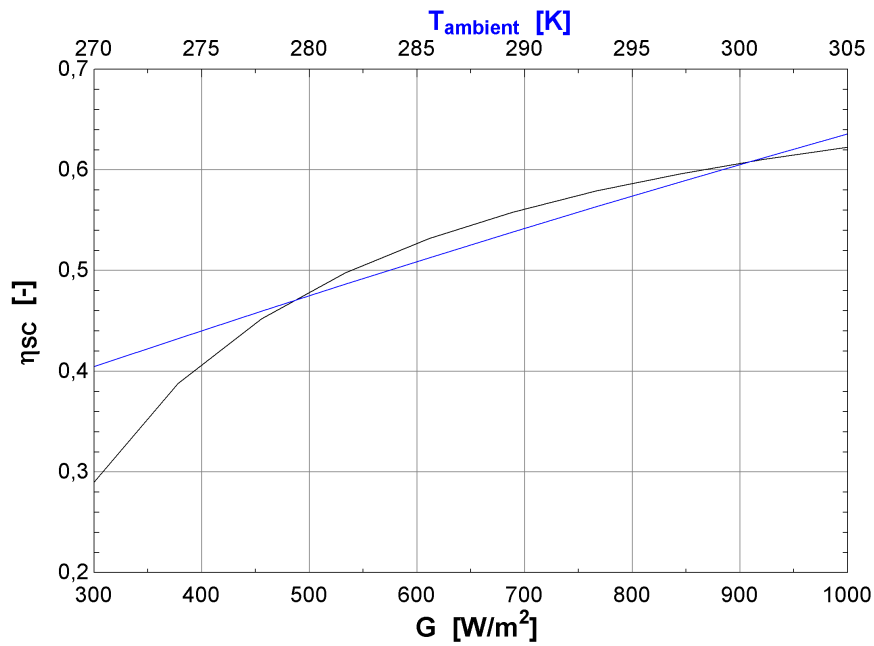


Figure 20: The variation in thermal efficiency with fixed fluid temperatures and varying solar flux and ambient temperature.

The thermal efficiency of the De Dietrich solar collector has a linear increase as the ambient temperature rises, shown in the blue line. An increase of the heat flux also has a positive impact on the thermal efficiency. When the solar flux falls below $500 W/m^2$, the negative influence on the thermal efficiency is higher than for a variation above $500 W/m^2$. This indicates that the SC's performance will be low when it is cloudy, even if the ambient temperature is high. The solar flux has an effect on the ambient temperature, which is not taken into consideration here.

5.2.3 Energy production

The energy production in the solar system is a fixed value at 510.6 W in the model, based on the DHW demand, in order to dimension the SC system. Nonetheless, it's interesting to observe how environmental factors influence the energy generation. As for the efficiency, the solar flux influence the thermal energy produced, which is illustrated in figure 21.

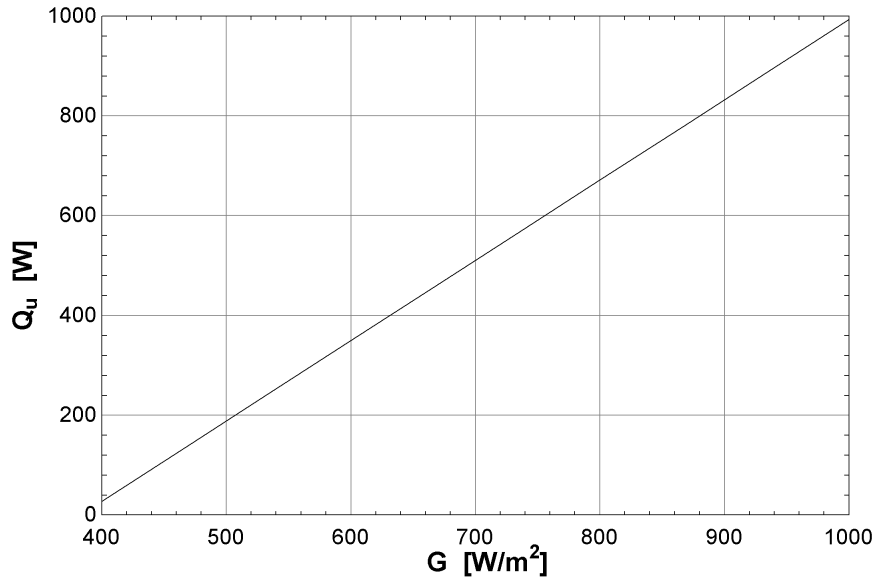


Figure 21: The impact of solar flux on the produced thermal energy from the SC.

The results emphasize the necessity of a clear or light clouded sky for optimal exploitation.

5.2.4 Exergy

The SC's exergy is assessed in the final section. The total exergy rate of the inlet was found to be 1379.0 W, where the working fluid at the inlet stands for 65.3 W and the solar flux stands for 1313.0 W. The exergy rate at the outlet of the SC was calculated to be 383.3 W under the dimensioned conditions. The corresponding exergy destruction and second law efficiency of the solar collector were found to be 982.3 W and 24.2 %. The ambient temperature varies greatly through the day and the year, and figure 22 illustrates how a variation of the ambient temperature affects the second law efficiency.

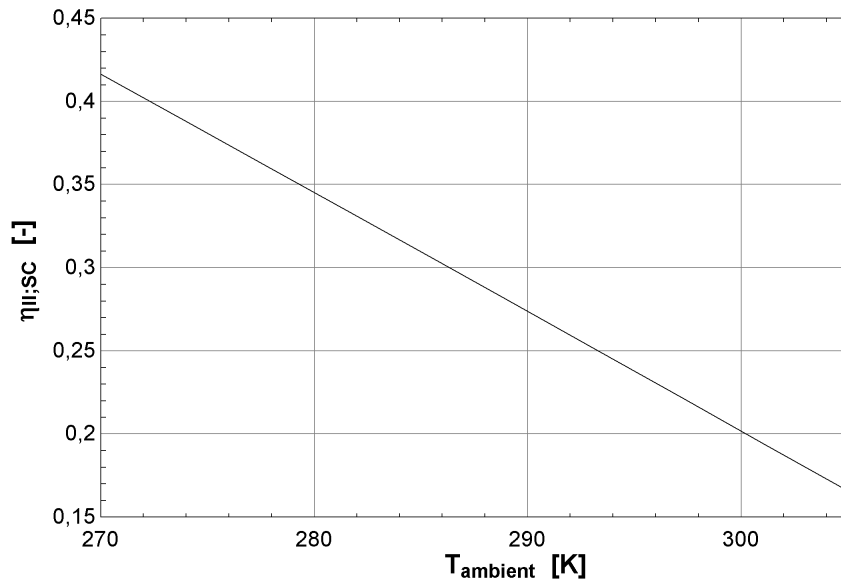


Figure 22: Relation between second law efficiency of the SC and the ambient temperature.

The second law efficiency decreases as the ambient temperature rises. At low temperatures, the exergy from the sun decreases more than the difference between the exergy of the fluid at the outlet and inlet of the SC, leading to higher efficiency.

The type of working fluid in the SC can also affect the exergy in the solar system. In figure 23 the behavior of the second law efficiency of the solar collector with a variation of the inlet temperature with three different working fluid is plotted.

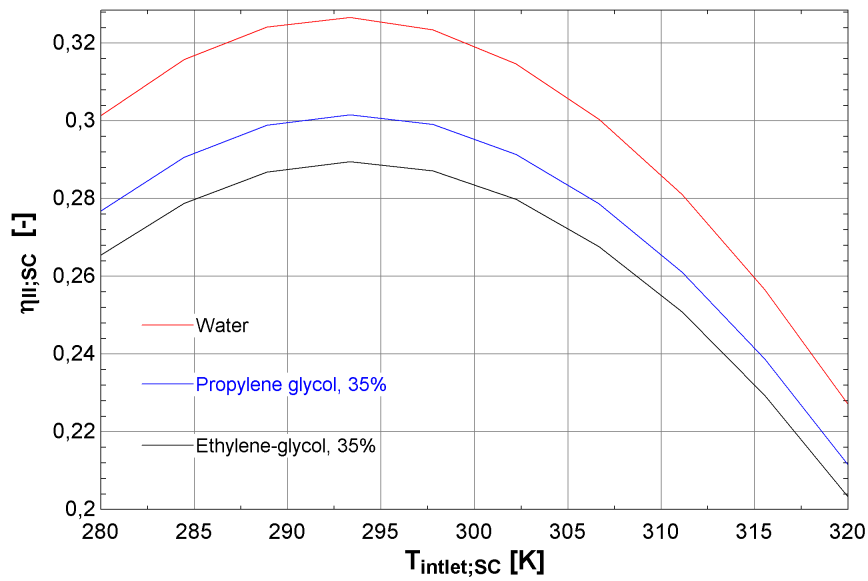


Figure 23: Relation between the second law efficiency and the inlet temperature of the SC with different working fluids.

The variation in the fluid inlet temperature to the SC reveals that the second law efficiency increases until the fluid reaches 293 K and then decreases as it rises further for all three fluids. When the fluid temperature increases up to the ambient temperature, the increase of the exergy efficiency is due to a higher absorber plate and outlet temperature, which increases the energy output. When the inlet temperature increases above the ambient temperature, the heat loss to the surroundings from the SC, making the system less efficient. This underlines the need for good insulation on the SC. In order to obtain a high second order efficient, the optimal inlet temperature in Norway is quite low. Water is the most efficient working fluid for second law efficiency. There is a possibility of the fluid freezing in Norway, hence propylene glycol, a frost-proof fluid, is recommended.

5.3 Ground heat exchanger model

In this section, the result of the thermodynamic analysis of the GHX model will be presented. The results from the EES model are presented in appendix N.

5.3.1 Dimensioning of the borehole field

The SGSHP is sized based on the school's energy need. As a result, in every evaluation of the GHX performance, the \dot{Q}_{ground} will be a fixed value. The needed heat transfer in the evaporator with R290 as the working fluid to produce 15 kW in the condenser was chosen as this value, 11 332 W.

The depth and number of the boreholes are critical to investigate in order to achieve optimal operation of the HP at a low cost. The optimal relation between the length of each borehole and the number of boreholes depends on several parameters, such as the types of grout materials. Figure 24 illustrates the effect of three different grout materials: water, cement and a Bentonite mixture consisting of 0,5%axilat and 15% water [71].

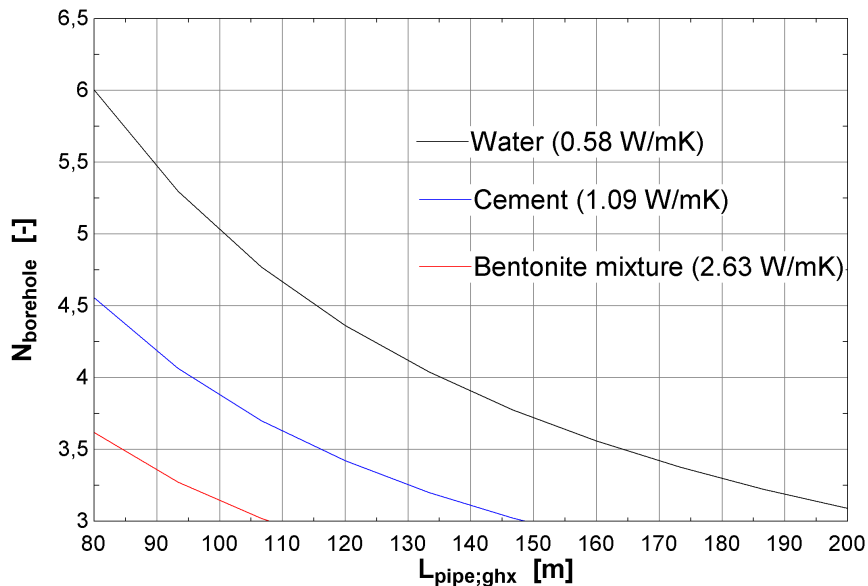


Figure 24: Relation between the length of each borehole and the needed number of boreholes to achieve the energy demand with different types of grout materials.

Since water has the lowest thermal conductivity, the number of boreholes required for this grout material is greater than those required for the other two grout materials. According to this graph, when the grout is water, one optimal relation is four 140-meter-deep boreholes. The bentonite mixture has a thermal conductivity of 2.63 W/mK, and when it replaces the cement the length of a borehole can be reduced up to 40%, which means a reduction in both investment and operation cost of the system. This is a higher reduction than Eslami-Nejad and Bernier reported [16].

The mass flow rate within the borehole was set to 0.5 kg/s. This resulted in a Reynolds number of 4287 inside the borehole when using the chosen pipes. As previously stated in the theory, this Reynolds number is advantageous since it provides a high heat transfer coefficient. How the mass flow rate of the brine in the boreholes influences the relationship between the depth and the number of boreholes is illustrated in figure 25 with three different flow rates, 0.3, 0.5 and 0.8 kg/s respectively.

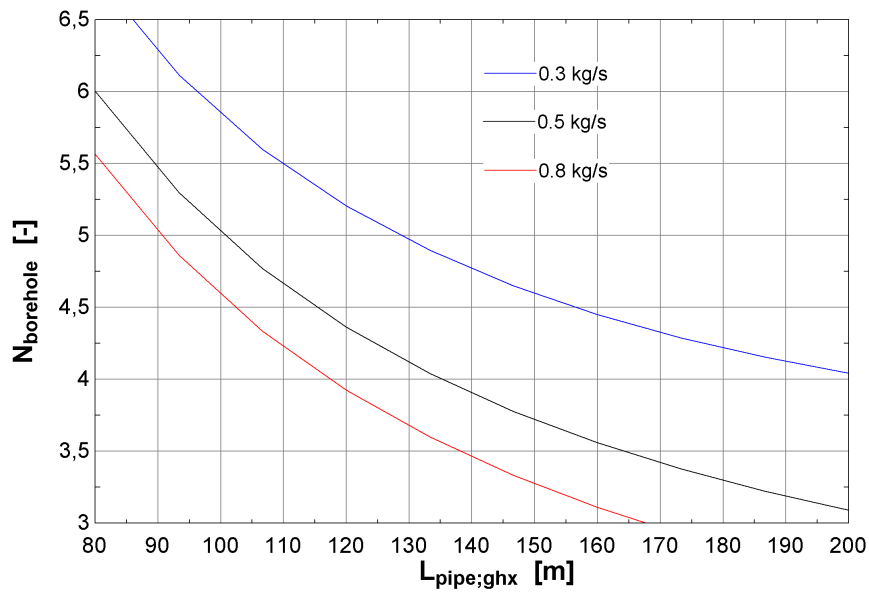


Figure 25: Relation between the length of each borehole and the needed number of boreholes to achieve the energy demand with different mass flow rate of the brine.

The result shows an increase in the mass flow rate reduces either the number of boreholes or the borehole length, which again affects both the investment and operation cost positively.

The needed length of the borehole also depends on the inlet temperature of the brine when the heat demand, the number of boreholes and the outlet temperature of the GHX remains constant. When the SC recharges the ground, the inlet temperature of the GHX can be raised, and figure 26 shows how this kind of temperature rise can affect the required depth of each borehole.

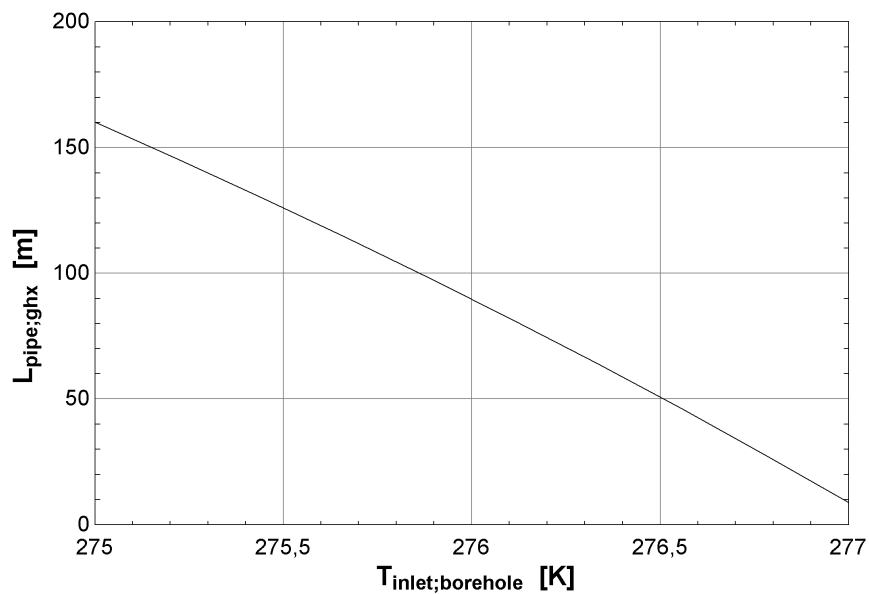


Figure 26: The effect of recharging the ground with SC on the needed length of each borehole.

Without the SC recharging the ground, the temperature down to the GHX will be 275 K, which is the

same as the HP's exit temperature. When this is the case, the boreholes must be 160 meters long, a 19% increase from when a 4.7 m^2 area of SC is fully utilized to transfer heat to the ground. From the equations 30 and 59, it can be seen that with a bigger area of SC and a higher mass flow rate of the solar working fluid, the temperature down to the GHX will increase, lowering the required depth of each borehole even more.

5.3.2 Outlet temperature

Because the borehole outlet temperature has a major impact on the evaporator and therefore the performance of the HP, it is a critical parameter affecting the performance of the GHX. With the approximated soil temperature at 282.3 K, and water as the grout, the outlet temperature of the GHX is equal to 277.5 K when the SC is solely used for recharging the ground. The temperature of the soil varies naturally throughout the year, and the thermal resistance in the borehole can be changed with the grout material. How the two parameters affect the outlet temperature of the GHX is illustrated in figure 27.

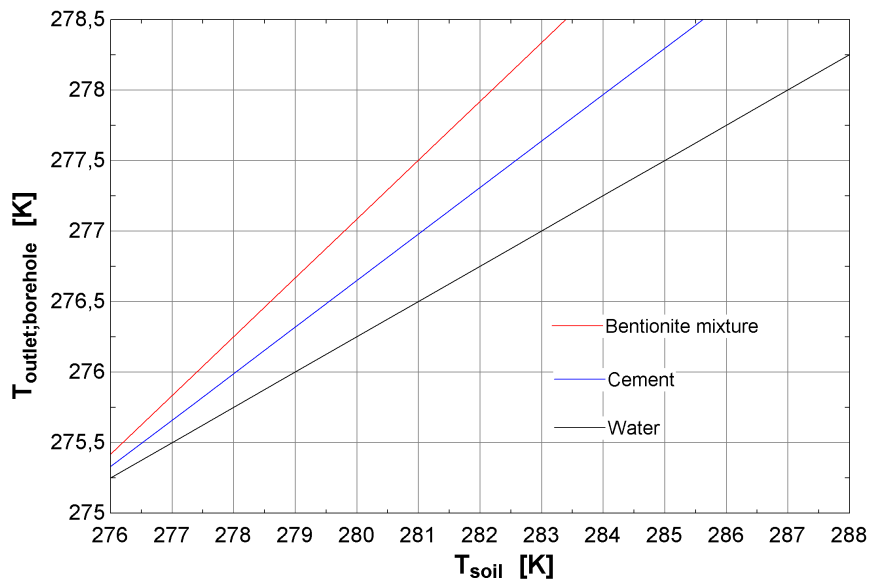


Figure 27: The impact of the soil temperature on the outlet temperature of the borehole with different types of grout materials.

The graph depicts a linear increase in outlet temperature as the soil temperature rises, and the higher conductivity of the grout, the lower the soil temperature is needed to achieve a high outlet temperature.

The temperature of the brine out from the HP also affects the outlet temperature of the brine. This is illustrated in figure 28.

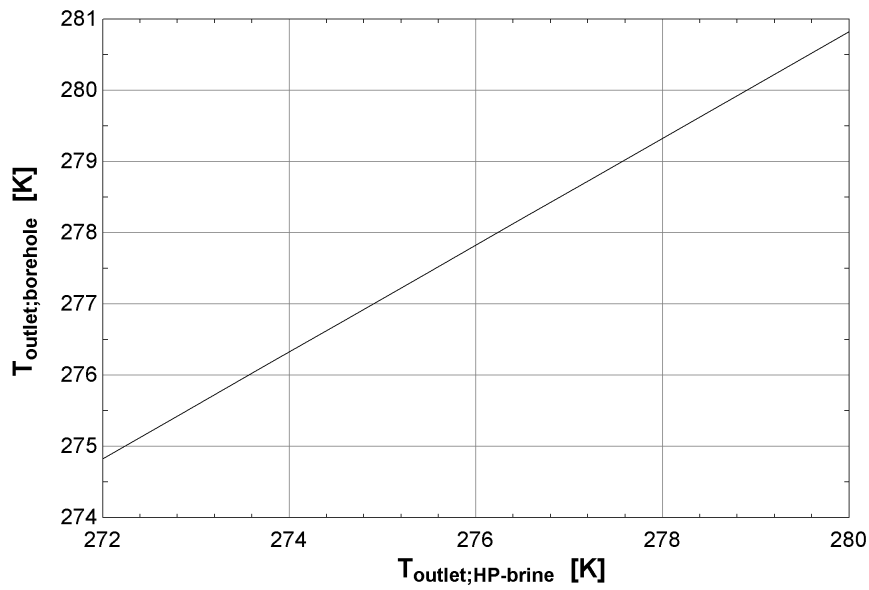


Figure 28: The impact of the temperature of the brine from the HP on the outlet temperature of the GHX.

The higher the temperature from the HP, the higher the outlet temperature of the borehole.

5.3.3 Exergy

The exergy, exergy destruction and the second law efficiency of the borehole field are presented in table 19.

Table 19: The calculated exergy of the GHX.

\dot{X}_i [W]	\dot{X}_o [W]	\dot{X}_{des} [W]	η_{II} [%]
817.9	533.1	294.7	65.2

The rate of exergy destruction in the borehole field is determined by the amount of energy produced, as well as the temperatures at the inlet and outlet. Figure 29 shows how the rate of exergy destruction in the borehole field is affected by the inlet and outlet temperature of brine to/from the borehole.

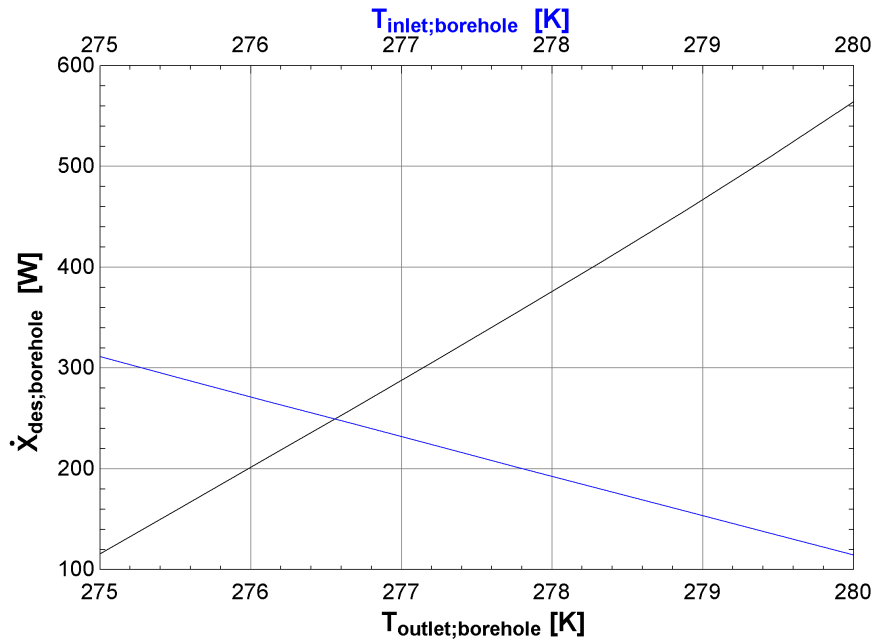


Figure 29: The influence of the inlet and outlet temperature on the exergy destruction of the borehole field.

The blue line in the graph above demonstrates that as the inlet temperature rises, the overall exergy destruction in the GHX reduces, but the black line shows that as the outlet temperature rises, the exergy destruction increases. As a result, the smallest temperature difference between the output and inlet is recommended to accomplish less exergy destruction.

5.3.4 Recharging the ground

The ground is recharged via a counterflow heat exchanger that transfers heat from the solar system and raises the borehole's inlet temperature. The maximum heat exchanger's area was calculated to be 0.14 m^2 using the dimensioned parameters and 100% of the mass flow rate from the SC. The modest size of this area is mostly due to the low mass flow rate of the working fluid in the solar system.

The exergy destruction in the HX was calculated to be, $16\,576 \text{ W}$, which is relatively high due to the high temperature differences on the cold and hot sides. The second law efficiency was 70.5 %.

The temperature out of the SC has an impact on the exchanged heat as well as the HX's exergy destruction. As a result, determining the ideal temperature here is of relevance. The black line in figure 30 illustrates how the SC outlet temperature influences the inlet temperature in the borehole, while the blue line indicates how the SC outlet temperature affects exergy destruction when the hot temperature out of the HX is fixed to 303K.

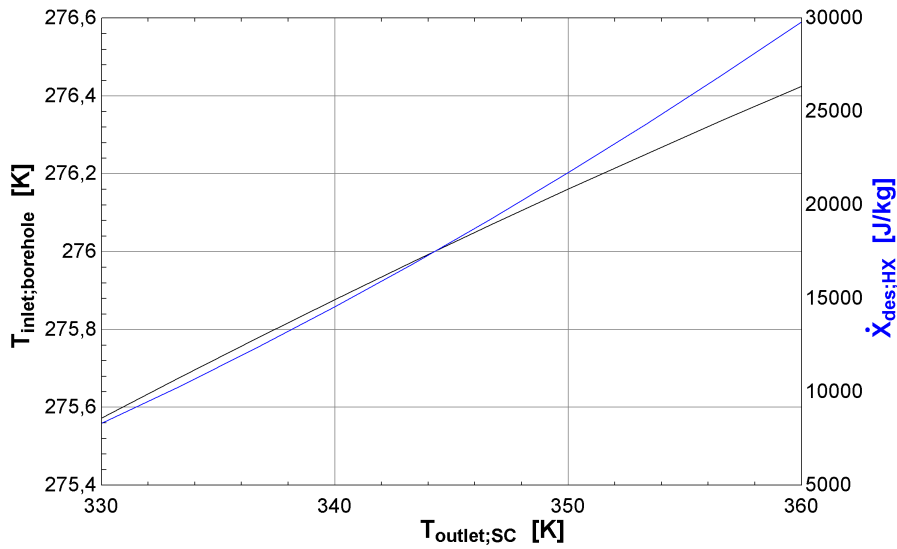


Figure 30: The impact of the hot inlet temperature to the HX on both the cold outlet temperature and the exergy destruction of the HX.

As seen from the figure, a higher temperature from the SC gives a higher inlet temperature of the borehole, which is expected. But, it is important to understand that higher temperature also gives higher exergy destruction of the HX, which is not preferable.

The solar energy produced vary over the year, so the amount of recharging will also vary. When the SC is able to recharge the ground, it helps to decrease long-term ground depletion. How much of the solar system's working fluid is utilized to recharge the ground has an effect on the heat exchanger's available energy transfer and, as a result, on the GHX's outlet temperature.

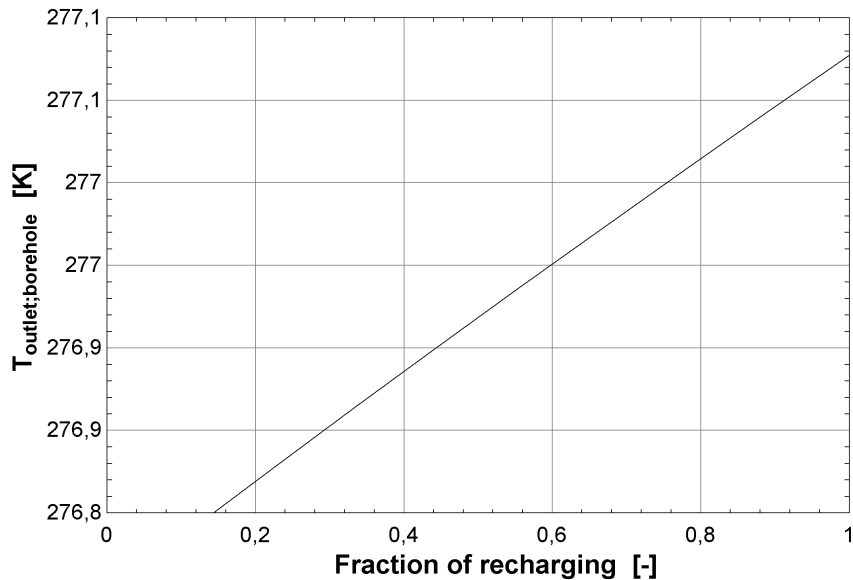


Figure 31: Effect of the energy from the SC on the outlet temperature of the brine from the borehole.

Figure 31 shows that when the HX receives more heat from the SC, the outlet temperature of the borehole increases. Increasing the inlet temperature through the HX can be a good option to reduce the exergy destruction in the borehole and help to get the right temperature into the evaporator. Using

longer boreholes instead of recharging the ground will increase the difference between the inlet and outlet temperature of the GHX, which was proven to increase the exergy destruction. The figure also illustrates that recharging with less than 20% of the mass flow rate of the solar system has little to no influence on the GHX's outlet temperature.

5.4 Heat pump model

For the last thermodynamic analysis, the results from the HP models will be presented. The output of EES models is presented in appendix O.

5.4.1 T-s and P-h diagrams

The changes in the states for the four different refrigerants are plotted in T-s and P-h diagrams. These diagrams will differ from one another due to the varied properties of each refrigerant, even though they are all utilized under the same conditions. The T-s diagrams are presented below in figure 32-35, and the P-h diagrams are presented in attachment L.

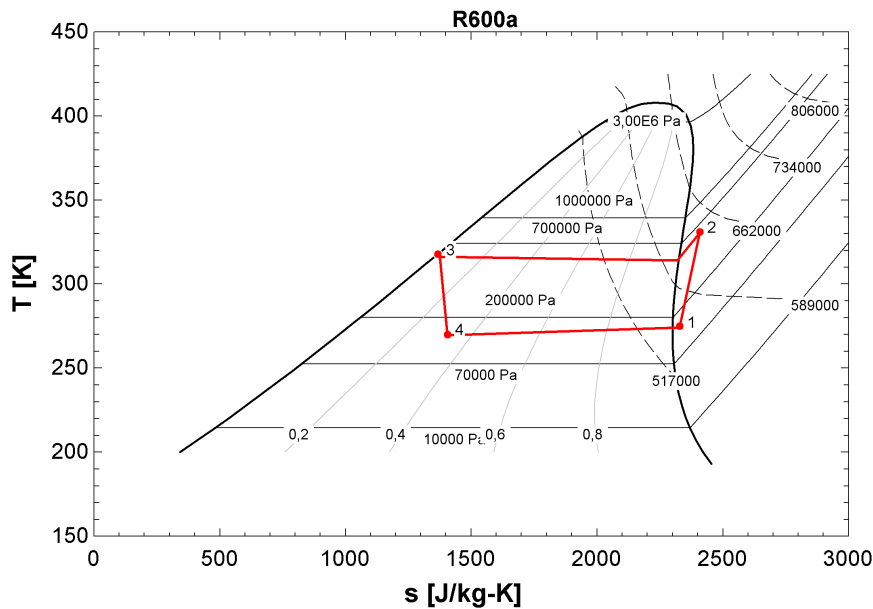


Figure 32: T-s diagram for R600a.

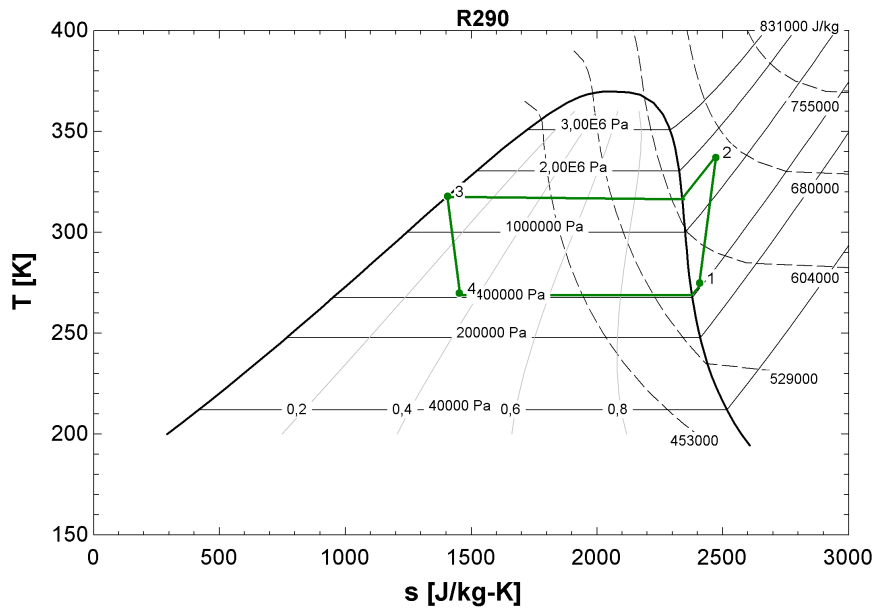


Figure 33: T-s diagram for R290.

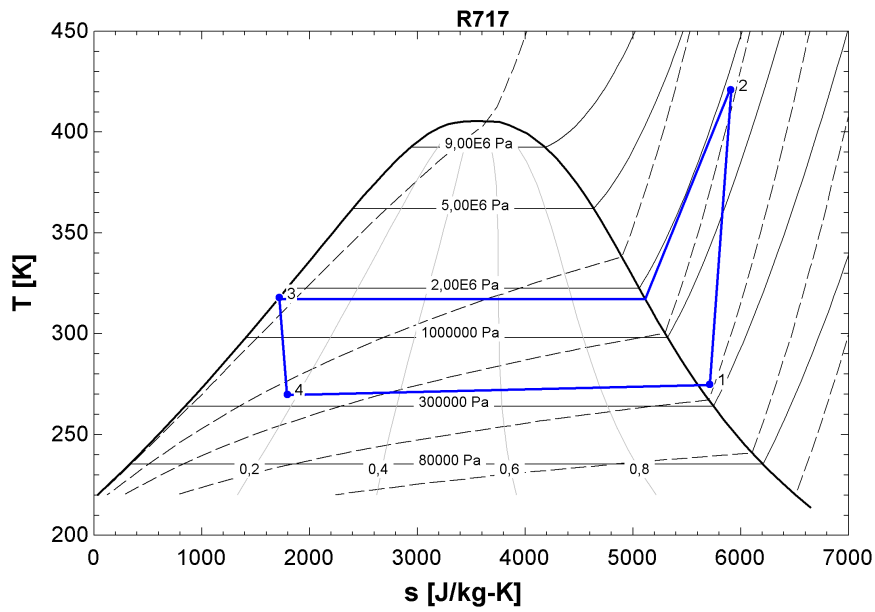


Figure 34: T-s diagram for R717.

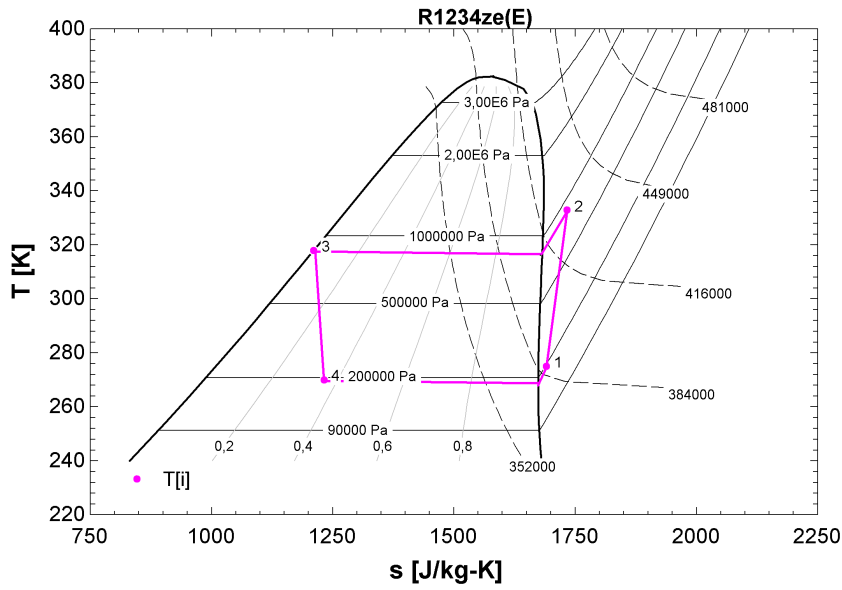


Figure 35: T - s diagram for R1234ze(E).

The graphs reveal that R600a and R290 has the most similar response. This could be due to the fact that these two have similar thermophysical properties. The critical pressure of R717 is higher than the others, hence it has the largest operation area, whereas R1234ze(E) has the smallest. R600a and R290 operation areas in this HP are in the upper part in the presented graphs, indicating a high condensation temperature. Flash steam can occur when this high temperature condensate passes through the expansion valve with low pressure. The flash steam is unable to absorb any energy from the brine during the face shift in the evaporator, resulting in a reduction in the evaporator's efficiency. It is a good idea to subcool the refrigerant at point 3 more than 5K or implement a flash vessel for the R290 and R600a heat pumps to reduce the risk of steam occurring.

5.4.2 Coefficient of performance

In order to investigate the performance of the working fluids, the COP of the HP was calculated for each refrigerant, the result is depicted in table 20.

Table 20: Calculated COP for all the refrigerants.

	R600a	R290	R717	R1234ze(E)
\dot{W}_{comp} [W]	3715	3668	3380	3846
\dot{m}_{refg} [kg/s]	0.045	0.044	0.011	0.09
η_i [%]	68.56	73.06	75.45	67.43
COP_{carnot} [-]	5.43	5.23	5.23	5.30
COP_{HP} [-]	4.04	4.09	4.44	3.90
$\frac{COP}{COP_{carnot}}$ [%]	74.4	78.2	84.9	73.6

With a COP of 4.44, R717 achieves the best performance of the HP. The R1234ze(E) HP's compressor has low isentropic efficiency, resulting in a high required work input at the compressor and a low COP. Due to the assumption of an adiabatic system, and neglecting the pressure drop and electricity loss in the compressor, the presented COPs will be higher than for a real HP suffering energy loss through the cycle.

Figure 36 illustrates how the mass flow rate of the refrigerant affects the COP.

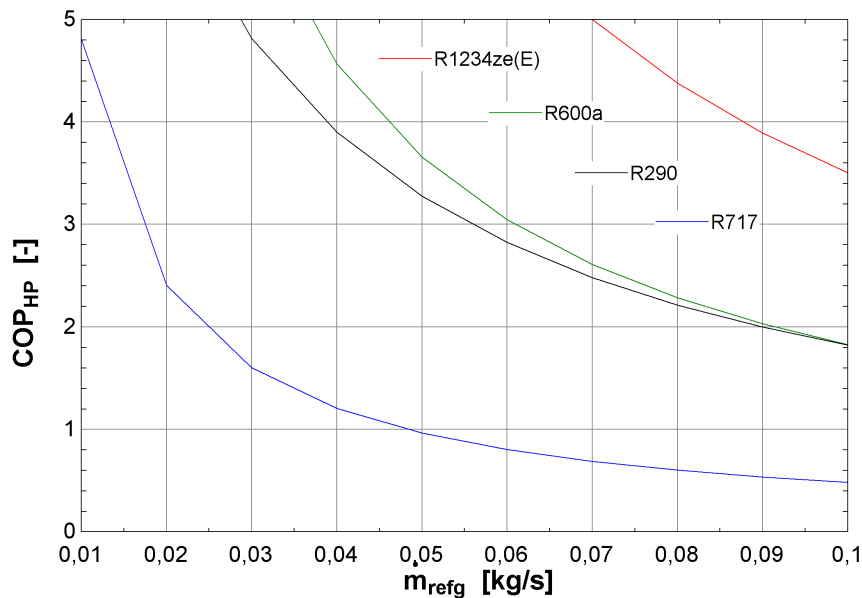


Figure 36: The COP of the HP with the different refrigerants when the mass flow rate is altered.

A higher mass flow rate of the refrigerant will give a lower COP for the HP. Due to the different thermodynamic properties for all the refrigerants, the correlation between the COP and the mass flow rate, with a fixed energy transfer in the condenser, will differ. As observed from the T-s diagrams, R600a and R290 behave similarly.

The brine temperature can affect the COP, and to illustrate this, the temperature of the brine at the outlet of the evaporator for the R290 HP has been altered, see figure 37.

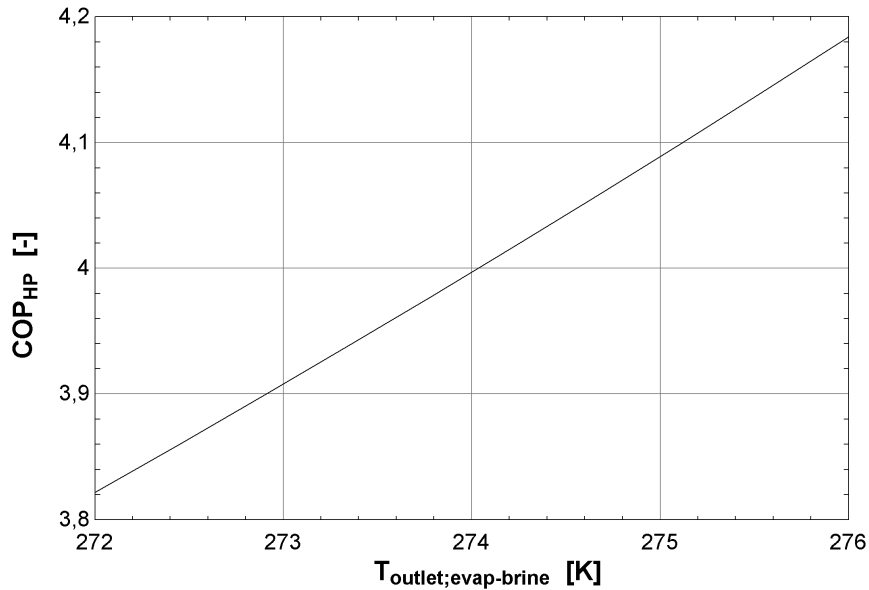


Figure 37: The impact of the brine temperature out of the evaporator on COP for the R290 HP.

The HPs COP increases as the temperature of the brine exiting the HP rises, which is consistent with results presented in the literature review, and the statement from Razavi et al.[18] that a higher evaporator temperature is beneficial for the COP. This will also imply that a higher temperature in the soil and a higher output temperature from the GHX is desired since it will result in a higher COP, as illustrated in figure 27 and 28. Because the temperature of the soil varies throughout the year, the COP of the HP varies as well, with the largest COP occurring in the summer. The fact that the HP's effectiveness is so dependent on the source temperature highlights the benefits of employing a ground source heat pump rather than air to water heat pump in northern climates, where the ambient temperature varies greatly and can have lower temperatures than the ground. This finding also underlines the advantage of implementing SC which can recharge the ground when they produce excess heat and increases the outlet temperature of the borehole.

5.4.3 Energy from the condenser

A higher COP in the HP will lead to more energy transfer to the hot water tank. Providing a higher brine temperature into the evaporator will ensure a greater heat transfer in the evaporator, which will lead to a greater energy transfer in the condenser. In the following figure, the R290 HP model is used and the outlet temperature of the GHX is varied depending on how much heat is provided from the SC, previously illustrated in figure 31. The temperatures of the HP and mass flow rate of the refrigerant remain the same, but the COP is varying with the regulation of T_6 when both formulas presented in equation 5 and the first part of equation 77 are implemented in EES.

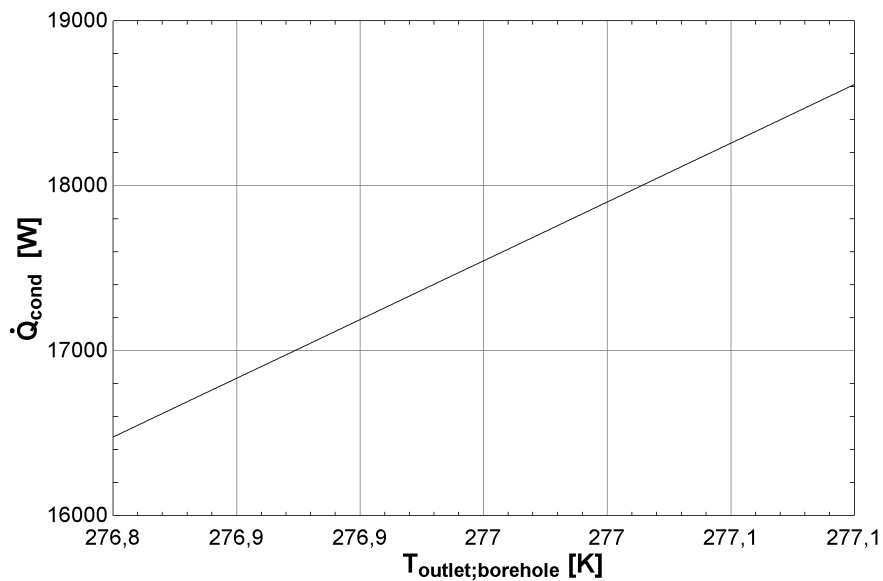


Figure 38: How an increase of the outlet temperature of the GHX impacts the produced energy of the HP.

The amount of energy produced increases in direct proportion to the brine's exit temperature from the GHX. This suggests that recharging the ground can raise the HP's energy output. The requirement for electricity from the electrical heater will be minimized when the SC produces extra heat that is delivered to the borehole.

5.4.4 Area evaporator

With the use of the LMTD method, the optimal area for the condenser and evaporator for the stated conditions was calculated for each HP. Table 21 list up the needed area for the evaporators with the various refrigerants.

Table 21: Calculated area of the evaporator area for the different refrigerants.

	R600a	R290	R717	R1234ez(E)
Evaporator [m ²]	3.3	3.5	3.4	2.9

Even though the refrigerants have different properties and it has been used different Nusselt correlations, the areas for the evaporators are quite similar. The overall heat transfer values are a bit bigger than in reality since fins are not taken into account in the calculations.

The inlet temperature of the brine and the mass flow rate of the refrigerant can affect the area of the evaporator when the heat extraded in the evaporator is constant. This has been illustrated in the figure 39, with the use of the EES model for the R290 HP.

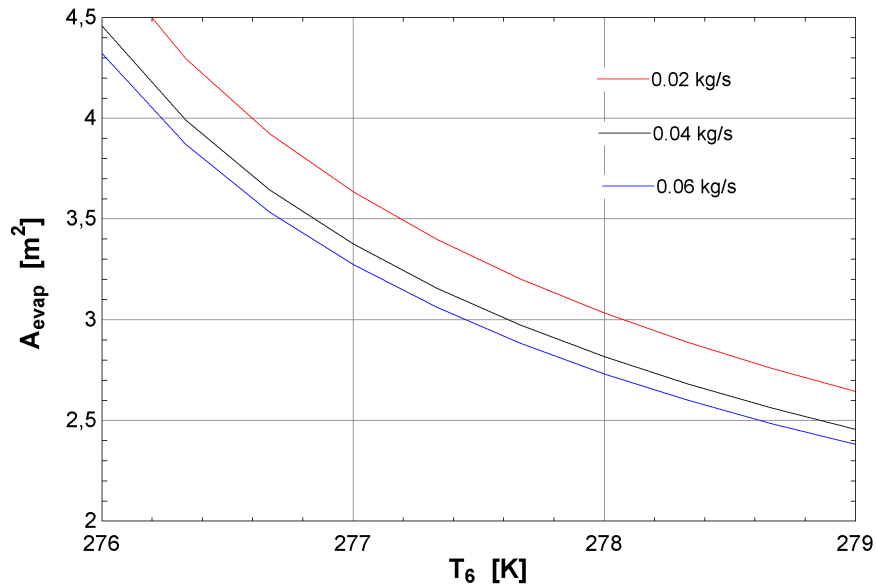


Figure 39: Area of the evaporator with different mass flow rates of the refrigerant with the variation of the inlet temperature of the brine for the R290 HP.

To be able to employ a smaller evaporator, a lower mass flow rate of the refrigerant and a high outlet temperature from the borehole is preferred. As previously stated, the grout affects the temperature of the brine, which in turn affects the area required for the evaporator. This underlines that the ideal grout to use is one with high thermal conductivity. The graph also proves that it is necessary to keep the thermal balance of the ground. If the temperature gets too low over time, the evaporator will not be able to extract the needed heat with the same area. This will reduce the COP of the HP and increase the need for energy from the electrical heater. The higher the mass flow rate of the refrigerant, the bigger the area needs to be. This is due to the amount of time the refrigerant has to absorb heat inside the evaporator.

5.4.5 Exergy

The exergy destruction in all four components and for the overall heat pump cycle is presented in table 22.

Table 22: Calculated exergy destruction in each component of the HP for the different refrigerants.

Component	R600a	R290	R717	R1234ze(E)
Evaporator [W]	265.5	260.1	265.4	251.7
Compressor [W]	1058.0	873.3	602.9	1129.0
Condenser [W]	243.3	275.3	589.6	251.9
Expansion valve [W]	504.4	605.8	246.2	577.6
Sum	2071.2	2014.5	1714.1	2210.2

The R1234ze(E) HP generates the most exergy destruction, while R717 generates the least. The results also show that the compressor incurs the most significant exergy destruction, and stands for over 35% of

the total exergy destruction in all four HPs.

In table 23 the second law efficiency, η_{II} , is listed for each component as well.

Table 23: Calculated second law efficiency in each component of the HP for the different refrigerants.

Component	R600a	R290	R717	R1234ze(E)
Evaporator [%]	73.4	74.1	73.3	74.2
Compressor [%]	71.5	76.2	82.2	70.6
Condenser [%]	78.9	76.8	60.7	78.3
Expansion valve [%]	0	0	0	0

Due to the assumptions of an adiabatic system, the second order efficiencies reported in the table above are greater than for a real system. The second law efficiency for the R717 condenser is notably lower than for the others. The temperature of the condenser has an effect on the component's exergy destruction, hence subcooling the refrigerant at state 3 will affect the condenser's performance. Figure 40 illustrates this effect.

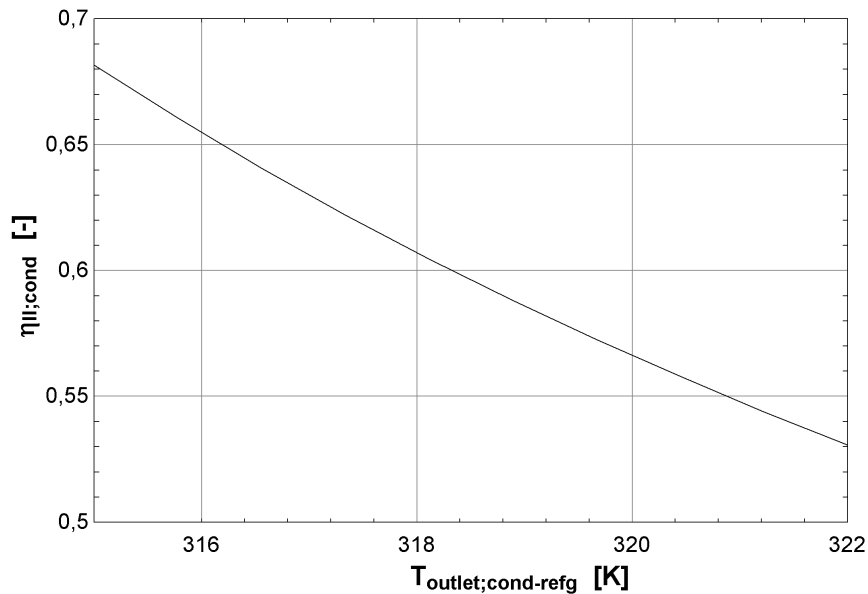


Figure 40: How subcooling the refrigerant after the condenser affects the second law efficiency of the condenser in the R717 HP.

Subcooling the refrigerants has given positive results on the second law efficiency, and is thus a strategy to implement in order to minimize the HP's total exergy destruction, which is shown in figure 41.

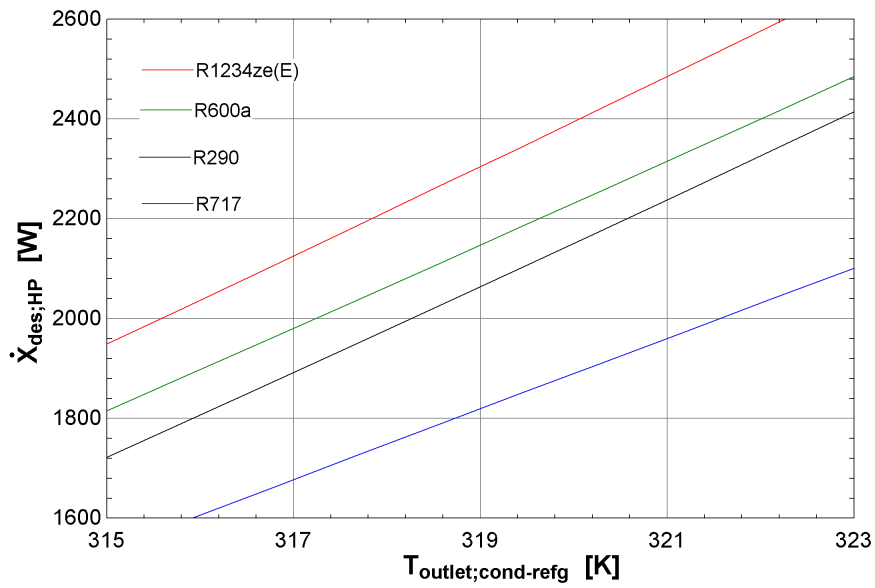


Figure 41: How subcooling the refrigerant after the condenser affects the total exergy destruction for the HP.

5.5 Solar collector to water tank

The findings from the dynamic simulation in IDA ICE of the plant where the SC is linked to the water tank are provided in this section.

A 1-year energy simulation was conducted for the energy plant, the results of which are reported in details in appendix P. The space heating demand was estimated to be 17 359.0 kWh/year, whereas the DHW demand was estimated to be 5 371.1 kWh/year. This is similar to the simplified calculation shown in table 3, which verifies the calculations and allows for comparisons between the EES models and the IDA ICE simulations. The amount of DHW that the SC can cover may be calculated from tables 28 and 29 shown in the appendix. On average, the SC can cover around 60% of the DHW during the solar system's operating period from Mars to September, however this percentage varies from month to month. The SC can only meet 30-40% of the DHW demand in Mars, April, and September, but they can cover 60-80 % for the remainder of the operation time. The solar collectors will provide less energy than expected from the mathematical model, indicating more loss in the solar system in the simulations, which is closer to a real solar system.

To evaluate the performance of the SGSHP, the use of the top heater electrical heater the default value is also used in this system to be able to compare the simulations. In the energy simulation, the mean required energy output from the top heater was simulated to be 16 834.2 W per month.

Over a seven-year period, the temperature at the bottom of the borehole was measured when the mass flow rate of the solar working fluid is set to the default for plant 2. This is illustrated in figure 42.

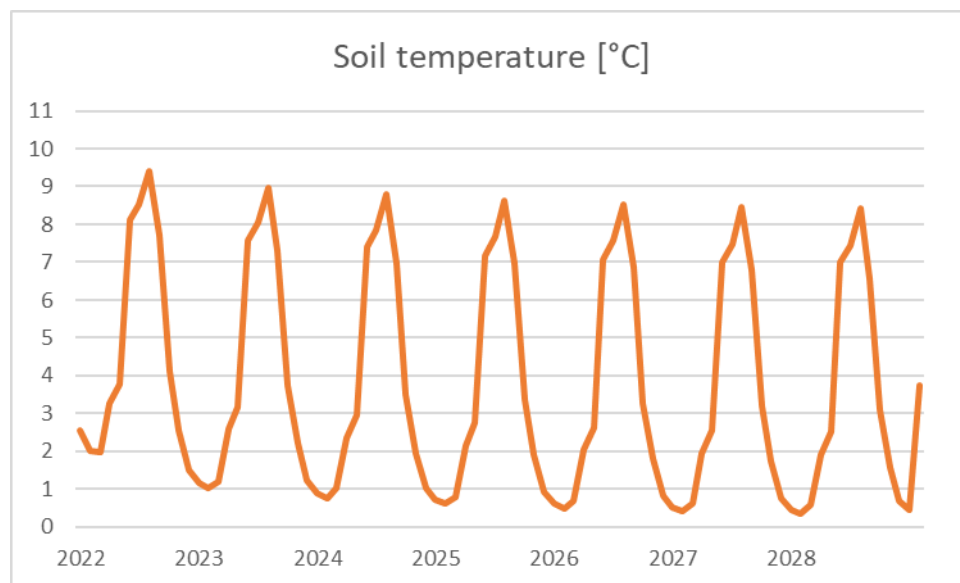


Figure 42: The soil temperature at 140 meters over a seven-year period without Sc recharging the ground.

The temperature of the soil changes significantly throughout the year and is expected to diminish over time. The temperature changes more throughout the year than the theory and literature suggest, but the pattern of the changes is expected and similar to the study of Gau et al., this behavior will therefore be discussed further [13]. The month with the greatest soil temperature is August, while the month with the lowest is February. Even with the usage of freecooling in the summer, the mean annual temperature dropped from 4.63 to 3.43°C from 2022 to 2028, over 1°C different, resulting in a 26% drop. This is a lesser drop than several GSHP system had in the literature review, most likely due to the freecooling.

5.6 Solar collector to ground heat exchanger

This section contains the results of the dynamic simulation of the plant where the SC is linked to the GHX in IDA ICE.

For the second plant, a 1-year energy simulation was also conducted, which achieved similar results as the first plant with 17 298 kWh/year for space heating and 5307 kWh/year for DHW.

This system's average monthly energy consumption from the electrical heater was determined to be 22 213.5 W. This represents a 5 378.8 W gain over the first plant, implying that the first configuration saves 24% energy in comparison. This is a significant amount, and differ from the statement from Thygesen and Karlsson [20].

How the soil temperature at 140 meters varies over a seven-year period is illustrated in figure 43.

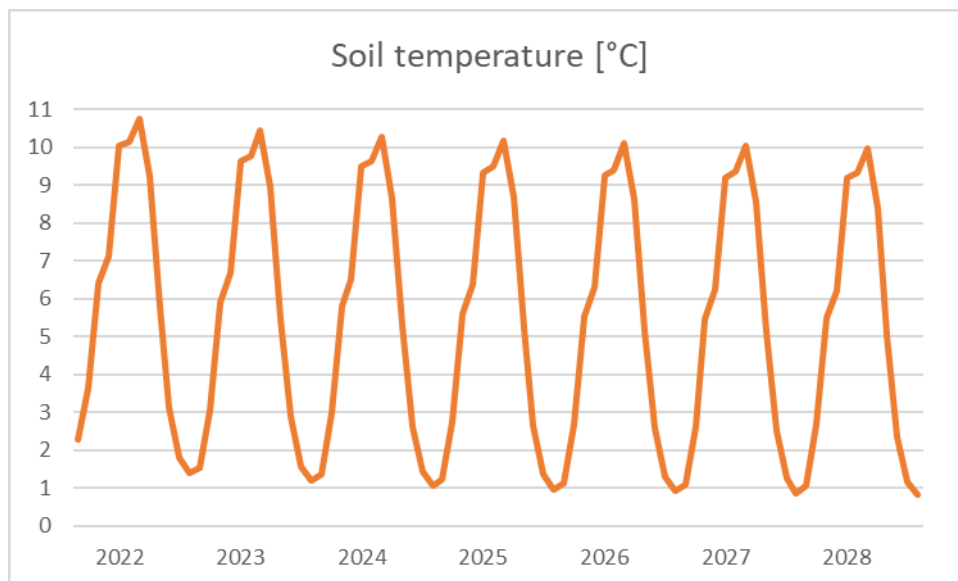


Figure 43: The soil temperature at 140 meters over a seven-year period with SC connected to the GHX.

Between 2022 and 2028, the mean soil temperature reduces from 5.98 to 5.15°C, a difference of less than 1°C and a 14 percent drop. This result is consistent with the findings in the literature review mentioned in section 2.3.1, and it was discovered that applying measures to achieve a thermal balanced soil was crucial in cold areas. According to the figures above, the second plant achieves a greater soil temperature during the operation period than the first plant. A greater soil temperature has been demonstrated to boost HP performance, another advantageous of connecting SC to the GHX. The COP for both the configuration is a fix value at 4, so how the higher soil temperature affects the COP in the these simulations will unfortunately not show.

Both of the evaluated system configurations have advantages and disadvantages. It is critical to implement efficient renewable energy systems that consume a minimal amount of provided energy and have a long lifetime to reduce energy consumption and greenhouse gas emissions in the building sector. Combining these two configurations, as shown in system configuration 1 in this thesis where SC prioritized to heat the water tank, is a good alternative for an SGSHP in a cold climate.

6 Conclusion

The main purpose of this thesis was to investigate the performance of a SGSHP, and provide information if it is beneficial to implement solar thermal energy to a GSHP in a colder climate and how such systems should be optimized. The studied SGSHP was connected to a school building in Oslo designed according to the Norwegian passive house standard, and the SC was able to provide heat to the hot water tank and recharge the GHX if excess heat was produced. The investigation was accomplished by performing thermodynamic analyzes in EES, and through dynamic simulations of the energy system in IDA ICE. The main results are listed below.

- The SC was able to cover around 60% of the DHW demand on average during the operation period from Mars to September, but the produced energy will vary a lot depending on the weather conditions.
- When recharging the ground with solar thermal energy from a 4.7 m^2 area of SC, the length of each borehole can be reduced by 19% compared to a reference case without SC.
- Recharging the ground with the solar thermal energy will increase the soil temperature, and slow down the depletion of the ground over time than if only freecooling is used as a measure, extending the lifespan of the energy system.
- Utilizing solar heat to heat the water tank reduced the need for an auxiliary unit, helping to reduce the energy consumption for the building.
- Keeping an inlet temperature to the SC close to the ambient temperature gave a positive outcome on the second law efficiency of the SC.
- A propylene glycol mixture gave a better second order efficiency of the SC than an ethylene glycol mixture and is therefore recommended for solar collectors in Norway.
- Choosing a grout with high thermal conductivity is favorable in order to increase the borehole outlet temperature and reduce the depth and number of boreholes, which is cost-beneficial.
- Recharging the ground through a HX is a good option to achieve a high brine temperature into the HP while not increasing the exergy destruction of the GHX.
- R717 was found to achieve the best overall performance of the HP under the specified conditions, having the highest COP at 4.44, lowest exergy destruction and was more flexible to different temperatures and pressures in the system due to the larger operation area.
- R1234ze(E) needed the smallest evaporator area, but had the lowest COP and highest exergy destruction.
- Keeping a low mass flow rate of the refrigerant will increase the COP.
- A higher soil temperature resulting in a higher outlet temperature of the GHX will give a higher COP.
- The compressor stood for a significant part of the HP's exergy destruction, and it was discovered that subcooling the refrigerant after the condenser will lower this amount, improving the HP's overall performance.
- A higher temperature of the brine at the inlet of the evaporator and a low mass flow rate of the refrigerant reduce the evaporator's area.
- A configuration of the SGSHP where the SC prioritizes heating the water tank and excess heat recharges the ground is a good option to achieve low energy usage and thermal balance in the soil.

In conclusion, the investigated SGSHP appears to be a well-suited approach for heating passive houses and low energy houses in Norway under the conditions studied. Utilizing an optimized SGSHP as described in this thesis will help reduce the energy consumption and therefore the greenhouse gas emissions in the building sector, and it is more suited for a cold environment than the literature review indicated.

7 Future work

Assumptions and simplifications have been made throughout the study due to time limitations, therefore some ideas and suggestions based on this study's experience have been compiled for future contributions.

It would have been beneficial to validate the SGSHP against a real system. This could provide more accurate and solid results since the majority of the simplification made in this study would be excluded.

EES does not provide properties for mixed refrigerants, but it would be interesting to investigate the performance of a HP with this kind of refrigerant and compare it to the others.

A variety of system solutions should be investigated. Only one solution was explored and confirmed to be efficient in a cold climate in this master's thesis, but it would be fascinating to see how alternative configurations affect the performance and which energy system is best suited for a cold climate. It's also worth checking to see if the type of building has an effect on which system should be used. Due to the scope of this study, the IDA ICE energy plants were not designed to simultaneously be able to heat the hot water tank and recharge the ground. A system more similar to system solution 1 might be examined further using macros.

The energy system's cost and profitability are not taken into consideration. In practice, this has a significant impact on the type and configuration of the system that will be used. When this viewpoint is taken into account, a more in-depth assessment can be conducted to see if the energy gains of adding SC will be profitable when compared to the increased startup and maintenance expenses of the system.

A SGSHP is a renewable energy system, and the ecological impact it can have has not been evaluated here. It could be interesting to see how the different parameters affect the environmental impact and if the energy benefits of SC compensates for the energy and emissions connected to the production and installation.

References

- [1] Umberto Berardi. “Building Energy Consumption in US, EU, and BRIC Countries”. In: (2015). DOI: <https://doi.org/10.1016/j.proeng.2015.08.411>.
- [2] UNFCCC. “The Paris Agreement”. In: (2015). URL: <https://unfccc.int/process-and-meetings/the-paris-agreement/the-paris-agreement>.
- [3] V. Masson-Delmotte et al. “Climate Change 2021: The Physical Science Basis. Contribution of Working Group I to the Sixth Assessment Report of the Intergovernmental Panel on Climate Change”. In: (2021). URL: <https://www.ipcc.ch/report/ar6/wg1/#TS>.
- [4] Åse Sørensen, Camilla Torp, and Kari Nylund. “Solvarme i kombinasjon med andre varmekilder. Norsk Solenergiforening”. In: (2017).
- [5] Hilary Arksey and Lisa O’Malley. “Scoping studies: towards a methodological framework”. In: (2005). URL: <https://eprints.whiterose.ac.uk/1618/1/Scopingstudies.pdf>.
- [6] Johannes de Beer. “Ground source energy”. In: (2017). URL: <https://www.ngu.no/en/topic/ground-sourced-energy>.
- [7] John Fialka. “Why China Is Dominating the Solar Industry”. In: (2016). URL: <https://www.scientificamerican.com/article/why-china-is-dominating-the-solar-industry/>.
- [8] Weibo Yang, Lulu Sun, and Yongping Sun. “Experimental investigations of the performance of a solar-ground source heat pump system operated in heating modes”. In: (2015).
- [9] Vikas Verma and K Murugesan. “Optimization of solar assisted ground source heat pump system for space heating application by Taguchi method and utility concept”. In: (2014).
- [10] Luis Pérez-Lombard, José Ortiz, and Christine Pout. “A review in buildings energy consumption information”. In: (2008). DOI: <https://doi.org/10.1016/j.enbuild.2007.03.007>.
- [11] Aleksandar Georgiev, Rumén Popov, and Emil Toshkov. “Investigation of a hybrid system with ground source heat pump and solar collectors: Charging of thermal storages and space heating”. In: (2020).
- [12] Yongming Ji et al. “Simplified method to determine the collector area of solar-assisted ground-source heat pump system”. In: (2017).
- [13] Yan Gao et al. “Designing and Optimizing Heat Storage of a Solar-Assisted Ground Source Heat Pump System in China”. In: (2020).
- [14] Minwoo Lee et al. “Performance improvement of solar-assisted ground-source heat pumps with parallelly connected heat sources in heating-dominated areas”. In: (2022).
- [15] Willian Duarte et al. “Feasibility of solar-geothermal hybrid source heat pump for producing domestic hot water in hot climates”. In: (2021).
- [16] Parham Eslami-Nejad and Michel Bernier. “Coupling of geothermal heat pumps with thermal solar collectors using double U-tube boreholes with two independent circuits”. In: (2011).
- [17] Massimo Cimmino and Parhan Eslami-Nejad. “A simulation model for solar assisted shallow ground heat exchangers in series arrangement”. In: (2017).
- [18] Seyed Houman Razavi, Rouhollah Ahmadi, and Alireza Zahedi. “Modeling, simulation and dynamic control of solar assisted ground source heat pump to provide heating load and DHW”. In: (2018).
- [19] Aymeric Girard et al. “Higher ground source heat pump COP in a residential building through the use of solar thermal collectors”. In: (2015).

- [20] Richard Thygesen and Bjorn Karlsson. “Economic and energy analysis of three solar assisted heat pump systems in near zero energy buildings”. In: (2013).
- [21] Jihyun Hwang, Doosam Song, and Taewon Lee. “The Effect of Coupling Solar Thermal System and Geothermal Heat Pump Systems in Areas with Unbalanced Heating and Cooling Demand”. In: (2021).
- [22] Vikas Verma and K Murugesan. “Experimental study of solar energy storage and space heating using solar assisted ground source heat pump system for Indian climatic conditions”. In: (2017).
- [23] Yongbao Chen, Zhisen Chen, and Zhe Xiaolei Chen Yuan. “Dynamic modeling of solar-assisted ground source heat pump using Modelica”. In: (2021).
- [24] Vikas Verma and K Murugesan. “Experimental study of solar assisted ground source heat pump system during space heating operation from morning to evening”. In: (2018).
- [25] Fabio Struckmann. “Analysus of a flat-plate solar collector”. In: (2008). DOI: https://www.lth.se/fileadmin/ht/Kurser/MVK160/Project_08/Fabio.pdf.
- [26] Jharkhand Dhanbad. “Solar thermal technology for Rual India”. In: (2015). URL: <https://www.slideshare.net/bapikumar144/solar-thermal-tech-pradhan>.
- [27] CEN-EN12975-1. “Thermal solar systems and components - Solar collectors Part 1: General requirements”. In: (2006).
- [28] Gjermund Stensrud. “Geotermisk energi-Fremtiden energikilde”. In: (2019). URL: <xn--strm-ira.no/geotermisk-energi>.
- [29] Knut Hofstad. “Grunnvarme”. In: (2019). URL: <snl.no/grunnvarme>.
- [30] Arne Petter Krogstad et al. “Bruk av grunnvarme til oppvarming av eneboliger og næringsbygg”. In: (2002).
- [31] Joseph Allen. “Avrenning fra borehull i fjell med fokus på Oslo kommune”. In: (2016).
- [32] Norsk Varmepumpeforening. “Væske-til-vann varmepumpe”. In: (2019). URL: <https://www.varmepumpeinfo.no/varmepumpetyper/vaske-til-vann-varmepumpe>.
- [33] Jens Petter Toldnæs. “Globale oppvarmingspotensialer”. In: (2022). URL: snl.no/eglobale_oppvarmingspotensialer.
- [34] Engineering ToolBox. “Refrigerants - Physical Properties”. In: (2005). URL: https://www.engineeringtoolbox.com/refrigerants-d_902.html.
- [35] Yunus A. Cengel and Michael A. Boles. “Thermodynamics An engineering approach”. In: (2015).
- [36] Bjørn Pedersen. “Entalpi”. In: (2019). URL: <snl.no/entalpi>.
- [37] Leyla Amiri, Edris Madadian, and P Ferri Hassani. “Ergo- and exergo-technical assessment of ground-source heat pump systems for geothermal energy production from underground mines”. In: (2019). DOI: 10.1080/09593330.2018.1481886.
- [38] Yunus A. Cengel and A. J. Ghajar. “. Heat and Mass Transfer Fundamentals Applications (5th ed.)” In: (2015).
- [39] Standard Norge. “NS 3701:2012 Criteria for passive houses and low energy buildings - Non-residential buildings”. In: (2012).
- [40] SINTEF byggforsk. “451.021 Klimadata for termisk dimensjonering og frostsikring”. In: (2018). URL: https://www.byggforsk.no/dokument/204/klimadata_for_termisk_dimensjonering_og_frostsikring.

- [41] Standard Norge. “SN-NSPEK 3031:2021 Energy performance og buildings- Calculation of energy needs and energy supply”. In: (2021).
- [42] Enova. “Solfanger”. In: (2016). URL: <https://www.enova.no/privat/alle-energitiltak/solenergi/solfanger-/>.
- [43] DE DIETRICH THERMIQUE. “Solar installations - solar collectors, tanks and systems for individual and collective installations”. In: (2017).
- [44] Direct Plastics. “Material data sheet - HDPE”. In: (). URL: <https://www.directplastics.co.uk/pub/pdf/datasheets/HDPE\%20Data\%20Sheet.pdf>.
- [45] David Zijdemans. “Vannbaserte oppvarmings-og kjølesystemer”. In: (2014).
- [46] SINTEF byggforsk. “552.403 Varmepumper i bygninger. Funksjonsbeskrivelse”. In: (2009). URL: https://www.byggforsk.no/dokument/541/varmepumper_i_bygninger_funksjonsbeskrivelse.
- [47] F-Chart Software. “Engineering Equation Solver”. In: (2021). URL: <https://fchartsoftware.com/ees/>.
- [48] Vidar Lunde, Line Ødegård Angeloff, and Frenndrik Jordhøy. “Legionellaveilederen - Fordelingsnett til dusjer og andre aerosoldannende tappepunkter”. In: (2020). URL: <https://www.fhi.no/nettpub/legionellaveilederen/temakapitler/interne-vannfordelingsnett-som-forsyner-dusjer-og-andre-aerosoldannende-tappepunkter/?term=&h=1>.
- [49] Thor Gjermund Eriksen and Ingrid Støver Jensen. “yr.no”. In: (2022). URL: <https://www.yr.no/en/statistics/graph/1-72837/Norway/Oslo/Oslo/Oslo>.
- [50] European commission. *PVGIS*. Computer Program. 2020. URL: https://re.jrc.ec.europa.eu/pvg_tools/en/.
- [51] David García-Menéndez et al. “Dynamic simulation and exergetic analysis of a solar thermal collector installation”. In: (2022). DOI: <https://doi.org/10.1016/j.aej.2021.06.075>.
- [52] Habtamu B. Madessa et al. “Parametric study of a vertically configured ground source heat pump system”. In: (2017).
- [53] Ali H. Tarrad. “A Borehole Thermal Resistance Correlation for a Single Vertical DX U-Tube in Geothermal Energy Application”. In: 3 (2019). DOI: [10.11648/j.ajese.20190304.12](https://doi.org/10.11648/j.ajese.20190304.12).
- [54] Dennis O’Neal and Yian Gu. “Development of an equivalent diameter expression for vertical U-Tubes used in ground-coupled heat pumps”. In: (1998). URL: https://www.researchgate.net/publication/279938328_Development_of_an_equivalent_diameter_expression_for_vertical_U-Tubes_used_in_ground-coupled_heat_pumps.
- [55] Andres A. Sánchez-Escalona et al. “Application of the ‘Nusselt-Equation Simulated Evolution Method’ in Forced Convective Heat Transfer Modeling”. In: (2020). DOI: <https://doi.org/10.18280/ijdne.160104>.
- [56] You-Rong Li Lan Xiao Shuang-Ying Wu Xiao-Feng Yuan. “Exergy transfer effectiveness on heat exchanger for finite pressure drop”. In: (2007). DOI: <https://doi.org/10.1016/j.energy.2007.04.010>.
- [57] Behzad Abolhassani Monfared. “Design and Construction of a Small Ammonia Heat Pump”. In: (2010). URL: <https://www.diva-portal.org/smash/get/diva2:483090/FULLTEXT01.pdf>.
- [58] Adrián Mota-Babiloni et al. “Optimisation of high-temperature heat pump cascades with internal heat exchangers using refrigerants with low global warming potential”. In: (2018). DOI: <https://doi.org/10.1016/j.energy.2018.09.188>.

- [59] Sung-Min Kim and Issam Mudawar. “Universal approach to predicting heat transfer coefficient for condensing mini/micro-channel flow”. In: (2013). DOI: <https://doi.org/10.1016/j.ijheatmasstransfer.2012.09.032>.
- [60] Jordan A. Morrow et al. “Flow condensation heat transfer performance of natural and emerging synthetic refrigerants”. In: (2021). DOI: <https://doi.org/10.1016/j.ijrefrig.2021.09.014>.
- [61] Mirza M. Shah. “Improved correlation for heat transfer during condensation in conventional and mini/micro channels”. In: (2019). DOI: <https://doi.org/10.1016/j.ijrefrig.2018.07.037>.
- [62] Ji Zhang et al. “Condensation heat transfer and pressure drop characteristics of R134a, R1234ze(E), R245fa and R1233zd(E) in a plate heat exchanger”. In: (2018). DOI: <https://doi.org/10.1016/j.ijheatmasstransfer.2018.08.124>.
- [63] EQUA Simulation AB. “IDA ICE”. In: (). URL: <https://www.equa.se/en/ida-ice>.
- [64] “Materialdata for natursetin”. In: (2003). URL: https://www.sintef.no/globalassets/upload/teknologi_og_samfunn/berg-og-geoteknikk/lister/typiske-materialdata-for-naturstein.pdf/.
- [65] Matweb. “Overview of materials for High Density Polyethylene (HDPE), Ultra High Molecular Weight”. In: (). URL: https://www.matweb.com/search/datasheet_print.aspx?matguid=f9470672aa5549cb9c7b157677d02062.
- [66] N. Hamlaoui et al. “Machining of tough polyethylene pipe material: surface roughness and cutting temperature optimization”. In: (2017). URL: [10.1007/s00170-017-0275-4](https://doi.org/10.1007/s00170-017-0275-4).
- [67] Ilaria Guarracino et al. “Systematic testing of hybrid PV-thermal (PVT) solar collectors in steady-state and dynamic outdoor conditions”. In: (2019).
- [68] Kristi Midttømme and Øystein Nordgulen. “Markedsundersøkelse om geotermisk energi - geologiske forhold”. In: (2000). URL: https://www.ngu.no/upload/Publikasjoner/Rapporter/2000/2000_083.pdf.
- [69] Hikmet Esen et al. “Energy and exergy analysis of a ground-coupled heat pump system with two horizontal ground heat exchangers”. In: (2007).
- [70] Emil Mikael Weiseth Kjellesvik and Håkon Haglund Norstrand. “Dimensjonering og optimalisering av CO2-varmepumpeanlegg”. In: (2018).
- [71] Chantal Maatouk. “Improvement Of Thermal Conductivity Of Grout Mixture For Geothermal Heat Pump Systems”. In: (2016). URL: <https://docs.lib.purdue.edu/cgi/viewcontent.cgi?article=2712&context=iracc#:~:text=The%20conventional%20cement%20grout%20has, reducing%20the%20heat%20exchanger%20length..>

A Draft of paper sent to a conference

Performance analysis of a solar thermal system coupled with a ground source heat pump in Nordic conditions

Abstract

The main objective of this work is to investigate the energy and exergy performance of a solar assisted ground source heat pump for a school building designed according to Norwegian passive house standard. The system is designed in such a way that the solar collector prioritizes to provide heat to the hot water tank and whenever there is excess heat from the solar collector it can be used to charge the ground borehole. A detailed thermodynamic analysis of the system has been carried out in Engineering Equation Solver (EES). Isobutane (R600a), propane (R290), ammonia (R717) and solstice (R1234ze(E)) have been investigated as working fluid for the heat pump. The result revealed that the solar collector and the different working media have affected both the COP and the exergy of the system. Moreover, the mass flow rate of the brine and the length of the borehole affect the performance of the system.

Introduction

The building sector's energy demand has been rising the last decades and it is now accounting for 30% of the global final energy consumption, making it one of the largest energy consumption sectors (Berardi (2015)). The Paris agreement is adopted by 196 countries in 2016 (UNFCCC (2015)), and the UN climate report is expressing a deep concern for the environment (Masson-Delmotte et al. (2021)), and it has heightened the focus on reducing energy usage. It is, therefore, vital to improve the performance of energy systems in buildings and minimize their greenhouse gas emissions to meet the Paris agreement's target of limiting global warming to 1.5 °C compared to the prediction.

As more passive houses and low-energy buildings have been built in recent years, the need for efficient energy systems has grown. As well, due to the change in weather pattern and cold climate in the north, there is still some uncertainty about how some types of energy sources can best be utilized for the building sector, like solar systems. Ground source heat pumps (GSHP) are a well-established technology in Norway today. Solar energy is, however, less used, particularly solar thermal energy systems. Nonetheless, there has been an increase in interest in combining these two technologies to improve the heat pump operating conditions and minimize the need of an auxiliary heating unit. Hwang et al. (2021), Razavi et al. (2018) and Girard et al. (2015) have compared the performance of the solar assisted ground source heat pump (SGSHP) to a conventional GSHP, and the results showed that the ben-

efits of having solar thermal energy combined with GSHP. The configurations of SGSHP can be done in a variety of ways. The heat generated by the solar collectors can be utilized to raise the evaporation temperature, recharge the ground, or used to produce the building's domestic hot water, or a combination of these methods. In recent years, there has been an increase in the number of published research works examining how system solutions for SGSHP affects performance, and Reda and Laitinen (2015) and Yang et al. (2015) reported different positive outcomes from each configuration studied.

The main objective of this paper is to investigate the energy and exergy performance of a SGSHP for a school building designed according to the Norwegian passive house standard, (NS3701 (2012)). The energy system will provide energy both for domestic hot water production and space heating. The system designed in such a way that flat plate solar collectors prioritize providing heat to the hot water tank and whenever there is excess heat from the solar collector, it can be used to charge the ground borehole. A detailed thermodynamic analysis of the selected system has been carried out in Engineering Equation Solver (EES) (Software (2021)), and the potential working fluids isobutane (R600a), propane (R290), ammonia (R717), and solstice (R1234ze(E)) have been investigated. Moreover, sensitivity analyses have been conducted to identify how different parameters influence the system's performance and provide important knowledge for system optimization.

Method

Case setup

The chosen solution for this work is illustrated in figure 1. The solar collector is used to heat the water tank and recharge the ground. The circulation pump before the SC will start when the surface temperature of the SC is 10°C or higher. Below this temperature, the SC will not be able to provide significant temperature rise in the water tank or heat exchanger, as mentioned by Sørensen (2017). If the temperature in the SC is 5K greater than the water tank temperature, the controller will direct the working fluid through the valve V_1 to the water tank. If this isn't the case, the controller will send the working fluid to the plate heat exchanger, which will heat the brine from the HP and to the ground heat exchanger (GHX). When the SC is unable to heat the water tank to 70 °C alone, the HP will start, and begin extracting heat from the GHX. If neither the GSHP nor the SC can maintain the set point in the tank, an electrical heater will be activated. Which

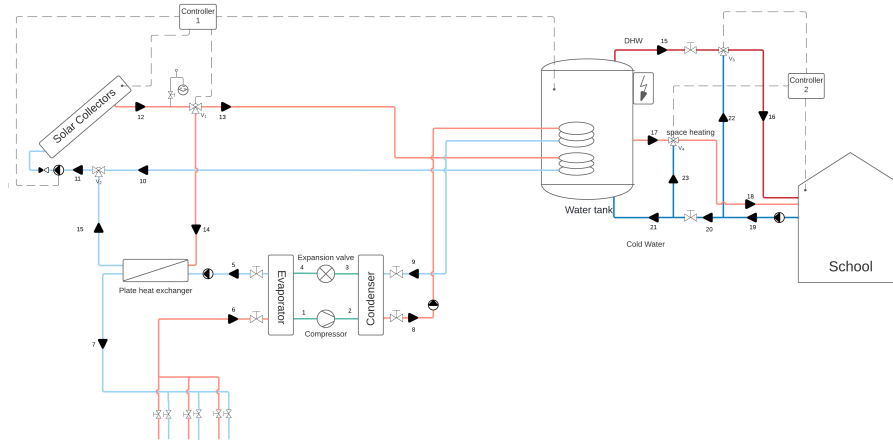


Figure 1: System solution for SGSHP

scenario the SC should work is determined by a controller which examines and compares the temperature at specified places and based on this adjust the flow through valve V_1 .

The water tank is split into three sections. The SC heats the low-temperature water at the bottom, where the cold water enters. In the middle, the HP connected to the heat exchanger (HX) heats the tank further and the space heating is extracted. The electrical heater is placed on the top section as an auxiliary unit, which will turn on when the water temperature falls below the set point. The domestic hot water (DHW) will also be distributed to the building from the top section. This is beneficial for the SC's efficiency, which is better at low temperatures, and it ensures that it doesn't compete with the electric energy.

The SGSHP system is dimensioned and analyzed based on a reference school building located in Oslo, Norway, where the mean temperature is $6.3\text{ }^\circ\text{C}$ and the designed outdoor temperature during the winter is $-19.8\text{ }^\circ\text{C}$, (byggforsk (2018)). The building is classified as a passive house and should therefore satisfy Criteria for passive houses and low energy buildings, (NS3701 (2012))

According to SN-NSPEK3031 (2021), the set point for heating the school building is $21\text{ }^\circ\text{C}$. As a result, ΔT in the energy calculation will be $21 - (-19.8) = 40.8\text{ }^\circ\text{C}$, which gives an energy and power demand of the building $23\,670\text{ kWh/year}$ and $26\,626\text{ W}$, respectively.

The SC is dimensioned to cover 60% of the DHW demand, 2700 kWh/year . The working fluid inside the solar system is Ethylene-Glycol mixture with a concentration of 35%.

The ground heat exchanger is made of single U-tube collectors, high-density polyethylene with a thermal conductivity of 0.35 W/mK , connected in parallel. The depth of the boreholes is selected to be 130 meters with an internal diameter of 0.1 meters.

In order to reduce the number of on-off time for the operation of a HP and improve its performance, a HP should be sized for 50-60% of the maximum building heating rate

demand and 80-95 percent of the energy demand, according to Zijdemans (2014). The HP in this study will therefore be dimensioned for 55% of the heating rate demand and 90% of the energy demand. The heat pump is dimensioned for 15 kW.

Solar collector

The thermal efficiency of the SC expresses the useful energy gain over the incident solar energy, and can be obtained from equation 1 (CEN-EN12975-1 (2006)).

$$\eta_{SC} = \eta_0 - \frac{a_1(T_m - T_a)}{G} - \frac{a_2(T_m - T_a)^2}{G} \quad (1)$$

η_0 , a_1 and a_2 is information given by the solar collector manufacturer, THERMIQUE (2017).

For the exergy analysis of the solar collector system, the general exergy balance from equation 2 is employed.

$$\Sigma X_{des} = \Sigma X_{in} - \Sigma X_{out} - \Sigma X_s \quad (2)$$

Since the system is under steady-state conditions, the stored exergy $\Sigma X_s = 0$. According to García-Menéndez et al. (2022), exergy into a solar system is separated into two parts: the working fluid and the solar radiation, and the following formulae are used to compute them.

$$X_{in,f} = m_{SC} c_{p,SC,f} (T_{11} - T_a - T_a \ln \frac{T_{11}}{T_a}) \quad (3)$$

$$X_{in,sr} = Q_i \left(1 - \frac{4}{3} \frac{T_a}{T_{sun}} + \frac{1}{3} \left(\frac{T_a}{T_{sun}} \right)^4 \right) \quad (4)$$

The exergy out of the system is only from the working fluid.

$$X_{out,f} = m_{SC} c_{p,sun} (T_{12} - T_a - T_a \ln \frac{T_{12}}{T_a}) \quad (5)$$

The second law efficiency is calculated using the following equation.

$$\eta_{II,sun} = \frac{X_{out,f} - X_{in,f}}{X_{in,f}} \quad (6)$$

Ground heat exchanger

Assuming that the pipe heat loss between the borehole and evaporator is negligible, the heat extracted from the borehole field is equal to the heat transfer to the working fluid in the evaporator.

$$Q_{Ground} = Q_{evap} \quad (7)$$

$$Q_{ground} = Q_{ghx} N_{boreholes} \quad (8)$$

The heat extracted from each borehole is determined by the following equations.

$$q_{ghx} = \frac{\Delta T}{R_{tot}} \quad (9)$$

$$Q_{ghx} = q_{ghx} L_{pipe,ghx} \quad (10)$$

ΔT represents the temperature difference between the soil and the brine temperature.

$$R_{tot} = R_{grount} + R_{pipe} + R_{brine} \quad (11)$$

Where $R_{grount} = \frac{\ln \frac{D_b}{D_{ed,o}}}{2\pi k_g}$, $R_{pipe} = \frac{\ln \frac{D_{ed,o}}{D_{ed,i}}}{2\pi k_p}$ and $R_{brine} = \frac{1}{\pi D_{ed,i} h_{brine}}$

The exergy and second law efficiency formula utilized for the SC were also employed in the exergy analysis of the GHX (García-Menéndez et al. (2022)).

$$X_{i,ghx} = m_{brine} c_{p,ghx} (T_7 - T_g - T_g \ln \frac{T_7}{T_g}) \quad (12)$$

$$X_{o,ghx} = m_{brine} c_{p,ghx} (T_6 - T_g - T_g \ln \frac{T_6}{T_g}) \quad (13)$$

$$\eta_{II,ghx} = \frac{X_{o,ghx}}{X_{i,ghx}} \quad (14)$$

The exergy destruction for the whole borehole field was determined.

$$X_{des,ghx} = m_{brine} (\psi_7 - \psi_6) + Q_{ground} (1 - \frac{T_0}{T_g}) \quad (15)$$

Heat pump

The COP of the HP is calculated using equation 16.

$$COP_{HP} = \frac{Q_{cond}}{W_{comp}} \quad (16)$$

Where the work done on the compressor, W_{comp} , is calculated by equation 17.

$$W_{comp} = m_{refg} (h_{2a} - h_1) \quad (17)$$

The second law of efficiency for the different components of the HP is calculated are follows.

$$\eta_{II,comp} = 1 - \frac{X_{des,comp}}{W_{comp}} \quad (18)$$

$$\eta_{II,cond} = 1 - \frac{X_{des,cond}}{m_{refg} (\psi_2 - \psi_3)} \quad (19)$$

$$\eta_{II,exp} = 0 \quad (20)$$

$$\eta_{II,evap} = 1 - \frac{X_{des,evap}}{m_{refg} (\psi_4 - \psi_1)} \quad (21)$$

The exergy flow due to mass transfer, when the kinetic and potential energy is neglected, is calculated by the following equation.

$$(\psi_i - \psi_e) = (h_i - h_e) - T_0 (s_i - s_e) \quad (22)$$

The exergy destruction is calculated by the following equations for the different components of the HP.

$$X_{des,comp} = T_0 m_{refg} (s_2 - s_1) \quad (23)$$

$$X_{des,cond} = T_0 m_{refg} (s_3 - s_2) + \frac{Q_{cond}}{T_{m,water}} \quad (24)$$

$$X_{des,exp} = T_0 m_{refg} (s_2 - s_1) \quad (25)$$

$$X_{des,evap} = T_0 m_{refg} (s_1 - s_4) - \frac{Q_{evap}}{T_{m,brine}} \quad (26)$$

Since the HP is placed inside the school building, the dead state temperature, T_0 , is set to 21°C.

The input data for the mathematical models is listed in table 1

Table 1: Input data for the mathematical models.

Parameter	Value
Ambient air temperature, T_a	286 K
Dead state temperature, T_0	279.3 K
Solar irradiance, G	800 W/m^2
Surface temperature of the sun, T_{sun}	4 333 K
Mass flow, m_{SC}	0.03 kg/s
Grout material	Water
Number of tubes, N_{tube}	2
Number of boreholes, $N_{borehole}$	4
Pipe outer diameter, $D_{pipe,o}$	0.04 m
Soil temperature, T_s	283.3 K
Brine temperature out of the HP, T_5	275 K
Mass flow rate, m_{GHX}	0.5 kg/s
Exit temperature of the refrigerant at state point 1, T_1	275 K
Exit temperature of the refrigerant at state point 3, T_3	318 K
Exit temperature of the refrigerant at state point 4, T_4	270 K
Pipe diameter of HP, D_{HP}	0,003 m

Validation of the models

The developed thermodynamics models were verified against other models to check the level of their accuracy. Using input data from the published articles, the findings were compared and evaluated, as shown in table 2.

Table 2: Validation of the mathematical model. *Guarracino et al. (2019)**Madessa et al. (2017)***Esen et al. (2007)

Value	This study	Models used for validation	Deviation
η_{th}	42%	41%*	2.4%
T_6	7.6-3.8°C	7.4-4.4°C **	10.6%
η_i	68%	70% ***	2.9%
COP	2.88	2.5-2.77 ***	3.8%

The small deviations for all the parameters presented in the table ensure the quality of the mathematical model and emphasizing the accuracy of the calculations used in this work. The highest deviation came from comparing how the mass flow rate in the borehole influence the temperature out of the GHX, T_6 . The obtained temperatures from this paper is lower than the validation model, and decreases more rapidly with the increase of the mass flow. This is maybe due to the of the use of equivalent diameter in this work. Moreover, the exact soil temperature is not mentioned in Madessa et al's study, and this can also contribute to differences.

Results and discussions

Solar collector

The thermal efficiency of a solar collector is used to assess its performance. For the chosen type of SC, ambient temperature at 293 K and solar irradiance at 800 W/m^2 , the thermal efficiency of the solar collectors was found to be 58%. This corresponds to the information given by Di-eTrich THERMIQUE (2017) for their flat plate solar collectors, emphasizing the accuracy of this calculation. As it can be seen from equation 1, the ambient temperature and solar flux, which can fluctuate greatly during the day, have an impact on the efficiency of the collector as shown in figure 2.

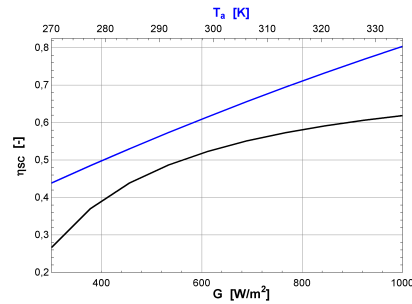


Figure 2: Variation in thermal efficiency with varying solar flux and ambient temperature

The exergy into and out of the SC was calculated for the chosen temperature and solar irradiance conditions, and was found to be 4282.9 W and 1309 W respectively. The corresponding second order efficiency of the solar collector was also found to be 33.44 %. Figure 3 shows how the inlet temperature effect this efficiency.

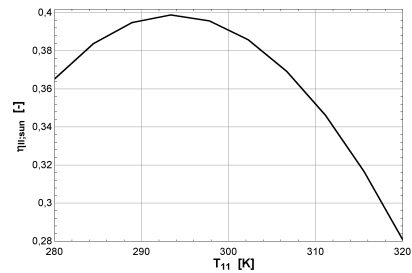


Figure 3: The impact of the inlet temperature of the SC on the second order efficiency

The variation in the fluid inlet temperature to the SC reveals that the exergy efficiency increases up to 294 K and then decreases as the inlet temperature rises further. This indicates that keeping a lower inlet temperature is generally preferable for the SC.

Ground heat exchanger

The depth and the number of the boreholes are critical to investigate in order to achieve optimal operation of the HP. The optimal relation between the length of each borehole

and the number of boreholes depends on several parameters, such as the types of grout materials. Figure 4 illustrates the effect of three different grout materials: water, cement and Bentonite mixture, on the number of boreholes for a fixed mass flow rate of 0.5 kg/s. The water used as grout is considered to be stagnant, and the effect of the convection heat transfer is ignored.

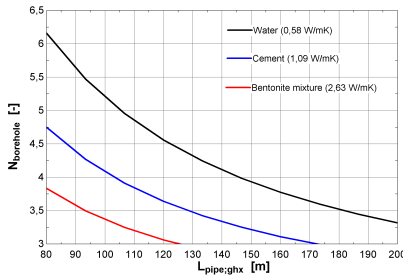


Figure 4: Relation between the depth and number of boreholes to achieve the energy demand with different types of grout

As shown in figure 4, Since water has the lowest thermal conductivity, the number of boreholes required for this grout material is greater than those required for the other two grout materials. The bentonite mixture has a thermal conductivity of 2.63 W/mK, and when it replaces the water with this mixture the length of a borehole can be reduced by 35%, which means reduction in both investment and operation of the system.

Another parameter influencing the relation between the depth and number of boreholes is the mass flow rate of the brine in each of the boreholes. In figure 5, three different flow rates were analyzed.

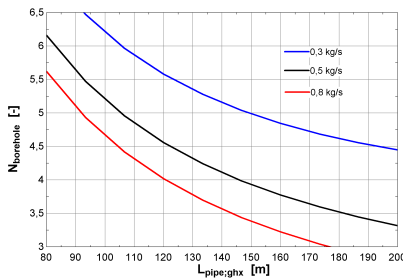


Figure 5: Relation between the depth and number of boreholes to achieve the energy demand with different mass flow rates

The results shows an increase in the mass flow rate reduce either the number of boreholes or the borehole length, which affects again both the investment and operation cost.

Figure 6 shows how the rate of exergy destruction in the borehole field is affected by inlet and outlet temperature of brine to/from the borehole.

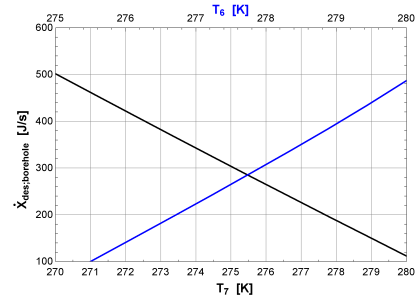


Figure 6: The influence the inlet and outlet temperature on the exergy destruction of the borehole

As the inlet temperature rises, the exergy destruction decreases, while the exergy destruction increases with increase in the outlet temperature. As a result, to achieve lesser exergy destruction, the minimal temperature difference between the outlet and inlet is preferred.

The DHW demand may be lower in the summer, and the SC can be able to charge the boreholes. Throughout this time, the SC can replenish the ground more effectively. This will help to reduce ground depletion in the long run.

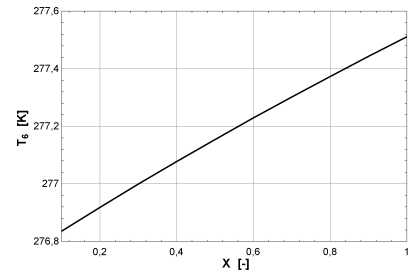


Figure 7: effect of the excess energy from the SC on the outlet temperature of the brine from the borehole

Figure 7 shows that when the heat exchanger receives more heat from the SC, the outlet temperature of the borehole increases, and this help to rise the exit temperature off the borehole. Therefor, increasing the inlet temperature through the heat exchanger is a good option to reduce the exergy destruction in the borehole and help to get the right temperature in to the evaporator.

Heat pump

In order to investigate the performance of the working fluids, COP of the HP was calculated for each refrigerant according to equation 19. The results shows that the COP for R600a, R290, R717, and R1234ze(E) were 4.04, 4.13, 4.39, and 3.89, respectively, when the heat transfer in the condenser was set at 15 kW and the length of each borehole was 130 meters. Figure 8 illustrates how the mass flow rate of the refrigerant effects the COP.

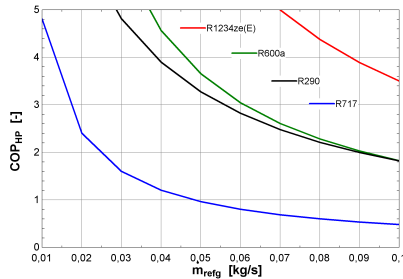


Figure 8: The COP of the HP with the different refrigerant when the mass flow rate is altered and the length of the borehole is set to 130 m.

The exergy destruction for the four components of the HP is presented in table 3.

Table 3: Calculated exergy destruction in each component of the HP for the different refrigerants

Component	R600a	R290	R717	R1234ze(E)
Evaporator [W]	259.0	260.9	267.8	245.0
Compressor [W]	1057.0	835.9	635,6	1140.0
Condenser [W]	243.3	273	599,5	252.5
Expansion valve [W]	504.4	607.7	245,3	577.0
Sum	2064.0	1978.0	1748.0	2215.0

R600a and R290 have the nearly the similar performance. This could be due to the fact that these two have nearly similar thermophysical properties. The R1234ze(E) HP generates the most exergy destruction, while R717 generates the least. The results also show that the compressor incurs the most significant exergy destruction, and stands for over 35% of the total exergy destruction. Figure 9 illustrates how subcooling of the refrigerant reduces the exergy destruction of the HP.

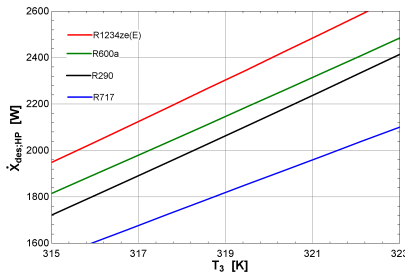


Figure 9: The total exergy destruction in the HP with variation in the outlet temperature of the condenser for each refrigerant.

Subcooling the refrigerants after the condenser has given positive result on the exergy destruction of the HP, and

is thus a strategy to implement in order to minimize the HP's total exergy destruction and the second order efficiency. In this study, the temperature out of the condenser is subcooled by 5K, and if this had not been done, the total exergy destruction would be increased by 17%.

Conclusion

The main purpose of this work was to investigate the performance of SGSHP for school building designed according to Norwegian passive house standard. EES was used to study the energy and exergy of the system.

When the SC produces excess heat, it can be directed to charge the borehole. This helps preventing thermal imbalance of the soil over time and increasing the borehole's outlet temperature. The inlet temperature of the SC has a substantial impact on the second order efficiency of the SC, and keeping a lower inlet temperature is generally preferable for the SC which is favorable for the cold climate in Norway.

For the borehole field, the optimal relation between the number of boreholes and length depend on the type of the grout material. The study shows, choosing a grout with high thermal conductivity is favorable in order to reduce the depth and number of boreholes, which is cost-beneficial.

R717 as a working fluid was found to achieve the best overall performance for the HP under the specified conditions, having the highest COP at 4.39 and lowest exergy destruction. The compressor stand for a significant part of the HP's exergy destruction, and it was discovered that subcooling the refrigerant after the condenser might reduce exergy destruction and improves the HP's overall performance.

In summary, SGSHP appear to be a well-suited energy system for heating school building in Norway under the conditions studied. Assumptions and simplifications have been made through the study, thus it's treated with caution.

Nomenclature

Greek letters Description

η_{th}	Thermal efficiency [-]
η_0	Optical efficiency [-]
$\eta_{II,SC}$	Second order efficiency-SC [-]
$\eta_{II,comp}$	Second order efficiency compressor [-]
$\eta_{II,cond}$	Second order efficiency condenser [-]
$\eta_{II,evap}$	Second order efficiency evaporator [-]
$\eta_{II,exp}$	Second order efficiency expansion valve [-]
ψ_1	Flow specific exergy at point 1 [kJ/kg]
ψ_2	Flow specific exergy at point 2 [kJ/kg]
ψ_3	Flow specific exergy at point 3 [kJ/kg]
ψ_4	Flow specific exergy at point 4 [kJ/kg]
Δ	Interval [-]

Abbreviation Explanation

COP	Coefficient of performance
EES	Engineering equation solver
GHX	Ground heat exchanger
GSHP	Ground source heat pump
GWP	Global warming potential
HP	Heat pump
HX	Heat exchanger
SC	Solar collector
SGSHP	Solar assisted ground source heat pump

Symbols Description

A	Area [m^2]
a_1	1st order heat loss coefficient [W/m^2K]
a_2	2nd order heat loss coefficient [W/m^2K^2]
$c_{p,SC,f}$	Heat capacity-working fluid in the SC [J/kgK]
$c_{p,ghx}$	Heat capacity of the brine [J/kgK]
D_b	diameter of the borehole [m]
$D_{ed,i}$	Equivalent inner diameter-borehole pipe [m]
$D_{ed,o}$	Equivalent outer diameter-borehole pipe [m]
G	Solar irradiance [W/m^2]
h_{brine}	Heat transfer coefficient-brine [W/m^2K]
h_1	Specific enthalpy at point 1 [J/kg]
h_{2a}	Specific enthalpy before the condenser [J/kg]
k_g	Thermal conductivity-grout [W/mK]
k_p	Thermal conductivity-borehole pipe [W/mK]
$L_{pipe,ghx}$	Length of the pipe in one borehole [m]
m_{brine}	Mass flow rate-brine [kg/s]
m_{SC}	Mass flow rate-SC working fluid [kg/s]
m_{refg}	Mass flow rate-refrigerant [kg/s]
$N_{boreholes}$	Number of boreholes [W]
Q_{cond}	Heat extracted in the condenser [W]
Q_{evap}	Heat extracted in the evaporator [W]
Q_{ground}	Heat extracted from the borehole field [W]
Q_i	Energy in to the solar system from the sun [W]
Q_{GHX}	Heat extracted from one boerhole [W]
q_{GHX}	Heat extracted from the borehole per meter [W/m]
R_{brine}	Thermal resistance-brine [mK/W]
R_{grout}	Thermal resistance-grout [mK/W]
R_{pipe}	Thermal resistance-pipe [mK/W]
s_1	Specif entropy at point 1 [J/kgK]
s_2	Specif entropy at point 2 [J/kgK]
s_3	Specif entropy at point 3 [J/kgK]
s_4	Specif entropy at point 4 [J/kgK]
T_a	Ambient temperature [K]
T_m	Mean temperature of the SC [K]
$T_{m,water}$	Mean temperature of the water in the condenser [K]
T_s	Mean temperature of the soil [K]
T_{sun}	Surface temperature of the sun [K]
T_0	Dead state temperature of the system [K]
T_6	Outlet temperature of the GHX [K]
T_7	Inlet temperature of the GHX [K]
T_{11}	Inlet temperature of the solar collector [K]
T_{12}	Outlet temperature of the solar collector [K]
U	Overall heat transfer coefficient [W/m^2K]
W_{comp}	Work in to the compressor [W]
$X_{des,comp}$	Exergy destruction-compressor [W]
$X_{des,cond}$	Exergy destruction-condenser [W]
$X_{des,evap}$	Exergy destruction-evaporator [W]
$X_{des,exp}$	Exergy destruction-expansion valve [W]
$X_{des,ghx}$	Exergy destruction-borehole field [W]
X_{in}	Exergy in to the system [W]
$X_{in,f}$	Exergy of the fluid in the inlet of the SC [W]
$X_{in,sr}$	Exergy due to the solar irradiance [W]
X_{in}	Exergy out of the system [W]
$X_{out,f}$	Exergy of the fluid in the outlet of the SC [W]

References

- Berardi, U. (2015). Building energy consumption in us, eu, and bric countries.
- byggforsk, S. (2018). 451.021 klimadata for termisk dimensjonering og frostsikring.
- CEN-EN12975-1 (2006). Thermal solar systems and components - solar collectors part 1: General requirements.
- Esen, H., M. Inalli, M. Esen, and K. Pihtili (2007). Energy and exergy analysis of a ground-coupled heat pump system with two horizontal ground heat exchangers.
- García-Menéndez, D., J. C. Ríos-Fernández, A. M. Blanco-Marigorta, and M. J. Suárez-López (2022). Dynamic simulation and exergetic analysis of a solar thermal collector installation.
- Girard, A., E. J. Gago, T. Muneer, and G. Caceres (2015). Higher ground source heat pump cop in a residential building through the use of solar thermal collectors.
- Guarracino, I., J. Freeman, A. Ramos, S. A. Kalogirou, N. J. Ekins-Daukes, and C. N. Markides (2019). Systematic testing of hybrid pv-thermal (pvt) solar collectors in steady-state and dynamic outdoor conditions.
- Hwang, J., D. Song, and T. Lee (2021). The effect of coupling solar thermal system and geothermal heat pump systems in areas with unbalanced heating and cooling demand.
- Madessa, H. B., T. B. P. F. Bye, and E. A (2017). Parametric study of a vertically configured ground source heat pump system.
- (2021). *Climate Change 2021: The Physical Science Basis. Contribution of Working Group I to the Sixth Assessment Report of the Intergovernmental Panel on Climate Change.*
- NS3701 (2012). Criteria for passive houses and low energy buildings - non-residential buildings.
- Razavi, S. H., R. Ahmadi, and A. Zahedi (2018). Modeling, simulation and dynamic control of solar assisted ground source heat pump to provide heating load and dhw.
- Reda, F. and A. Laitinen (2015). Different strategies for long term performance of sagshp to match residential energy requirements in a cold climate.
- SN-NSPEK3031 (2021). Energy performance og buildings- calculation of energy needs and energy supply.
- Software, F.-C. (2021). Engineering equation solver.
- Sørensen, Å. L., T. C. B. . N. H. K. (2017). Solvarme i kombinasjon med andre varmekilder. norsk solenergiforening.
- THERMIQUE, D. D. (2017). Solar installations - solar collectors, tanks and systems for individual and collective installations.
- UNFCCC (2015). The paris agreement.
- Yang, W., L. Sun, and Y. Sun (2015). Experimental investigations of the performance of a solar-ground source heat pump system operated in heating modes.
- Zijdemans, D. (2014). *Vannbaserte oppvarmings-og kjølesystemer.*

B Literature review - Articles

Table 24: Articles gathered in the literature review from Science Direct, Scopus and Web of Science

Mehrpanahi et al. "Extraction of optimal SAGSHP sizing based on the various control logic in specific climate condition," 2019.
Shamsabadi et al. "The design of a seasonal heat storage system with a geothermal heat pump for a residential building in Tehran," 2021.
Georgiev et al. "Investigation of a hybrid system with ground source heat pump and solar collectors: Charging of thermal storages and space heating," 2020.
Girard et al. "Higher ground source heat pump COP in a residential building through the use of solar thermal collectors," 2015.
Carbonell et al. " Simulations of Combined Solar Thermal and Heat Pump Systems for Domestic Hot Water and Space Heating," 2014.
Jonas et al. "Simulation and performance analysis of combined parallel solar thermal and ground or air source heat pump systems," 2017.
Taler et al. "Operation assessment of hybrid heat source for heating the building and preparation of hot water in the fire brigade building," 2019.
Rad et al. "Feasibility of combined solar thermal and ground source heat pump systems in cold climate, Canada," 2013.
Reda and Laitinen , "Different strategies for long term performance of SAGSHP to match residential energy requirements in a cold climate," 2015.
Nouri et al. "Designing and optimization of solar assisted ground source heat pump system to supply heating, cooling and hot water demands," 2019.
Fadejev et al. "Geothermal Heat Pump Plant Performance in a Nearly Zero-energy Building," 2016.
Hwang et al. "The Effect of Coupling Solar Thermal System and Geothermal Heat Pump Systems in Areas with Unbalanced Heating and Cooling Demand " 2021.
Huang et al. "Demonstration and optimization of a solar district heating system with ground source heat pumps," 2020.
Fong and Lee "Investigation on hybrid system design of renewable cooling for office building in hot and humid climate," 2014.
Bakirci et al. "Energy analysis of a solar-ground source heat pump system with vertical closed-loop for heating applications," 2011.
Lazzarin "Dual source heat pump systems: Operation and performance," 2012.
Cimmino and Eslami-Nejad "A simulation model for solar assisted shallow ground heat exchangers in series arrangement," 2017.
Lee et al. "Performance improvement of solar-assisted ground-source heat pumps with parallelly connected heat sources in heating-dominated areas," 2022.
Eslami-Nejad and Bernier "Coupling of geothermal heat pumps with thermal solar collectors using double U-tube boreholes with two independent circuits," 2011.

Si et al. " Performance evaluation and optimization of a novel solar-ground source heat pump system," 2014.
Reda "Long term performance of different SAGSHP solutions for residential energy supply in Finland," 2015.
Thygesen and Karlsson "Economic and energy analysis of three solar assisted heat pump systems in near zero energy buildings," 2013.
Elhashmi et al. "Low-energy opportunity for multi-family residences: A review and simulation-based study of a solar borehole thermal energy storage system," 2020.
Razavi et al."Modeling, simulation and dynamic control of solar assisted ground source heat pump to provide heating load and DHW," 2018.
Qu et al."Study of operational strategies for a hybrid solar-geothermal heat pump system," 2019.
Verma and Murugesan "Optimization of solar assisted ground source heat pump system for space heating application by Taguchi method and utility concept," 2014.
Verma and Murugesan "Experimental study of solar energy storage and space heating using solar assisted ground source heat pump system for Indian climatic conditions," 2017.
Verma and Murugesan"Experimental study of solar assisted ground source heat pump system during space heating operation from morning to evening," 2018.
Yang et al."Experimental investigations of the performance of a solar-ground source heat pump system operated in heating modes," 2015.
Duarte et al. "Feasibility of solar-geothermal hybrid source heat pump for producing domestic hot water in hot climates," 2021.
Gao et al."Designing and Optimizing Heat Storage of a Solar-Assisted Ground Source Heat Pump System in China," 2020.
Chen et al. "Dynamic modeling of solar-assisted ground source heat pump using Modelica," 2021.
Ji et al."Simplified method to determine the collector area of solar-assisted ground-source heat pump system," 2017.

C Gjennestad High School



Figure 44: Gjennestad High School

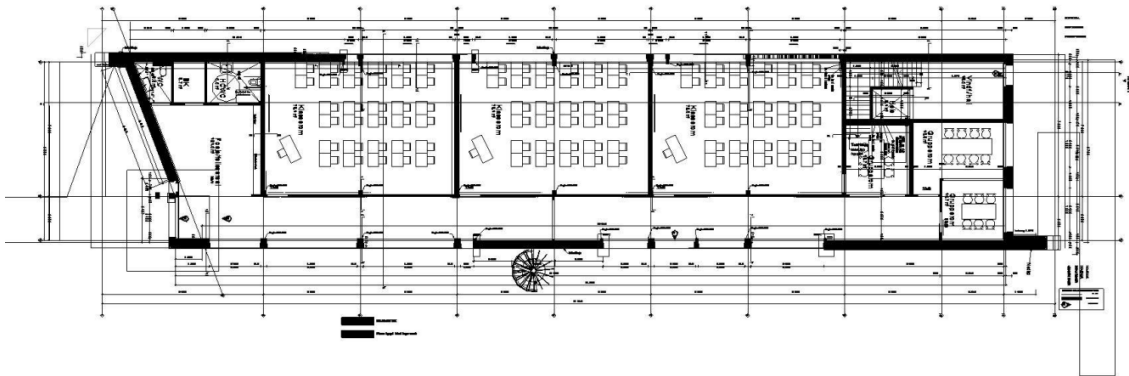


Figure 45: 1. floor of Gjennestad High School

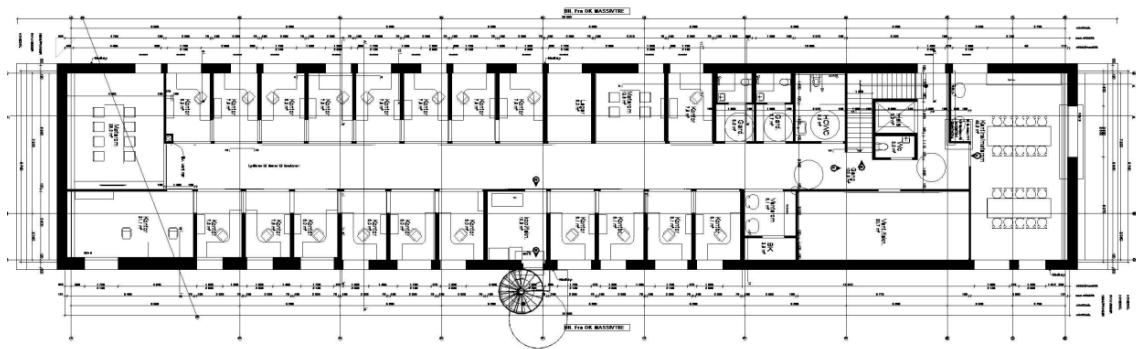


Figure 46: 2. floor of Gjennestad High School

D Data sheet for the solar collectors

DH 200 AND CH 250 FLAT SOLAR COLLECTORS

For DH 200/CH 250 flat collectors, serial connection is possible up to 10 collectors for installation on a roof or terrace. For installing more than 10 collectors, the hydraulic connection must be divided into branches connected in parallel in a

Tichelmann loop, with each branch having the same number of collectors. The fields will need to be balanced using balancing valves.

USES

All hot water production applications at temperatures < 80 °C with more or less regular requirements in case of pressurised systems, or irregular requirements in the case of self-draining systems, with heat-transporting fluid only.
In self-draining configuration, the collector field must be installed level, with no gradient on either side, to enable the heat exchangers to be drained. Some residual fluid will remain the manifold tube whenever circulation is stopped.

PACKAGE LIST

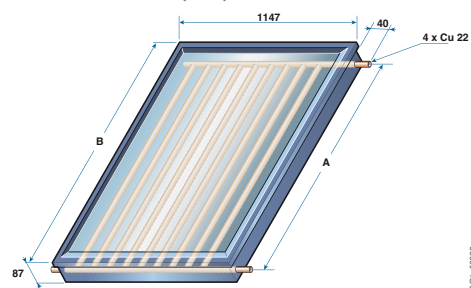
- 1 DH 200 flat collector: package ER646
- 1 CH 250 flat collector: package ER647

The collectors are delivered in an upright individual package on a pallet (up to 8 collectors).
The pallets delivered must be stored until the collectors are installed, in a dry, sun-free and aerated place with no risk of condensation.

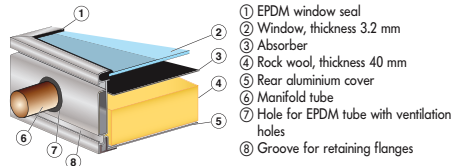
DESCRIPTION

- Flat glass high-efficiency solar collector for installation of up to 10 serial collectors, comprising:
- an anthracite grey coloured frame made from aluminium profiles with a fastening groove around the perimeter, and anticorrosion-treated aluminium base sheet,
 - a translucent glass safety window, thickness 3.2 mm and translucency > 91 %,
 - a flat aluminium absorber with selective coating and drainable sinusoidal heat exchanger connected to 2 Ø 22 mm manifold tubes for serial connection to 4 points in a bank,
 - rear and lateral rock wool insulation, thickness 40 mm.

MAIN DIMENSIONS (mm)



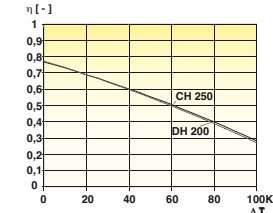
	A (mm)	B (mm)
DH 200	1 610	1 753
CH 250	2 044	2 187



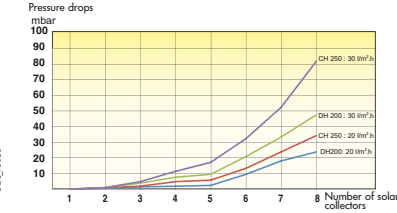
TECHNICAL SPECIFICATIONS

Collector		DH 200	CH 250
Overall surface area A_G	m^2	2.01	2.51
Inlet surface area A_a	m^2	1.92	2.40
Absorber area A_A	m^2	1.87	2.35
Fluid capacity	L	1.5	1.7
Recommended flow rate	$L/h.m^2$	30	30
Max. operating temperature	$^{\circ}C$	180	180
Stagnation temperature	$^{\circ}C$	198	198
Operating pressure	bar	2.5	2.5
Max. operating pressure	bar	10	10
Optical efficiency η_{0A}	%	0.770	0.765
Transfer loss coefficient a_{1A}	$W/m^2.K$	3.924	3.653
Transfer loss coefficient a_{2A}	$W/m^2.K^2$	0.011	0.012
Incidence angle factor K_{θ} for 50 °C	%	0.91	0.91
Net weight	kg	37	44

Efficiency curve

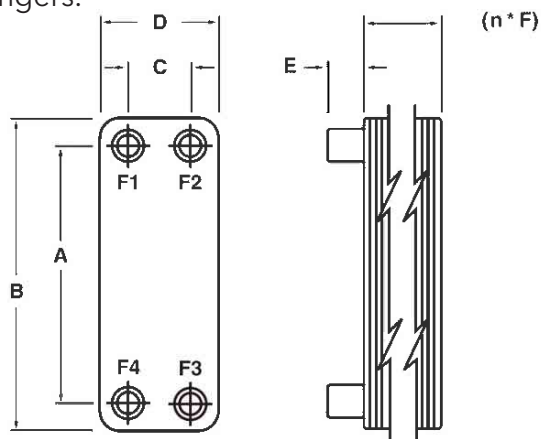


Pressure drop curve



E Data sheet for the heat exchanger

Copper Heat Exchangers.



Model Type	a	b	c	d	e	f	g	Connection	Volume Liter/channel	Weight (kgs.)	Max. # of plates
BP400	171.8	214.5	41.9	80.7	24.1	1.98	10.2	G3/4"	0.029	.06 x n + 1.18	50
BP405	354.8	397.5	41.9	80.7	24.1	1.98	10.2	G3/4"	0.059	0.11 x n + 1.60	75
BP410	249.7	309.6	50	112	24.1	2.462	10.2	G1"	0.060	0.13 x n + 1.60	150
BP411	249.7	309.6	50	112	24.1	2.462	10.2	G1"	0.060	0.13 x n + 1.60	150
BP412	249.7	309.6	50	112	24.1	2.462	10.2	G1"	0.060	0.13 x n + 1.60	150
BP415	465.7	525.4	50	112	24.1	2.462	10.2	G1"	0.103	0.23 x n + 2.04	150
BP422	518.5	616.8	91.9	190	48.2	2.921	10.2	G2"	0.266	0.44 x n + 7.00	200
BP423	518.5	616.8	91.9	190	48.2	2.921	10.2	G2"	0.266	0.44 x n + 7.00	200
BP424	518.5	616.8	91.9	190	48.2	2.921	10.2	G2"	0.266	0.44 x n + 7.00	200
BP432	622.3	892.1	211	430	88.8	2.898	31.02	DN 80 PN 25	0.815	0.95 x n + 71.70	250
BP433	863.5	1194	256	515	88.8	2.898	31.02	DN 100 PN 25	1.220	1.47 x n + 111.60	250
BP434	863.5	1194	256	515	88.8	2.898	31.02	DN 100 PN 25	1.220	1.47 x n + 111.60	250
BP435	863.5	1194	256	515	88.8	3.909	31.02	DN 100 PN 25	1.220	1.47 x n + 111.60	180

Dimensions in mm

n = number of plates

Typical Connection Locations (Side-1: F1 & F4, Side-2: F2 & F3)

Sensible Application (liquids or gases - no phase change)

- For all models the F2 - F3 side has one extra channel, ie. BP 410-10 has 4 channels on the F1 - F4 side and 5 on the F2 - F3 side.
- Liquid applications should be plumbed in a counter-current, parallel, flow arrangement, (for example: Hot in at F1/Hot out at F4; Cold in at F3/Cold out at F2). Hot and cold side in and out locations aren't critical as long as the piping is in a counter-current, parallel, flow arrangement. Unit may be mounted in any orientation.
- Connections may be on the front (ie. F1, F2, F3, F4) or back (ie. B1, B2, B3, B4) of the unit.

Phase Change Applications

- Units should be mounted in the vertical direction, similar to the figure above and plumbed with the vapor connection up and the liquid connection down on the phase change side see below.

Phase Change

Condensers	
Vapor In:	F1/B1
Condensate Out:	F4/B4
Liquid In:	F3/B3
Liquid Out:	F2/B2

Standard Materials

Cover Plate:	ASTM 316L stainless steel
Channel Plates:	ASTM 316L stainless steel
Connections:	ASTM 316L stainless steel
Brazing Material:	Copper

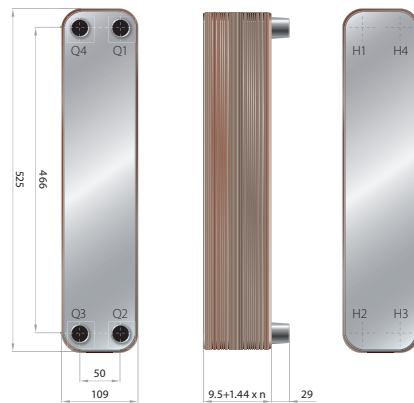
Design Specifications Copper Brazed

Design Pressure:	30 Bar.
Design Temperature:	232°C.
	-190°C.

F Data sheet for the condenser



H55-C Heat pump Condenser Micro Plate Heat Exchanger



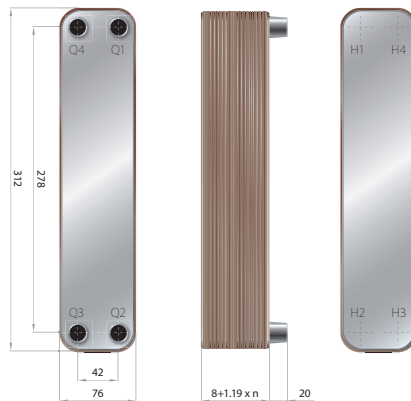
Introduction	Condenser optimised for R407C in high efficiency residential heat pumps with capacities between 4-40 kW. The heat exchanger features innovative Micro Plate technology that improves heat transfer and reduces the amount of material used. To meet demands for higher COPs in heat pumps, the H55-C is designed to work efficiently with close temperature approaches. The low hold-up volume reduces the refrigerant charge and offers valuable savings.	
Key features	<ul style="list-style-type: none"> • Minimal hold up volume: Less refrigerant charge • High heat transfer: For a more efficient heat pump • Smaller footprint: Enabling more compact heat pumps • Reduced CO₂ footprint: Environmentally friendly with high heat transfer and minimal refrigerant charge. 	
Technical data n = number of plates	Min. working temperature: -190 °C Max. working temperature: 200 °C Max. working pressure: 30 bar Hold up volume Q1-Q2/Q3-Q4 (l): $0.061 \times n / 2 + 0.061 \times (n-2) / 2$ Weight (kg): $2.32 + 0.135 \times n$	
Standard materials	Cover plates: AISI 304 Connections: AISI 304 Other material combinations are available on request. Please contact your Danfoss sales representative for more information.	Plates: AISI 316 Brazing filler: Pure copper Max. no. of plates: 150
Standard connections	Standard connections as per below are optimised for this product as condenser in heat pump system. For other connections, please contact your Danfoss representative. Q3 (Refrigerant outlet): soldering 1/2", 5/8" or 7/8" Q4 (Refrigerant inlet): soldering 1/4", 3/8" or 5/8" Q1-Q2 (Brine side): External threaded G 1"	
Third party approvals	Europe: Pressure Equipment Directive (PED), America: Underwriters Laboratory Inc (UL). The third party approvals stated are standard for all our products. For details of other existing approvals or to discuss how we can meet your local needs, please contact your Danfoss representative.	
Accessories – stud bolts	Stud bolts on front and/or back plates for mounting support are available upon request. Please contact your Danfoss sales representative for further information.	
Corresponding evaporator	A corresponding MPHE for evaporator duties (H55-E) is also available, fully tested and ready for heat pump applications	

Danfoss can accept no responsibility for possible errors in catalogues, brochures and other printed material. Danfoss reserves the right to alter its products without notice. This also applies to products already on order provided that such alterations can be made without consequential changes being necessary in specifications already agreed. All trademarks in this material are property of the respective companies. Danfoss and the Danfoss logotype are trademarks of Danfoss A/S. All rights reserved.

G Data sheet for the evaporator



H22-E Heat pump Evaporator Micro Plate Heat Exchanger



Introduction	Evaporator optimised for R407C in small high-efficiency residential ground source heat pumps with capacities between 2-8 kW. The heat exchanger features innovative Micro Plate technology that improves heat transfer and reduces the amount of material used. To meet demands for higher COPs in heat pumps, the H22-E is designed to work efficiently with close temperature approaches, while a low pressure drop on the brine side reduces the pump power and keeps the overall COP high. The low hold-up volume reduces the refrigerant charge and offers valuable savings.	
Key features	<ul style="list-style-type: none"> • Minimal hold-up volume: Less refrigerant charge • Reduced pressure drop: For a more efficient heat pump • Smaller footprint: Enabling more compact heat pumps • Reduced CO₂ footprint: Environmentally friendly with high heat transfer and minimal refrigerant charge. 	
Technical data n = number of plates	Min. working temperature: -196 °C Max. working temperature: 200 °C Max. working pressure: 30 bar Hold-up volume Q1Q2/ Q3-Q4 (l): $0.021 \times n / 2$ / $0.021 \times (n-2) / 2$ Weight (kg): $0.58 + 0.045 \times n$	
Standard materials	Cover plates: AISI 304 Connections: AISI 304 Other material combinations can be provided upon request. Please contact your Danfoss sales representative for more information.	Plates: AISI 316 Brazing filler: Pure copper
Standard connections	The standard connections below are optimised for this product as an evaporator in heat pump systems. For other connections, please contact your Danfoss representative. Q3 (Refrigerant inlet): soldering 1/4", 3/8" or 1/2" Q4 (Refrigerant outlet): soldering 1/2", 3/4" or 7/8" Q1-Q2 (Brine side): External threaded G 3/4"	
Third-party approvals	Europe: Pressure Equipment Directive (PED). America: Underwriters Laboratory Inc (UL). The third-party approvals stated are standard for all our products. For details of other existing approvals or to discuss how we can meet your local needs, please contact your Danfoss representative.	
Accessories – stud bolts	Stud bolts on front and/or back plates for mounting support are available upon request. Please contact your Danfoss sales representative for more information.	
Corresponding condensers	A corresponding Micro Plate heat exchanger for condenser duties (H22-C) is also available, fully tested and ready for heat pump applications.	

Danfoss can accept no responsibility for possible errors in catalogues, brochures and other printed material. Danfoss reserves the right to alter its products without notice. This also applies to products already on order provided that such alterations can be made without consequential changes being necessary in specifications already agreed. All trademarks in this material are property of the respective companies. Danfoss and the Danfoss logo are trademarks of Danfoss A/S. All rights reserved.

H Formulas implemented in EES

H.1 Nusselt correlation for R290 and R600a

Lockhart-Martinelli parameter's general definition:

$$X = \sqrt{\frac{(\frac{dP}{dz})_f}{(\frac{dP}{dz})_g}} \quad (95)$$

where

$$-(\frac{dP}{dz})_f = \frac{2f_f v_f G^2 (1-x)^2}{D_h} \quad (96)$$

and

$$-(\frac{dP}{dz})_g = \frac{2f_g v_g G^2 x^2}{D_h} \quad (97)$$

Mass flux in a circular pipe:

$$G = \frac{\dot{m}_{refg}}{\pi D^2} \quad (98)$$

To determine the frictions factors f_f and f_g the Reynolds number for the liquid and vapor phase is implemented.

$$Re_f = \frac{G(1-x)D_h}{\mu_f} \quad (99)$$

$$Re_g = \frac{GxD_h}{\mu_g} \quad (100)$$

For $Re_k > 20,000$ the friction factors is given by

$$f_k = 0.046 Re_k^{-0.2} \quad (101)$$

k detonates f for fluid and g for vapor.

$$C = 0,39 Re_{fo}^{0,03} Su_{go}^{0,10} (\frac{\rho_f}{\rho_g})^{0,35} \quad (102)$$

$$Su = \frac{\rho_g \sigma D_h}{\mu_g^2} \quad (103)$$

H.2 Nusselt correlation for R717 and R1234ze(E)

$$J_g = \frac{xG}{(gD\rho_g(\rho_f - \rho_g))^{0,5}} \quad (104)$$

$$Z = (\frac{1}{x} - 1)^{0,8} p_r^{0,4} \quad (105)$$

$$p_r = \frac{P}{P_c} \quad (106)$$

$$J_g \geq 0,98(Z + 0,263)^{-0,62} \quad (107)$$

I EES SC model

File:C:\Users\s351343\Downloads\SC.EES

24.05.2022 17:04:51 Page 1

EES Ver. 10.836: #3911: For use only by the Department of Civil Engineering and Energy Technology, HiOA

"Solar collector system"
_____ "

"Parameters"
_____ "

T_a=293 [K]
"Ambient temperature"

T_s=5778 [K]
"The black body temperature of the sun"

R_f_sun=**foulingfactor**("Ethylene glycol solution")
"Fouling factor of the working fluid in the SC"

C_EG=35 [%]
"Ethylene Glycol-Water, 35% mixture"

beta_SC=35 [deg]
"Surface tilt angle of the SC"

phi_SC=60 [deg]
"Latitude of Oslo"

A=2,51 [m^2]
"Total are for one SC - Data sheet"

A_aa_SC= 2,35 [m^2]
"Aperature area of one SC - Datas heet"

P=250000 [Pa]
"Operation pressure - Data sheet"

G=700 [W/m^2]
"Solar irradiance"

c_p_solar=**cp**(EG;T=T_m;C=C_EG)
"Heat capacity of the working fluid in the SC"

"At the inlet of SC"
....."

T_11=313 [K]
h_11=**enthalpy**(EG;T=T_11;C=C_EG;P=P)

"At the outlet of SC"
....."

h_12=**enthalpy**(EG;T=T_12;C=C_EG;P=P)
T_12=343 [K]

"Mass balance"
_____ "

m_dot_SC=0,02 [kg/s]
"Mass flow rate inside one solar collector - Data sheet"

m_dot_10=m_dot_11

m_dot_11=m_dot_12

m_dot_12=m_dot_13

m_dot_13=m_dot_solar_f

m_dot_solar_f=m_dot_SC*N_SC
"The total mass flow rate in the solar system"

File:C:\Users\s351343\Downloads\SC.EES 22.05.2022 14:41:49 Page 2
 EES Ver. 10.836: #3911: For use only by the Department of Civil Engineering and Energy Technology, HiOA

$m_{dot_11} = m_{dot_12}$
 $m_{dot_12} = m_{dot_13}$
 $m_{dot_13} = m_{dot_solar_f}$
 $m_{dot_solar_f} = m_{dot_SC} * N_{SC}$
 "The total mass flow rate in the solar system"
 "Thermal efficiency"
 $eta_{SC} = eta_0 - ((a_1 * (T_m - T_a)) / G) - (a_2 * (T_m - T_a)^2) / G$
 "Thermal efficiency of the SC"
 $T_m = (T_{11} + T_{12}) / 2$
 "Mean temperature of working fluid the SC"
 $eta_0 = 0,765$
 "Optical efficiency of the SC - Data sheet"
 $a_1 = 3,653 \text{ [W/m}^2\text{-K]}$
 "First order heat loss coefficient of the SC - Data sheet"
 $a_2 = 0,012 \text{ [W/m}^2\text{-K}^2]$
 "Second order heat loss coefficient of the SC - Data sheet"
 "Total Aperature area"
 $Q_u = F_R * A_{aa} * (G * (\tau * \alpha) - U_L * (T_m - T_a))$
 "The usefule energy collected from the SC"
 $N_{SC} = A_{aa} / A_{aa_SC}$
 "Number of solar collectors in the system"
 $A_{tot_SC} = N_{SC} * A$
 "Total area of the SC"
 $F_R = 0,8$
 "Heat removal factor"
 $\tau = 0,8$
 "Transmittance of the cover on the SC"
 $\alpha = 0,8$
 "Absorbance of the cover on the SC"
 $U_L = 7 \text{ [W/m}^2\text{-K]}$
 "Heat loss coeficcient"
 $Q_u = 510,6 \text{ [W]}$
 "The SC is dimensioned based on 60% of the DHW demand"
 "Energy to water tank"
 $Q_{dot_tank} = m_{dot_coil} * (h_{13} - h_{10})$
 "Energy transfer in the coil inside the water tank"
 $m_{dot_coil} = m_{dot_solar_f}$
 $h_{13} = h_{12}$
 $h_{10} = h_{11}$
 "Exergy of SC"

File:C:\Users\s351343\Downloads\SC.EES 22.05.2022 14:41:49 Page 3
EES Ver. 10.836: #3911: For use only by the Department of Civil Engineering and Energy Technology, HiOA

_____"
 $X_{\dot{i}} - X_{\dot{o}} - X_{\dot{s}} - X_{\dot{des}} = 0$
"Exergy balance"
 $X_{\dot{s}} = 0$
"Stored energy under steady state conditions"
 $X_{\dot{i}} = X_{\dot{i}_f} + X_{\dot{i}_{sr}}$
"Total exergy in to SC"
 $X_{\dot{i}_f} = \dot{m}_{solar} \cdot C_{p,sun} \cdot (T_{11} - T_a - T_a \cdot \ln(T_{11}/T_a))$
"Fluid exergy in to SC"
 $X_{\dot{i}_{sr}} = Q_{\dot{i}} \cdot (1 - (4/3) \cdot (T_a/T_s) + (1/3) \cdot (T_a/T_s)^4)$
"Exergy due to energy from the solar radiation in to SC"
 $Q_{\dot{i}} = G \cdot A_{aa} \cdot \tau \cdot \alpha$
"Total energy on the SC from the sun"
 $X_{\dot{o}} = \dot{m}_{solar} \cdot C_{p,sun} \cdot (T_{12} - T_a - T_a \cdot \ln(T_{12}/T_a))$
"Exergy out of the SC due to the fluid"
 $\eta_{II,SC} = (X_{\dot{o}} - X_{\dot{i}_f}) / X_{\dot{i}_{sr}}$
"Second law efficiency of SC"

J EES GHX model

File:C:\Users\s351343\Downloads\GHX-final.EES

16.05.2022 12:33:44 Page 1

EES Ver. 10.836: #3911: For use only by the Department of Civil Engineering and Energy Technology, HiOA

```

"
Ground heat exchanger model
"

"Parameters
"

"Dead state
....."

T_0=279,3 [K]
"The mean temperature in Oslo"

P_0=101000 [Pa]
"Dead state pressure at 1 atm"

h_0=enthalpy(EG;T=T_0;C=C_EG;P=P_0)
"Dead state enthalpy"

"Soil
....."

T_s=T_0+1,5[K]+2,5[K]
"Soil temperature, Madessa et al."

"Grout
....."

T_g=282,5 [K]
k_g=conductivity(Water;T=T_g;P=P_borehole)
cp=cp(Water;T=T_g;P=P_borehole)
rho_w=density(Water;T=T_g;P=P_borehole)

"Brine
....."

C_EG=35 [%]
T_F=freezingpt(EG;C=C_EG)
P_borehole=200000 [Pa]
T_m_brine=(T_6+T_7)/2
R_f_brine=foulingfactor('Ethylene glycol solution')
Pr_GHX=prandtl(EG;T=T_5;C=C_EG)
k_GHX=conductivity(EG;T=T_5;C=C_EG)
mu_GHX=viscosity(EG;T=T_5;C=C_EG)
rho_GHX=density(EG;T=T_5;C=C_EG)
c_p_brine_6=cp(PG;T=T_6;C=C_EG)
h_6=enthalpy(EG;T=T_6;C=C_EG;P=P_borehole)
c_p_brine_7=cp(EG;T=T_7;C=C_EG)
h_7=enthalpy(EG;T=T_7;C=C_EG;P=P_borehole)
c_p_brine_m=cp(EG;T=T_m_brine;C=C_EG)

"Heat exchanger sun side
....."

T_m_HX_solar=(T_14+T_15)/2
P_solar=250000 [Pa]
T_14=343 [K]
T_15=313 [K]
m_dot_solar_f=0,027 [kg/s]
R_f_solar=foulingfactor('Ethylene glycol solution')
rho_HX_solar=density(EG;T=T_m_HX_solar;C=C_EG)
Pr_HX_solar=prandtl(EG;T=T_m_HX_solar;C=C_EG)
mu_HX_solar=viscosity(EG;T=T_m_HX_solar;C=C_EG)

```

File:C:\Users\s351343\Downloads\GHX-final.EES 16.05.2022 12:33:44 Page 2
 EES Ver. 10.836: #3911: For use only by the Department of Civil Engineering and Energy Technology, HiOA

c_p_HX_solar=cp(EG;T=T_m_HX_solar;C=C_EG)
 k_HX_solar=conductivity(EG;T=T_m_HX_solar;C=C_EG)
 h_15=enthalpy(EG;T=T_15;C=C_EG;P=P_solar)
 h_14=enthalpy(EG;T=T_14;C=C_EG;P=P_solar)

"Heat exchanger ground side

....."
 T_m_HX_brine=(T_7+T_5)/2
 T_5=275 [K]
 rho_HX_brine=density(EG;T=T_m_HX_brine;C=C_EG)
 Pr_HX_brine=prandtl(EG;T=T_m_HX_brine;C=C_EG)
 mu_HX_brine=viscosity(EG;T=T_m_HX_brine;C=C_EG)
 c_p_HX_brine=cp(EG;T=T_5;C=C_EG)
 k_HX_brine=conductivity(EG;T=T_m_HX_brine;C=C_EG)
 h_5=enthalpy(EG;T=T_5;C=C_EG;P=P_borehole)

"Mass balance

....."
 m_dot_GHX=0,5 [kg/s]
 "Mass flow rate of the brine in one borehole"
 m_dot_6=m_dot_7
 m_dot_7=m_dot_brine
 m_dot_brine=N_borehole*m_dot_GHX
 "Total mass flow rate of the brine in the borehole field"

"Temperature out of the GHX

....."
 D_b=0,11 [m]
 "Diameter of the borehole"
 D_pipe_o=0,04 [m]
 "Outer diameter of the pipe inside the GHX"
 k_pipe_GHX=0,35 [W/m*K]
 "Thermal conductivity of the pipe in the GHX"
 L_pipe_GHX=130 [m]
 "Length of the borehole"
 N_tube=2
 "Number of tubes in one borehole, singel U-tube"
 T_6=T_s-(T_s-T_7)*exp(-1/(m_dot_GHX*c_p_brine_6*R_tot/L_pipe_GHX))
 "Temperature in to the evaporator from the GHX"
 R_tot=R_grout+R_pipe+R_brine
 R_grout=(ln(D_b/D_ed_o))/(2*PI*k_g)
 "Thermal resistance in the grout, only conductive heat transfer considered"
 R_pipe=(ln(D_ed_o/D_ed_i))/(2*PI*k_pipe_GHX)
 "Thermal resistance of the pipe"
 R_brine=1/(PI*D_ed_i*h_ghx)
 "Thermal resistance of the brine"
 Nu_GHX=(h_GHX*D_pipe_i)/k_GHX
 "Average Nusselt number for the brine in the ghxr"
 Nu_GHX=(z_1*(f_GHX/8)*(Re_GHX-z_2)*Pr_GHX)/(1+z_3*sqrt(f_GHX/8)*(Pr_GHX^(2/3)-1))
 "The nussel number correlation from Sándhez-Escalona et al. (2021) for the brine in the GHX"

File:C:\Users\s351343\Downloads\GHX-final.EES 16.05.2022 12:33:44 Page 3
 EES Ver. 10.836: #3911: For use only by the Department of Civil Engineering and Energy Technology, HiOA

z_1=0,8761
 z_2=147,3
 z_3=10,3

f_GHX=(1,82*log10((Re_GHX)-1,64))⁽⁻²⁾
 "Filonenko model of the friction factor"

Re_GHX=(rho_GHX*v_avg_GHX*D_pipe_i)/mu_GHX
 "Average Reynolds number for the brine in the GHX"

v_avg_GHX=(m_dot_GHX/rho_GHX)/(PI*D_pipe_i²/4)
 "Average velocity of the brine in the GHX"

D_pipe_i=0,032[m]
 "Inner diameter of the pipe inside the GHX"

D_ed_o=sqrt(N_tube)*D_pipe_o
 "Ekvivalent outer diameter of the pipe in the GHX, by Gu and O'Neal"

D_ed_i=sqrt(N_tube)*D_pipe_i
 "Ekvivalent inner diameter of the pipe in the GHX, by Gu and O'Neal"

"Heat extracted from the GHX "

q_GHX=(T_s-T_6)/(R_tot)
 "Heat flux of the borehole"

Q_dot_GHX=q_GHX*L_pipe_GHX
 "Total heat extracted from one borehole"

N_borehole=Q_dot_ground/Q_dot_GHX
 "Number of required boreholes"

Q_dot_ground=Q_dot_evap
 "Energy needed from the GHX to the HP"

Q_dot_evap=11332 [W]
 "The needed energy transfer in the evaporator collected from the R290 HP model"

"Circulation pump "

W_pump=DELTA_P_pump*(m_dot_brine/rho_GHX)
 "Work done by the circulation pumpe"

DELTA_P_pump=(P_evap-P_borehole)
 "The pressure difference before and after the pump"

P_evap=430514 [Pa]
 "Pressure in the evaporator collected from R290 HP model"

"Exergy "

X_dot_i=m_dot_brine*c_p_brine_7*(T_7-T_s-T_s*ln(T_7/T_s))
 "exergy in to the system"

X_dot_o=m_dot_brine*c_p_brine_6*(T_6-T_s-T_s*ln(T_6/T_s))
 "Exergy out of the system"

eta_II_borehole=X_dot_o/X_dot_i
 "Second order thermal efficiency of the SC system"

X_dot_des_borehole=m_dot_brine*(DELTA_psi_76)+Q_dot_ground*(1-T_0/T_s)
 "Exergy destruction of the borehole"

File:C:\Users\s351343\Downloads\GHX-final.EES 16.05.2022 12:33:44 Page 4
 EES Ver. 10.836: #3911: For use only by the Department of Civil Engineering and Energy Technology, HiOA

DELTA_psi_76=(h_7-h_6)-T_0*(c_p_brine_m*ln(T_7/T_6))
 "Spesifix flow exergy where entropy change for pure substanses is employed"

"Area heat exchanger "

"Components values
"

D_pipe_HX=0,01576 [m]
 "Inner diameter for the pipes inside the HX"

d_plate=0,00198 [m]
 "Plate thickness of the heat exchanger, data sheet for BP400 Lowara"

lambda_HX_wall=386 [W/m-K]
 "Thermal conductivity of the heat exchanger with plates with cobber brazing"

"Main equations
"

A_HX=Q_dot_HX/(U_HX*deltaT_lm)
 "Newton's Law of cooling"

Q_dot_HX=m_dot_solar*f*(h_14-h_15)
 "Heat extracted in the HX"

DELTA_T_lm=((T_14-T_7)-(T_15-T_5))/ln((T_14-T_7)/(T_15-T_5))
 "The logarithmic mean temperature in the HX"

U_HX=1/((1/h_solar)+R_f_solar+(d_plate/lambda_HX_wall)+R_f_brine+(1/h_brine))
 "The overall heat transfer in the HX"

"Nusselt correlation for working fluid in the SC in the heat exchanger
"

h_solar=(Nus_solar*k_HX_solar)/D_pipe_HX
 "Average Nusselt number for the working fluid in the SC system in the HX"

Nus_solar=(z_1*(f_solar/8)*(Re_solar-z_2)*Pr_HX_solar)/(1+z_3*sqrt(f_solar/8)*(Pr_HX_solar^(2/3)-1))
 "The nussel number correlation from Sándhez-Escalona et al. (2021)"

f_solar=(1,82*log10(Re_solar)-1,64)^(-2)
 "Filonenko model of the friction factor"

Re_solar=(rho_HX_solar*v_avg_solar*D_pipe_HX)/mu_HX_solar
 "Average Reynoldsnumber number"

v_avg_solar=(m_dot_solar_f/rho_HX_solar)/((PI*D_pipe_HX^2)/4)
 "Avaregae velocity"

"Nusselt correlation for brine in the heat exchanger
"

h_brine=(Nus_brine*k_HX_brine)/D_pipe_i
 "Average Nusselt number for the brine in the HX"

Nus_brine=(0,8761*(f_brine/8)*(Re_brine-147,3)*Pr_HX_brine)/(1+10,3*sqrt(f_brine/8)*(Pr_HX_brine^(2/3)-1))
 "The nussel number correlation from Sándhez-Escalona et al. (2021) for the brine in the evaporator"

f_brine=(1,82*log10(Re_brine)-1,64)^(-2)
 "Filonenko model of the friction factor"

File:C:\Users\s351343\Downloads\GHX-final.EES 16.05.2022 12:33:44 Page 5
 EES Ver. 10.836: #3911: For use only by the Department of Civil Engineering and Energy Technology, HiOA

Re_brine=(rho_HX_brine*v_avg_brine*D_pipe_i)/mu_HX_brine
 "Average Reynolds number number"

v_avg_brine=(m_dot_brine/rho_HX_brine)/((PI*D_pipe_i^2)/4)
 "Average velocity"

T_7=((m_dot_solar_f*c_p_HX_solar*(T_14-T_15))/(m_dot_brine*c_p_HX_brine))+T_5
 "Temperature of the brine after the HX"

"Exergy heat exchanger "

X_dot_14+X_dot_5=X_dot_15+X_dot_7+X_dot_des_HX
 "Exergy balance in the HX"

"Exergy balance for each state
"

X_dot_5=(h_5-h_0)-T_0*DELTA_5
 DELTA_5=c_p_HX_brine*ln(T_5/T_0)

X_dot_7=(h_7-h_0)-T_0*DELTA_7
 DELTA_7=c_p_HX_brine*ln(T_7/T_0)

X_dot_14=(h_14-h_0)-T_0*DELTA_14
 DELTA_14=c_p_HX_solar*ln(T_14/T_0)

X_dot_15=(h_15-h_0)-T_0*DELTA_15
 DELTA_15=c_p_HX_solar*ln(T_15/T_0)

eta_II_HX=(T_0*ln(T_14/T_15)-(T_14-T_15))/(T_0*ln(T_14/T_7)-(T_14-T_7))
 "Second order thermal efficiency of the HX"

K EES HP model

K.1 R600a HP model

File:C:\Users\s351343\Downloads\HP R600a.EES 16.05.2022 12:52:44 Page 1
 EES Ver. 10.836: #3911: For use only by the Department of Civil Engineering and Energy Technology, HiOA

```

"
Heat Pump model - R600a
"

"Parameters
"

R$='R600a'
"Isobutane as the refrigerant in the HP"

R_f_refg=foulingfactor('Refrigerant liquids')
"Fouling factor of refrigerant in liquid state"

R_f_w=foulingfactor('Closed-loop treated water')
"Fouling factor of water"

R_f_brine=foulingfactor('Ethanol solution')
"Fouling factor of the brine"

C_EG= 35 [%]
"Ethylene- Glycol-Water, 35%mixture, as the brine in the GHX"

T_0=294 [K]
"Dead state temperature of the HP inside the school"

"Point 1: before compressor"

T_1=T_4+5 [K]
s_1=s_2s
h_1=enthalpy(R$;T=T_1;P=P_1)
s_1=entropy(R$;P=P_1;T=T_1)

"Point 2: before condenser"

P_2=P_3
h_2s=enthalpy(R$;P=P_2;s=s_2s)
s_2=entropy(R$;P=P_2;h=h_2a)
T_2=temperature(R$;s=s_2;h=h_2a)
h_2a=((h_2s-h_1))/eta_i+h_1

"Condenser"

T_sat_cond=323 [K]
P_sat_cond=pressure(R$;T=T_sat_cond;x=0,5)
Pr_cond_f=prandtl(R$;T=T_sat_cond;P=P_2)
mu_cond_f=viscosity(R$;T=T_sat_cond;x=0)
mu_cond_g=viscosity(R$;T=T_sat_cond;x=1)
nu_cond_f=kinematicviscosity(R$;T=T_sat_cond;x=0)
nu_cond_g=kinematicviscosity(R$;T=T_sat_cond;x=1)
rho_cond_f=density(R$;T=T_sat_cond;x=0)
rho_cond_g=density(R$;T=T_sat_cond;x=1)
sigma_cond=surfacetension(R$;T=T_sat_cond)
k_cond_refg=conductivity(R$;T=T_sat_cond;P=P_2)

T_8=323 [K]
T_9=303 [K]
T_m_w=(T_8+T_9)/2
P_heating= 60000 [Pa]
cp_w=cp(Water;T=T_m_w;P=P_heating)
Pr_cond_w=prandtl(Water;T=T_m_w;P=P_heating)
k_cond_w=conductivity(Water;T=T_m_w;P=P_heating)
mu_cond_w=viscosity(Water;T=T_m_w;x=0)
rho_cond_w=density(Water;T=T_m_w;x=0)

"Point 3: before expansion vavle"

```

File:C:\Users\s351343\Downloads\HP R600a.EES 16.05.2022 12:52:45 Page 2
 EES Ver. 10.836: #3911: For use only by the Department of Civil Engineering and Energy Technology, HiOA

```
h_3=h_4
s_3=entropy(R$;P=P_3;h=h_3)
x_3=0
T_3=T_sat_cond-5[K]
h_3=enthalpy(R$;T=T_3;x=x_3)
P_3=pressure(R$;T=T_3;x=x_3)
```

"Point 4: before evaporator"

```
P_4=P_sat_evap
P_4=P_1
T_4=T_5-5[K]
P_sat_evap=p_sat(R$;T=T_4)
s_4=entropy(R$;T=T_4;h=h_4)
```

"Evaporator"

```
T_m_evap=(T_1+T_4)/2
mu_evap_f=viscosity(R$;T=T_m_evap;x=0)
mu_evap_g=viscosity(R$;T=T_m_evap;x=1)
nu_evap_f=kinematicviscosity(R$;T=T_m_evap;x=0)
nu_evap_g=kinematicviscosity(R$;T=T_m_evap;x=1)
rho_evap_f=density(R$;T=T_m_evap;x=0)
rho_evap_g=density(R$;T=T_m_evap;x=1)
sigma_evap=surfacetension(R$;T=T_m_evap)
k_evap_refg=conductivity(R$;T=T_m_evap;P=P_4)
Pr_evap_f=prandtl(R$;T=T_m_evap;P=P_4)

T_5=275 [K]
T_m_evap_brine=(T_5+T_6)/2
cp_brine=cp(EG;T=T_m_w;C=C_EG)
k_evap_brine=conductivity(EG;T=T_m_evap_brine;C=C_EG)
mu_evap_brine=viscosity(EG;T=T_m_evap_brine;C=C_EG)
rho_evap_brine=density(EG;T=T_m_evap_brine;C=C_EG)
Pr_evap_brine=prandtl(EG;T=T_m_evap_brine;C=C_EG)
```

"Massbalance "

```
m_dot_1=m_dot_2
m_dot_2=m_dot_3
m_dot_3=m_dot_4
m_dot_4=m_dot_refg
```

"COP "

```
COP_carnot=(h_2s-h_3)/(h_2s-h_1)
"COP of a Carnot HP"
```

```
Q_dot_cond=15000 [W]
"The energy demand for the HP based on the energy calculations of the school"
```

```
m_dot_refg=Q_dot_cond/(h_2a-h_3)
"Mass flow rate of the refrigerant based on the heat transfer in the condenser"
```

```
W_dot_comp=m_dot_refg*(h_2a-h_1)
"The work input in the compressor"
```

```
COP_HP=Q_dot_cond/W_dot_comp
"COP of the HP"
```

```
eta_v/eta_i=(1+k_e*(((T_1-273[K])-18[K])/100[K]))*exp(a*(T_sat_cond/T_m_evap)+b)
"Pierre's correlation for isentropic volume and efficiency"
```

```
eta_v=k_1*(1+k_s*(((T_1-273[K])-18[K])/100[K]))*exp(k_2*(P_sat_cond/P_sat_evap))
```

File:C:\Users\s351343\Downloads\HP R600a.EES 16.05.2022 12:52:45 Page 3
 EES Ver. 10.836: #3911: For use only by the Department of Civil Engineering and Energy Technology, HiOA

"Pierre's constants for the chosen refrigerant
"

k_1=1,04
 k_2=-0,07
 k_s=0,15
 k_e=0,1
 a=-2,4
 b=2,88

"Area condenser
"

"Components values
"

D_pipe_w=0,028 [m]
 "Inner diameter for pipes with water - Datasheet "

D_pipe_HP=0,003 [m]
 "Inner diameter for the pipes inside the HP"

d_plate=0,00144 [m]
 "Plate thickness of the condenser - Data sheet"

mu_wall=**viscosity(Water;T=T_wall;x=0)**
 "The viscosity of the water by the wall in the condenser"

T_wall=(T_sat_cond+T_m_w)/2
 "The temperature of the wall in the condenser"

lambda_cond_wall=15 [W/m-K]
 "Thermal conductivity of the condenser with plates of stainless steel, Data sheet"

"Main equations
"

A_c=Q_dot_cond/(U_cond*DELTAT_lm_cond)
 "Newton's Law of cooling"

DELTAT_lm_cond=((T_2-T_8)-(T_3-T_9))/ln((T_2-T_8)/(T_3-T_9))
 "The logarithmic mean temperature in the condenser"

U_cond=1/((1/h_cond_refg)+R_f_refg+(d_plate/lambda_cond_wall)+R_f_w+(1/h_w))
 "The overall heat transfer in the condenser"

"Nusselt correlation for refrigerant
"

Nu_cond_refg=(h_cond_refg*D_pipe_HP)/k_cond_refg
 "Average Nusselt number for the refrigerant in the condenser"

Nu_cond_refg=0,04*(Re_cond_f)^0,69*(Pr_cond_f)^0,34*(phi_cond_g/X_tt_cond)
 "The nussel number correlation from Kim and Mudawar (2013)"

X_tt_cond=(mu_cond_f/mu_cond_g)^0,1*((1-x)/x)^0,9*(rho_cond_g/rho_cond_f)^0,5
 "Convensional turbulent-turbulent Lockhart-Martinelli parameter"

x=0,5
 "Flow quality of the refrigerant in the condenser"

phi_cond_g^2=1+C_cond*X_cond+X_cond^2
 "two-phase pressure drop multiplier based on gas flow"

X_cond^2=D_pz_f/D_pz_g
 "Lockhart-Martinelli parameter's general definition"

File:C:\Users\s351343\Downloads\HP R600a.EES 16.05.2022 12:52:45 Page 4
 EES Ver. 10.836: #3911: For use only by the Department of Civil Engineering and Energy Technology, HiOA

-D_pz_f=(2*f_cond_f*nu_cond_f*(G_cond)^2*(1-x)^2)/D_pipe_HP
 "Frictional pressuer gradient for the refrigerant in the liquid state"

-D_pz_g=(2*f_cond_g*nu_cond_g*(G_cond)^2*(x)^2)/D_pipe_HP
 "Frictional pressuer gradient for the refrigerant in the gaseous state"

Re_cond_f=((G_cond)*(1-x)*D_pipe_HP)/mu_cond_f
 "Superficial liquid Reynolds number of the refrigerant"

Re_cond_g=(G_cond*x*D_pipe_HP)/mu_cond_g
 "Superficial vapor Reynolds number of the refrigerant"

f_cond_f=0,046*(Re_cond_f)^(-0,2)
 "Friction factor of the refrigerant in the condenser in liquid state"

f_cond_g=0,046*(Re_cond_g)^(-0,2)
 "Friction factor of the refrigerant in the condenser in gaseous state"

C_cond=0,39*(Re_cond_fo)^0,03*(Su_cond_go)^0,1*(rho_cond_f/rho_cond_g)^0,35
 "The constant in the two-phase pressure drop multiplier for turbulet turbulent flow"

Su_cond_go=(rho_cond_g*sigma_cond*D_pipe_HP)/(mu_cond_g)^2
 "Surtman number of the refrigerant in gaseous state only"

Re_cond_fo=((G_cond)*D_pipe_HP)/mu_cond_f
 "Liquid only Reynolds number of the refrigerant"

G_cond=m_dot_refg/(PI*D_pipe_HP^2/4)
 "Mass velocity of the refrigerant in the condenser"

"Nusselt correlation for water
"

Nu_cond_w=(h_w*D_pipe_w)/k_cond_w
 "Average Nusselt number for the water in the condenser"

Nu_cond_w=0,4225*(Re_cond_w)^(0,733)*(Pr_cond_w)^(0,33)*(mu_cond_w/mu_wall)^(0,14)
 "The nussel number correlation from Zhang (2020)"

Re_cond_w=(rho_cond_w*v_avg_w*D_pipe_w)/mu_cond_w
 "Reynolds number for water in the condenser"

v_avg_w=(m_dot_w/rho_cond_w)/((PI*D_pipe_w^2)/4)
 "Average velocity of the water in the condenser"

m_dot_w=(Q_dot_cond)/(cp_w*(T_8-T_9))
 "Mass flow rate of the water through the condenser"

"Area evaporator
"

"Components values
"

d_plate_evap=0,00174 [m]
 "Plate thickness of the evaporator, data sheet for H55-C heat pump evaporator, Danfoss"

lambda_evap_wall=15 [W/m-K]
 "Thermal conductivity of the condenser with plates of stainless steel - Data sheet "

D_pipe_brine=0,028 [m]
 "Inner diamenter for pipes with brine into the evaporator- Data sheet "

File:C:\Users\s351343\Downloads\HP R600a.EES 16.05.2022 12:52:45 Page 5
 EES Ver. 10.836: #3911: For use only by the Department of Civil Engineering and Energy Technology, HiOA

```
"Main equations
....."

A_evap= Q_dot_evap/(U_evap*DELTAT_lm_evap)
"Newton's Law of cooling"

Q_dot_evap=m_dot_refg*(h_1-h_4)
"the useful heat obtained by the evaporator"

DELTAT_lm_evap=((T_6-T_1)-(T_5-T_4))/ln((T_6-T_1)/(T_5-T_4))
"The logarithmic mean temperature in the evaporator"

U_evap=1/((1/h_evap_refg)+R_f_refg+(d_plate_evap/lambda_evap_wall)+R_f_brine+(1/h_evap_brine))
"The overall heat transfer in the evaporator"

"Nusselt correlation for refrigerator in the evaporator
....."

Nu_evap_refg=(h_evap_refg*D_pipe_HP)/k_evap_refg
"Average Nusselt number for the refrigerant in the evaporator"

Nu_evap_refg=0,048*(Re_evap_f)^0,69*(Pr_evap_f)^0,34 *(phi_evap_g/X_tt_evap)
"The nussel number correlation from Kim and Mudawar (2013)"

X_tt_evap=(mu_evap_f/mu_evap_g)^0,1*((1-x)/x)^0,9*(rho_evap_g/rho_evap_f)^0,5
"Convensional turbulent-turbulent Lockhart-Martinelli parameter"

phi_evap_g^2=1+C_evap*X_evap+X_evap^2
"Two-phase pressure drop multiplier based on gas flow"

X_evap^2=D_pz_evap_f/D_pz_evap_g
"Lockhart-Martinelli parameter's general definition"

-D_pz_evap_f=(2*f_evap_f*nu_evap_f*(G_evap)^2*(1-x)^2)/D_pipe_HP
"Frictional pressuer gradient for the refrigerant in the liquid state"

-D_pz_evap_g=(2*f_evap_g*nu_evap_g*(G_evap)^2*(x)^2)/D_pipe_HP
"Frictional pressuer gradient for the refrigerant in the gaseous state"

Re_evap_f=((G_evap)*(1-x)*D_pipe_HP)/mu_evap_f
"Superficial liquid Reynolds number of the refrigerant"

Re_evap_g=(G_evap*x*D_pipe_HP)/mu_evap_g
"Superficial vapor Reynolds number of the refrigerant"

f_evap_f=0,046*(Re_evap_f)^(-0,2)
"Friction factor of the refrigerant in the condenser in liquid state"

f_evap_g=0,046*(Re_evap_g)^(-0,2)
"Friction factor of the refrigerant in the condenser in gaseous state"

C_evap=0,39*(Re_evap_fo)^0,03*(Su_evap_go)^0,1*(rho_evap_f/rho_evap_g)^0,35
"The constant in the two-phase pressure drop multiplier for turbulet turbulent flow"

Su_evap_go=(rho_evap_g*sigma_evap*D_pipe_HP)/(mu_evap_g)^2
"Surtman number of the refrigerant in gaseous state only"

Re_evap_fo=((G_evap)*D_pipe_HP)/mu_evap_f
"Liquid only Reynolds number of the refrigerant"

G_evap=m_dot_refg/(PI*D_pipe_HP^2/4)
"Mass velocity of the refrigerant in the evaporator"

"Nusselt correlation for brine in the evaporator
....."
```

File:C:\Users\s351343\Downloads\HP R600a.EES 16.05.2022 12:52:45 Page 6
 EES Ver. 10.836: #3911: For use only by the Department of Civil Engineering and Energy Technology, HiOA

```

h_evap_brine=(Nu_evap_brine*k_evap_brine)/D_pipe_brine
"Average Nusselt number for the brine in the evaporator"

Nu_evap_brine=(0,8761*(f_brine/8)*(Re_evap_brine-147,3)*Pr_evap_brine)/((1+10,3*sqrt(f_brine/8)*(Pr_evap_brine^(2/3)-1)))
"The nussel number correlation from Sándhez-Escalona et al. (2021) for the brine in the evaporator"

f_brine=(1,82*log10(Re_evap_brine)-1,64)^(-2)
"Filonenko model of the friction factor"

Re_evap_brine=(rho_evap_brine*v_avg_brine*D_pipe_brine)/mu_evap_brine
"Average Reynoldsnumber number for the brine in the evaporator"

v_avg_brine=(m_dot_brine/rho_evap_brine)/((PI*D_pipe_brine^2)/4)
"Avaregae velocity of the water in the condenser"

T_6=277,1 [K]
"Temperatur in to the evaporator from the GHX"

m_dot_brine=1,908 [kg/s]
"Mass flow of the brine in the evaporator, collected from the GHX model"

" Exergy "
....."

"Compressor
....."
eta_II_comp=1-(X_dot_des_comp/W_dot_comp)
"Second order thermal efficiency of the compressor"

X_dot_des_comp=T_0*m_dot_refg*(s_2-s_1)
"Exergy destruction in the compressor"

"Condenser
....."

eta_II_cond=1-(X_dot_des_cond)/(m_dot_refg*((h_2a-h_3)-T_0*(s_2-s_3)))
"Second order thermal efficiency of the condenser"

X_dot_des_cond=T_0*(m_dot_refg*(s_3-s_2)+(Q_dot_cond/T_m_w))
"Exergy destruction in the condenser"

"Expansion valve
....."

eta_II_exp=0
"Second order thermal efficiency of the expansion valve"

X_dot_des_exp=m_dot_refg*T_0*(s_4-s_3)
"Exergy destruction in the expansion valve"

"Evaporator
....."

eta_II_evap=1-(X_dot_des_evap)/(m_dot_refg*((h_4-h_1)-T_0*(s_4-s_1)))
"Second order thermal efficiency of the Evaporator"

X_dot_des_evap=T_0*(m_dot_refg*(s_1-s_4)-(Q_dot_evap/T_m_evap_brine))
"Exergy destruction in the evaporator"

X_dot_des_HP=X_dot_des_comp+X_dot_des_cond+X_dot_des_exp+X_dot_des_evap
"Total exergy destruction for the HP"

```

File:C:\Users\s351343\Downloads\HP R600a.EES

16.05.2022 12:52:45 Page 7

EES Ver. 10.836: #3911: For use only by the Department of Civil Engineering and Energy Technology, HiOA

K.2 R290 HP model

File:C:\Users\351343\Downloads\HP R290.EES 19.05.2022 10:00:30 Page 1
 EES Ver. 10.836: #3911: For use only by the Department of Civil Engineering and Energy Technology, HiOA

```
"
Heat Pump model - R290
"

"Parameters
"

R$='R290'
"Propane as the refrigerant in the HP"

R_f_refg=foulingfactor('Refrigerant liquids')
"Fouling factor of refrigerant in liquid state"

R_f_w=foulingfactor('Closed-loop treated water')
"Fouling factor of water"

R_f_brine=foulingfactor('Ethanol solution')
"Fouling factor of the brine"

C_EG= 35 [%]
"Ethylene- Glycol-Water, 35%mixture, as the brine in the GHX"

T_0=294 [K]
"Deat state temperature of the HP inside the school"

"Point 1: before compressor"

T_1=T_4+5[K]
s_1=s_2s
h_1=enthalpy(R$;T=T_1;P=P_1)
s_1=entropy(R$;P=P_1;T=T_1)

"Point 2: before condenser"

P_2=P_3

h_2s=enthalpy(R$;P=P_2;s=s_2s)
s_2=entropy(R$;P=P_2;h=h_2a)
T_2=temperature(R$;P=P_2;h=h_2a)
h_2a=((h_2s-h_1))/eta_i+h_1

"Condenser"

T_sat_cond=323 [K]
P_sat_cond=pressure(R$;T=T_sat_cond;x=0,5)
Pr=prandtl(R$;T=T_sat_cond;P=P_2)
mu_cond_f=viscosity(R$;T=T_sat_cond;x=0)
mu_cond_g=viscosity(R$;T=T_sat_cond;x=1)
nu_cond_f=kinematicviscosity(R$;T=T_sat_cond;x=0)
nu_cond_g=kinematicviscosity(R$;T=T_sat_cond;x=1)
rho_cond_f=density(R$;T=T_sat_cond;x=0)
rho_cond_g=density(R$;T=T_sat_cond;x=1)
sigma_cond=surfacetension(R$;T=T_sat_cond)
k_cond_refg=conductivity(R$;T=T_sat_cond;P=P_2)

T_8=323 [K]
T_9=303 [K]
T_m_w=(T_8+T_9)/2
P_heating= 60000 [Pa]
cp_w=cp(Water;T=T_m_w;P=P_heating)
Pr_cond_w=prandtl(Water;T=T_m_w;P=P_heating)
k_cond_w=conductivity(Water;T=T_m_w;P=P_heating)
mu_cond_w=viscosity(Water;T=T_m_w;x=0)
rho_cond_w=density(Water;T=T_m_w;x=0)
```

File:C:\Users\s351343\Downloads\HP R290.EES 19.05.2022 10:00:30 Page 2
 EES Ver. 10.836: #3911: For use only by the Department of Civil Engineering and Energy Technology, HiOA

"Point 3: before expansion valve"

```
h_3=h_4
s_3=entropy(R$,P=P_3;h=h_3)
x_3=0
T_3=T_sat_cond-5[K]
h_3=enthalpy(R$,T=T_3;x=x_3)
P_3=pressure(R$,T=T_3;x=x_3)
```

"Point 4: before evaporator"

```
P_4=P_sat_evap
P_4=P_1
T_4=T_5-5[K]
P_sat_evap=p_sat(R$,T=T_4)
s_4=entropy(R$,T=T_4;h=h_4)
```

"Evaporator"

```
T_m_evap=(T_1+T_4)/2
mu_evap_f=viscosity(R$,T=T_m_evap;x=0)
mu_evap_g=viscosity(R$,T=T_m_evap;x=1)
nu_evap_f=kinematicviscosity(R$,T=T_m_evap;x=0)
nu_evap_g=kinematicviscosity(R$,T=T_m_evap;x=1)
rho_evap_f=density(R$,T=T_m_evap;x=0)
rho_evap_g=density(R$,T=T_m_evap;x=1)
sigma_evap=surfacetension(R$,T=T_m_evap)
k_evap_refg=conductivity(R$,T=T_m_evap;P=P_4)
Pr_evap_f=prandtl(R$,T=T_m_evap;P=P_4)

T_5=275 [K]
T_m_evap_brine=(T_5+T_6)/2
cp_brine=cp(EG;T=T_m_evap_brine;C=C_EG)
k_evap_brine=conductivity(EG;T=T_m_evap_brine;C=C_EG)
mu_evap_brine=viscosity(EG;T=T_m_evap_brine;C=C_EG)
rho_evap_brine=density(EG;T=T_m_evap_brine;C=C_EG)
Pr_evap_brine=prandtl(EG;T=T_m_evap_brine;C=C_EG)
```

"Mass balance"

```
m_dot_1=m_dot_2
m_dot_2=m_dot_3
m_dot_3=m_dot_4
m_dot_4=m_dot_refg
```

"COP"

```
COP_carnot=(h_2s-h_3)/(h_2s-h_1)
"COP of a Carnot HP"
```

```
Q_dot_cond=15000 [J/s]
"The energy demand for the HP based on the energy calculations of the school"
```

```
m_dot_refg=Q_dot_cond/(h_2a-h_3)
"Mass flow rate of the refrigerant based on the heat transfer in the condenser"
```

```
W_dot_comp=m_dot_refg*(h_2a-h_1)
"The work input in the compressor"
```

```
COP_HP=Q_dot_cond/W_dot_comp
"COP of the HP"
```

```
eta_veta_i=(1+k_e*(((T_1-273[K])-18[K])/100[K]))*exp(a*(T_sat_cond/T_m_evap)+b)
"Pierre's correlation for isentropic volume and efficiency"
```

File:C:\Users\s351343\Downloads\HP R290.EES 19.05.2022 10:00:30 Page 3
 EES Ver. 10.836: #3911: For use only by the Department of Civil Engineering and Energy Technology, HiOA

$\text{eta_v} = k_1 * (1 + k_s * ((T_1 - 273[K]) - 18[K]) / 100[K]) * \exp(k_2 * (P_sat_cond / P_sat_evap))$

"Pierre's constants for the chosen refrigerant
"

k_1=1,04
 k_2=-0,07
 k_s=0,15
 k_e=-0,1
 a=-2,4
 b=2,88

"Area condenser
 _____"

"Components values
"

D_pipe_w=0,028 [m]
 "Inner diameter for pipes with water - Data sheet "

D_pipe_HP=0,003 [m]
 "Inner diameter for the pipes inside the HP"

d_plate=0,00144 [m]
 "Plate thickness of the condenser- Data sheet"

$\mu_{wall} = \text{viscosity}(\text{Water}, T=T_{wall}; x=0)$
 "The viscosity of the water by the wall in the condenser"

$T_{wall} = (T_{sat_cond} + T_{m_w}) / 2$
 "The temperature of the wall in the condenser"

lambda_cond_wall=15
 "Thermal conductivity of the condenser with plates of stainless steel- Data sheet "

"Main equations
"

$A_c = Q_{dot_cond} / (U_{cond} * \Delta T_{lm_cond})$
 "Newton's Law of cooling"

$\Delta T_{lm_cond} = ((T_2 - T_8) - (T_3 - T_9)) / \ln((T_2 - T_8) / (T_3 - T_9))$

$U_{cond} = 1 / ((1/h_{cond_refg}) + R_{f_refg} + (d_{plate} / \lambda_{cond_wall}) + R_{f_w} + (1/h_w))$
 "The overall heat transfer in the condenser"

"Nusselt correlation for refrigerant
"

$Nu_{cond_refg} = (h_{cond_refg} * D_{pipe_HP}) / k_{cond_refg}$
 "Average Nusselt number for the refrigerant in the condenser"

$Nu_{cond_refg} = 0,048 * (Re_{cond_f})^{0,69} * (Pr)^{0,34} * (\phi_{cond_g} / X_{tt_cond})$
 "The nusselt number correlation from Kim and Mudawar (2013)"

$X_{tt_cond} = (\mu_{cond_f} / \mu_{cond_g})^{0,1} * ((1-x)/x)^{0,9} * (\rho_{cond_g} / \rho_{cond_f})^{0,5}$
 "Convensional turbulent-turbulent Lockhart-Martinelli parameter"

x=0,5
 "Flow quality of the refrigerant in the condenser"

$\phi_{cond_g}^2 = 1 + C_{cond} * X_{cond} + X_{cond}^2$
 "Two-phase pressure drop multiplier based on gas flow"

$X_{cond}^2 = D_{pz_f} / D_{pz_g}$
 "Lockhart-Martinelli parameter's general definition"

File:C:\Users\s351343\Downloads\HP R290.EES 19.05.2022 10:00:30 Page 4
 EES Ver. 10.836: #3911: For use only by the Department of Civil Engineering and Energy Technology, HiOA

-D_pz_f=(2*f_cond_f*nu_cond_f*(G_cond)^2*(1-x)^2)/D_pipe_HP
 "Frictional pressuer gradient for the refrigerant in the liquid state"

-D_pz_g=(2*f_cond_g*nu_cond_g*(G_cond)^2*(x)^2)/D_pipe_HP
 "Frictional pressuer gradient for the refrigerant in the gaseous state"

Re_cond_f=((G_cond)*(1-x)*D_pipe_HP)/mu_cond_f
 "Superficial liquid Reynolds number of the refrigerant"

Re_cond_g=(G_cond*x*D_pipe_HP)/mu_cond_g
 "Superficial vapor Reynolds number of the refrigerant"

f_cond_f=0,046*(Re_cond_f)^(-0,2)
 "Friction factor of the refrigerant in the condenser in liquid state"

f_cond_g=0,046*(Re_cond_g)^(-0,2)
 "Friction factor of the refrigerant in the condenser in gaseous state"

C_cond=0,39*(Re_cond_fo)^0,03*(Su_cond_go)^0,1*(rho_cond_f/rho_cond_g)^0,35
 "The constant in the two-phase pressure drop multiplier for turbulet turbulent flow"

Su_cond_go=(rho_cond_g*sigma_cond*D_pipe_HP)/(mu_cond_g)^2
 "Surtman number of the refrigerant in gaseous state only"

Re_cond_fo=((G_cond)*D_pipe_HP)/mu_cond_f
 "Liquid only Reynolds number of the refrigerant"

G_cond=m_dot_refg/(PI*D_pipe_HP^2/4)
 "Mass velocity of the refrigerant in the condenser"

"Nusselt correlation for water
"

Nus_cond_w=(h_w*D_pipe_w)/k_cond_w
 "Average Nusselt number for the water in the condenser"

Nus_cond_w=0,4225*(Re_cond_w)^(0,733)*(Pr_cond_w)^(0,33)*(mu_cond_w/mu_wall)^(0,14)
 "The nussel number correlation from Zhang (2020)"

Re_cond_w=(rho_cond_w*v_avg_w*D_pipe_w)/mu_cond_w
 "Reynolds number for water in the condenser"

v_avg_w=(m_dot_w/rho_cond_w)/((PI*D_pipe_w^2)/4)
 "Average velocity of the water in the condenser"

m_dot_w=(Q_dot_cond)/(cp_w*(T_8-T_9))
 "Mass flow rate of the water through the condenser"

"Area evaporator
 _____"

"Components values
"

d_plate_evap=0,00174 [m]
 "Plate thickness of the evaporator- Data sheet"

lambda_evap_wall=15
 "Thermal conductivity of the condenser with plates of stainless steel- Data sheet"

D_pipe_brine=0,028 [m]
 "Inner diamenter for pipes with brine into the evaporator- Data sheet "

"Main equations

File:C:\Users\s351343\Downloads\HP R290.EES 19.05.2022 10:00:30 Page 5
 EES Ver. 10.836: #3911: For use only by the Department of Civil Engineering and Energy Technology, HiOA

```

....."
A_evap= Q_dot_evap/(U_evap*DELTA_T_lm_evap)
"Newton's Law of cooling"

Q_dot_evap=m_dot_refg*(h_1-h_4)
"The useful heat obtained by the evaporator"

DELTA_T_lm_evap=((T_6-T_1)-(T_5-T_4))/ln((T_6-T_1)/(T_5-T_4))
"The logarithmic mean temperature in the evaporator"

U_evap=1/((1/h_evap_refg)+R_f_refg+(d_plate_evap/lambda_evap_wall)+R_f_brine+(1/h_evap_brine))
"The overall heat transfer in the evaporator"

"Nusselt correlation for refrigerator in the evaporator
....."

Nus_evap_refg=(h_evap_refg*D_pipe_HP)/k_evap_refg
"Average Nusselt number for the refrigerant in the evaporator"

Nus_evap_refg=0,048*(Re_evap_f)^0,69*(Pr_evap_f)^0,34 *(phi_evap_g/X_tt_evap)
"The nussel number correlation from Kim and Mudawar (2013)"

X_tt_evap=(mu_evap_f/mu_evap_g)^0,1*((1-x)/x)^0,9*(rho_evap_g/rho_evap_f)^0,5
"Convensional turbulent-turbulent Lockhart-Martinelli parameter"

phi_evap_g^2=1+C_evap*X_evap+X_evap^2
"Two-phase pressure drop multiplier based on gas flow"

X_evap^2=D_pz_evap_f/D_pz_evap_g
" Lockhart-Martinelli parameter's general definition"

-D_pz_evap_f=(2*f_evap_f*nu_evap_f*(G_evap)^2*(1-x)^2)/D_pipe_HP
"Frictional pressuer gradient for the refrigerant in the liquid state"

-D_pz_evap_g=(2*f_evap_g*nu_evap_g*(G_evap)^2*(x)^2)/D_pipe_HP
"Frictional pressuer gradient for the refrigerant in the gaseous state"

Re_evap_f=((G_evap)*(1-x)*D_pipe_HP)/mu_evap_f
"Superficial liquid Reynolds number of the refrigerant"

Re_evap_g=(G_evap*x*D_pipe_HP)/mu_evap_g
"Superficial vapor Reynolds number of the refrigerant"

f_evap_f=0,046*(Re_evap_f)^(-0,2)
"Friction factor of the refrigerant in the condenser in liquid state"

f_evap_g=0,046*(Re_evap_g)^(-0,2)
"Friction factor of the refrigerant in the condenser in gaseous state"

C_evap=0,39*(Re_evap_fo)^0,03*(Su_evap_go)^0,1*(rho_evap_f/rho_evap_g)^0,35
"The constant in the two-phase pressure drop multiplier for turbulet turbulent flow"

Su_evap_go=(rho_evap_g*sigma_evap*D_pipe_HP)/(mu_evap_g)^2
"Surtman number of the refrigerant in gaseous state only"

Re_evap_fo=((G_evap)*D_pipe_HP)/mu_evap_f
"Liquid only Reynolds number of the refrigerant"

G_evap=m_dot_refg/(PI*D_pipe_HP^2/4)
"Mass velocity of the refrigerant in the evaporator"

"Nusselt correlation for brine in the evaporator
....."

```

```

File:C:\Users\s351343\Downloads\HP R290.EES
19.05.2022 10:00:30 Page 6
EES Ver. 10.836: #3911: For use only by the Department of Civil Engineering and Energy Technology, HiOA

h_evap_brine=(Nus_evap_brine*k_evap_brine)/D_pipe_brine
"Average Nusselt number for the brine in the evaporator"

Nus_evap_brine=(0,8761*(f_brine/8)*(Re_evap_brine-147,3)*Pr_evap_brine)/(1+10,3*sqrt(f_brine/8)*(Pr_evap_brine^(2/3)-1))
"The nussel number correlation from Sándhez-Escalona et al. (2021) for the brine in the evaporator"

f_brine=(1,82*log10(Re_evap_brine)-1,64)^(-2)
"Filonenko model of the friction factor"

Re_evap_brine=(rho_evap_brine*v_avg_brine*D_pipe_brine)/mu_evap_brine
"Average Reynoldsnumber number for the brine in the evaporator"

v_avg_brine=(m_dot_brine/rho_evap_brine)/((PI*D_pipe_brine^2)/4)
"Average velocity of the water in the condenser"

T_6=276,8 [K]
"Temperatur in to the evaporator from the GHX"

m_dot_brine=2 [kg/s]
"Mass flow rate of the brine in the evaporator, collected from the GHX model"

" Exergy "
_____

"Compressor
....."
eta_II_comp=1-(X_dot_des_comp/W_dot_comp)
"Second order thermal efficiency of the compressor"

X_dot_des_comp=T_0*m_dot_refg*(s_2-s_1)
"Exergy destruction in the compressor"

"Condenser
....."

eta_II_cond=1-(X_dot_des_cond)/(m_dot_refg*((h_2a-h_3)-T_0*(s_2-s_3)))
"Second order thermal efficiency of the condenser"

X_dot_des_cond=T_0*(m_dot_refg*(s_3-s_2)+(Q_dot_cond/T_m_w))
"Exergy destruction in the condenser"

"Expansion valve
....."

eta_II_exp=0
"Second order thermal efficiency of the expansion valve"

X_dot_des_exp=m_dot_refg*T_0*(s_4-s_3)
"Exergy destruction in the expansion valve"

"Evaporator
....."

eta_II_evap=1-(X_dot_des_evap)/(m_dot_refg*((h_4-h_1)-T_0*(s_4-s_1)))
"Second order thermal efficiency of the Evaporator"

X_dot_des_evap=T_0*(m_dot_refg*(s_1-s_4)-(Q_dot_evap/T_m_evap_brine))
"Exergy destruction in the evaporator"

X_dot_des_HP=X_dot_des_comp+X_dot_des_cond+X_dot_des_exp+X_dot_des_evap
"Total exergy destruction of the HP"

```

K.3 R717 HP model

File:C:\Users\s351343\Downloads\HP R717.EES 16.05.2022 12:59:23 Page 1
 EES Ver. 10.836: #3911: For use only by the Department of Civil Engineering and Energy Technology, HiOA

```
"
Heat Pump model - R717
"

"Parameters
"

R$=R717'
"Ammonia as the refrigerant in the HP"

R_f_refg=foulingfactor('Refrigerant liquids')
"Fouling factor of refrigerant in liquid state"

P_c=p_crit(R717)
"Critical pressure of the refrigerant"

R_f_w=foulingfactor('Closed-loop treated water')
"Fouling factor of water"

R_f_brine=foulingfactor('Ethanol solution')
"Fouling factor of the brine"

C_EG= 35 [%]
"Ethylene- Glycol-Water, 35%mixture, as the brine in the GHX"

T_0=294 [K]
"Dead state temperature of the HP inside the school"

"Point 1: before compressor"

T_1=T_4+5[K]
s_1=s_2s
h_1=enthalpy(R$;T=T_1;P=P_1)
s_1=entropy(R$;P=P_1;T=T_1)

"Point 2: before condenser"

P_2=P_3

h_2s=enthalpy(R$;P=P_2;s=s_2s)
s_2=entropy(R$;P=P_2;h=h_2a)
T_2=temperature(R$;s=s_2;h=h_2a)
h_2a=((h_2s-h_1)/eta_i+h_1

"Condenser"

T_sat_cond=323 [K]
T_m_cond=(T_2+T_3)/2
P_sat_cond=pressure(R$;T=T_sat_cond;x=0,5)
P_cond=pressure(R$;T=T_m_cond;x=0,5)
Pr_cond_f=prandtl(R$;T=T_sat_cond;P=P_2)
mu_cond_f=viscosity(R$;T=T_sat_cond;x=0)
mu_cond_g=viscosity(R$;T=T_sat_cond;x=1)
nu_cond_f=kinematicviscosity(R$;T=T_sat_cond;x=0)
nu_cond_g=kinematicviscosity(R$;T=T_sat_cond;x=1)
rho_cond_f=density(R$;T=T_sat_cond;x=0)
rho_cond_g=density(R$;T=T_sat_cond;x=1)
sigma_cond=surfactension(R$;T=T_sat_cond)
k_cond_refg=conductivity(R$;T=T_sat_cond;P=P_2)
k_cond_refg_fo=conductivity(R$;T=T_sat_cond;x=0)

T_8=323 [K]
T_9=303 [K]
T_m_w=(T_8+T_9)/2
P_heating= 60000 [Pa]
cp_w=cp(Water;T=T_m_w;P=P_heating)
```

```
Pr_cond_w=prandtl(Water,T=T_m_w;P=P_heating)
k_cond_w=conductivity(Water,T=T_m_w;P=P_heating)
mu_cond_w=viscosity(Water,T=T_m_w;x=0)
rho_cond_w=density(Water,T=T_m_w;x=0)
```

"Point 3: before expansion vavle"

```
h_3=h_4
x_3=0
T_3=T_sat_cond-5[K]
h_3=enthalpy(R$;T=T_3;x=x_3)
s_3=entropy(R$;P=P_3;h=h_3)
P_3=pressure(R$;T=T_3;x=x_3)
```

"Expansion valve"

"Point 4: before evaporator"

```
P_4=P_sat_evap
P_4=P_1
T_4=T_5-5[K]
P_sat_evap=p_sat(R$;T=T_4)
s_4=entropy(R$;T=T_4;h=h_4)
```

"Evaporator"

```
T_m_evap=(T_1+T_4)/2
P_evap=pressure(R$;T=T_m_evap;x=0,5)
mu_evap_f=viscosity(R$;T=T_m_evap;x=0)
mu_evap_g=viscosity(R$;T=T_m_evap;x=1)
nu_evap_f=kinematicviscosity(R$;T=T_m_evap;x=0)
nu_evap_g=kinematicviscosity(R$;T=T_m_evap;x=1)
rho_evap_f=density(R$;T=T_m_evap;x=0)
rho_evap_g=density(R$;T=T_m_evap;x=1)
sigma_evap=surfacetension(R$;T=T_m_evap)
k_evap_refg=conductivity(R$;T=T_m_evap;P=P_4)
k_evap_refg_fo=conductivity(R$;T=T_m_evap;x=0)
Pr_evap_f=prandtl(R$;T=T_m_evap;P=P_4)

T_5=275 [K]
C_PG= 50 [%]
T_m_evap_brine=(T_5+T_6)/2
cp_brine=cp(EG;T=T_m_evap_brine;C=C_EG)
k_evap_brine=conductivity(EG;T=T_m_evap_brine;C=C_EG)
mu_evap_brine=viscosity(EG;T=T_m_evap_brine;C=C_EG)
rho_evap_brine=density(EG;T=T_m_evap_brine;C=C_EG)
Pr_evap_brine=prandtl(EG;T=T_m_evap_brine;C=C_EG)
```

"Mass balance"

```
m_dot_1=m_dot_2
m_dot_2=m_dot_3
m_dot_3=m_dot_4
m_dot_4=m_dot_refg
```

"COP"

```
COP_carnot=(h_2s-h_3)/(h_2s-h_1)
"COP of a Carnot HP"
```

```
Q_dot_cond=15000 [J/s]
```

"The energy demand for the HP based on the energy calculations of the school"

$$m_dot_refg=Q_dot_cond/(h_2a-h_3)$$

"Mass flow rate of the refrigerant based on the heat transfer in the condenser"

$$W_dot_comp=m_dot_refg*(h_2a-h_1)$$

"The work input in the compressor"

$$COP_HP=Q_dot_cond/W_dot_comp$$

"COP of the HP"

$$\eta_{v/\eta_i}=(1+k_e*\left(\frac{(T_1-273[K])-18[K]}{100[K]}\right))^{\exp(a*(T_{sat_cond}/T_{m_evap})+b)}$$

"Pierre's correlation for isentropic volume and efficiency"

$$\eta_v=k_1*(1+k_s*\left(\frac{(T_1-273[K])-18[K]}{100[K]}\right))^{\exp(k_2*(P_{sat_cond}/P_{sat_evap}))}$$

"Pierre's constants for the chosen refrigerant"

....."

$$k_1=1,02$$

$$k_2=-0,063$$

$$k_s=0$$

$$k_e=0$$

$$a=-1,69$$

$$b=1,97$$

"Area condenser "

"

"Components values"

....."

$$D_pipe_w=0,028 \text{ [m]}$$

"Inner diameter for pipes with water- Data sheet "

$$D_pipe_HP=0,004 \text{ [m]}$$

"Inner diameter for the pipes inside the HP"

$$d_plate=0,00144 \text{ [m]}$$

"Plate thickness of the condenser - Data sheet"

$$\mu_{wall}=\text{viscosity}(\text{Water}; T=T_{wall}; x=0)$$

"The viscosity of the water by the wall in the condenser"

$$T_{wall}=(T_{sat_cond}+T_{m_w})/2$$

"The temperature of the wall in the condenser"

$$\lambda_{cond_wall}=15$$

"Thermal conductivity of the condenser with plates of stainless steel - Data sheet "

"Main equations"

....."

$$A_{cond}=Q_{dot_cond}/(U_{cond}*DELTA T_{lm_cond})$$

"Newton's Law of cooling"

$$DELTA T_{lm_cond}=\frac{(T_2-T_8)-(T_3-T_9)}{\ln((T_2-T_8)/(T_3-T_9))}$$

"The logarithmic mean temperature in the condenser"

$$U_{cond}=1/((1/h_{cond_refg})+R_{f_refg}+(d_{plate}/\lambda_{cond_wall})+R_{f_w}+(1/h_w))$$

"The overall heat transfer in the condenser"

"Nusselt correlation for refrigerant"

....."

$$x=0,5$$

"Flow quality of the refrigerant in the condenser"

$$G_{\text{cond}} = m_{\text{dot_refg}} / (\pi * D_{\text{pipe_HP}}^2) / 4$$

"Mass velocity of the refrigerant in the condenser"

$$J_{\text{g_cond}} = (x * G_{\text{cond}}) / (g * D_{\text{pipe_HP}} * \rho_{\text{cond_g}} * (\rho_{\text{cond_f}} - \rho_{\text{cond_g}}))^{(0,5)}$$

"The dimensionless vaopr velocity"

$$g = 9,81 \text{ [m/s}^2\text{]}$$

"The gravity of the Earth"

$$Z_{\text{cond}} = ((1/x) - 1)^{(0,8)} * P_{\text{r_cond}}^{(0,4)}$$

"Correlation parameter"

$$P_{\text{r_cond}} = P_{\text{cond}} / P_{\text{c}}$$

$$h_{\text{cond_refg}} = h_{\text{cond_fo}} * (1 + 1,128 * x^{(0,817)} * (\rho_{\text{cond_f}} / \rho_{\text{cond_g}})^{(0,3635)} * (\mu_{\text{cond_f}} / \mu_{\text{cond_g}})^{(0,2362)} * (1 - \mu_{\text{cond_g}} / \mu_{\text{cond_f}})^{(2,144)} * Pr_{\text{cond_f}}^{(-0,1)})$$

$$h_{\text{cond_fo}} = 0,023 * Re_{\text{cond_fo}}^{(0,8)} * Pr_{\text{cond_f}}^{0,4} * k_{\text{cond_refg_fo}} / D_{\text{pipe_HP}}$$

$$Re_{\text{cond_fo}} = (G_{\text{cond}} * D_{\text{pipe_HP}}) / \mu_{\text{cond_f}}$$

"Liquid only Reynolds number of the refrigerant"

"Nusselt correlation for water"

....."

$$Nu_{\text{cond_w}} = (h_{\text{w}} * D_{\text{pipe_w}}) / k_{\text{cond_w}}$$

"Average Nusselt number for the water in the condenser"

$$Nu_{\text{cond_w}} = 0,4225 * (Re_{\text{cond_w}})^{(0,733)} * (Pr_{\text{cond_w}})^{(0,33)} * (\mu_{\text{cond_w}} / \mu_{\text{wall}})^{(0,14)}$$

"The nusselt number correlation from Zhang (2020)"

$$Re_{\text{cond_w}} = (\rho_{\text{cond_w}} * v_{\text{avg_w}} * D_{\text{pipe_w}}) / \mu_{\text{cond_w}}$$

"Reynolds number for water in the condenser"

$$v_{\text{avg_w}} = (m_{\text{dot_w}} / \rho_{\text{cond_w}}) / ((\pi * D_{\text{pipe_w}}^2) / 4)$$

"Average velocity of the water in the condenser"

$$m_{\text{dot_w}} = (Q_{\text{dot_cond}}) / (c_{\text{p_w}} * (T_{\text{8-T_9}}))$$

"Mass flow rate of the water through the condenser"

"Area evaporator "

....."

"Components values"

....."

$$d_{\text{plate_evap}} = 0,00174 \text{ [m]}$$

"Plate thickness of the evaporator- Data sheet"

$$\lambda_{\text{evap_wall}} = 15$$

"Thermal conductivity of the condenser with plates of stainless steel- Data sheet "

$$D_{\text{pipe_brine}} = 0,028 \text{ [m]}$$

"Inner diameter for pipes with brine into the evaporator- Data sheet "

"Main equations"

....."

$$A_{\text{evap}} = Q_{\text{dot_evap}} / (U_{\text{evap}} * \Delta T_{\text{AT_Im_evap}})$$

"Newton's Law of cooling"

$$Q_{\text{dot_evap}} = m_{\text{dot_refg}} * (h_{\text{1-h_4}})$$

"the useful heat obtained by the evaporator"

DELTA_T_lm_evap=((T_6-T_1)-(T_5-T_4))/ln((T_6-T_1)/(T_5-T_4))
 "The logarithmic mean temperature in the evaporator"

U_evap=1/((1/h_evap_refg)+R_f_refg+(d_plate_evap/lambda_evap_wall)+R_f_brine+(1/h_evap_brine))
 "The overall heat transfer in the evaporator"

"Nusselt correlation for refrigerator in the evaporator
"

J_g_evap=(x*G_evap)/(g*D_pipe_HP*rho_evap_g*(rho_evap_f-rho_evap_g))^(0,5)
 "The dimensionless vapor velocity"

G_evap=m_dot_refg/(PI*D_pipe_HP^2)/4
 "Mass velocity of the refrigerant in the evaporator"

Z_evap=((1/x)-1)^(0,8)*P_r_evap^(0,4)
 "Correlation parameter"

P_r_evap=P_evap/P_c

h_evap_refg=h_evap_fo*(1+1,128*x^(0,817)*(rho_evap_f/rho_evap_g)^(0,3635)*(mu_evap_f/mu_evap_g)^(0,2362)*(1-(mu_evap_g/mu_evap_f))^(2,144)*Pr_evap_f^(-0,1))

h_evap_fo=0,023*Re_evap_fo^(0,8)*Pr_evap_f^0,4*k_evap_refg/D_pipe_HP

Re_evap_fo=((G_evap)*D_pipe_HP)/mu_evap_f
 "Liquid only Reynolds number of the refrigerant"

"Nusselt correlation for brine in the evaporator
"

h_evap_brine=(Nu_evap_brine*k_evap_brine)/D_pipe_brine
 "Average Nusselt number for the brine in the evaporator"

Nu_evap_brine=(0,8761*(f_brine/8)*(Re_evap_brine-147,3)*Pr_evap_brine)/(1+10,3*sqrt(f_brine/8)*(Pr_evap_brine^(2/3)-1))
 "The nusselt number correlation from Sándhez-Escalona et al. (2021) for the brine in the evaporator"

f_brine=(1,82*log10(Re_evap_brine)-1,64)^(-2)
 "Filonenko model of the friction factor"

Re_evap_brine=(rho_evap_brine*v_avg_brine*D_pipe_brine)/mu_evap_brine
 "Average Reynolds number for the brine in the evaporator"

v_avg_brine=(m_dot_brine/rho_evap_brine)/((PI*D_pipe_brine^2)/4)
 "Average velocity of the water in the condenser"

T_6=277,1 [K]
 "Temperature in to the evaporator from the GHX"

m_dot_brine=2 [kg/s]
 "Mass flow rate of the brine in the evaporator, collected from the GHX model"

" Exergy
 _____ "

"Compressor
"

eta_II_comp=1-(X_dot_des_comp/W_dot_comp)
 "Second order thermal efficiency of the compressor"

X_dot_des_comp=T_0*m_dot_refg*(s_2-s_1)
 "Exergy destruction in the compressor"

"Condenser
....."

$\eta_{II_cond} = 1 - (X_{dot_des_cond}) / (m_{dot_refg} * ((h_{2a} - h_3) - T_{0} * (s_2 - s_3)))$
"Second order thermal efficiency of the condenser"

$X_{dot_des_cond} = T_0 * (m_{dot_refg} * (s_3 - s_2) + (Q_{dot_cond} / T_{m_w}))$
"Exergy destruction in the condenser"

"Expansion valve
....."

$\eta_{II_exp} = 0$
"Second order thermal efficiency of the expansion valve"

$X_{dot_des_exp} = m_{dot_refg} * T_0 * (s_4 - s_3)$
"Exergy destruction in the expansion valve"

"Evaporator
....."

$\eta_{II_evap} = 1 - (X_{dot_des_evap}) / (m_{dot_refg} * ((h_4 - h_1) - T_0 * (s_4 - s_1)))$
"Second order thermal efficiency of the Evaporator"

$X_{dot_des_evap} = T_0 * (m_{dot_refg} * (s_1 - s_4) - (Q_{dot_evap} / T_{m_evap_brine}))$
"Exergy destruction in the evaporator"

$X_{des_HP} = X_{dot_des_comp} + X_{dot_des_cond} + X_{dot_des_exp} + X_{dot_des_evap}$
"Total exergy destruction of the HP"

K.4 R1234ze(E) HP model

File:C:\Users\ls351343\Downloads\HP R1234ze(E).EES 19.05.2022 09:56:53 Page 1
 EES Ver. 10.836: #3911: For use only by the Department of Civil Engineering and Energy Technology, HiOA

```
"
Heat Pump model - R1234ze(E)
"

"Parameters
"

R$='R1234ze(E)'
"Solstice as the refrigerant in the HP"

R_f_refg=foulingfactor('Refrigerant liquids')
"Fouling factor of refrigerant in liquid state"

P_c=p_crit(R1234ze(E))
"Critical pressure of the refrigerant"

R_f_w=foulingfactor('Closed-loop treated water')
"Fouling factor of water"

R_f_brine=foulingfactor('Ethanol solution')
"Fouling factor of the brine"

C_EG= 35 [%]
"Ethylene- Glycol-Water, 35%mixture, as the brine in the GHX"

T_0=294 [K]
"Dead state temperature of the HP inside the school"

"Point 1: before compressor"

T_1=T_4+5 [K]
s_1=s_2s
h_1=enthalpy(R$;T=T_1;P=P_1)
s_1=entropy(R$;P=P_1;T=T_1)

"Point 2: before condenser"

P_2=P_3
h_2s=enthalpy(R$;P=P_2;s=s_2s)
s_2=entropy(R$;P=P_2;h=h_2a)
T_2=temperature(R$;P=P_2;h=h_2a)
h_2a=((h_2s-h_1))/eta_i+h_1

"Condenser"

T_sat_cond=323 [K]
T_m_cond=(T_2+T_3)/2
P_sat_cond=pressure(R$;T=T_sat_cond;x=0,5)
P_cond=pressure(R$;T=T_m_cond;x=0,5)
Pr_cond_f=prandtl(R$;T=T_sat_cond;P=P_2)
mu_cond_f=viscosity(R$;T=T_sat_cond;x=0)
mu_cond_g=viscosity(R$;T=T_sat_cond;x=1)
nu_cond_f=kinematicviscosity(R$;T=T_sat_cond;x=0)
nu_cond_g=kinematicviscosity(R$;T=T_sat_cond;x=1)
rho_cond_f=density(R$;T=T_sat_cond;x=0)
rho_cond_g=density(R$;T=T_sat_cond;x=1)
sigma_cond=surfacetension(R$;T=T_sat_cond)
k_cond_refg=conductivity(R$;T=T_sat_cond;P=P_2)
k_cond_refg_fo=conductivity(R$;T=T_sat_cond;x=0)

T_8=323 [K]
T_9=303 [K]
T_m_w=(T_8+T_9)/2
P_heating= 60000 [Pa]
cp_w=cp(Water;T=T_m_w;P=P_heating)
Pr_cond_w=prandtl(Water;T=T_m_w;P=P_heating)
```

File:C:\Users\s351343\Downloads\HP R1234ze(E).EES 19.05.2022 09:56:53 Page 2
 EES Ver. 10.836: #3911: For use only by the Department of Civil Engineering and Energy Technology, HiOA

k_cond_w=**conductivity**(Water,T=T_m_w;P=P_heating)
 mu_cond_w=**viscosity**(Water,T=T_m_w;x=0)
 rho_cond_w=**density**(Water,T=T_m_w;x=0)

"Point 3: before expansion vavle"

h_3=h_4
 x_3=0
 T_3=T_sat_cond-5[K]
 h_3=**enthalpy**(R\$;T=T_3;x=x_3)
 s_3=**entropy**(R\$;P=P_3;h=h_3)
 P_3=**pressure**(R\$;T=T_3;x=x_3)

"Point 4: before evaporator"

P_4=P_1
 T_4=T_5-5[K]
 P_4=**p_sat**(R\$;T=T_4)
 s_4=**entropy**(R\$;T=T_4;h=h_4)

"Evaporator"

T_m_evap=(T_1+T_4)/2
 P_sat_evap=**p_sat**(R\$;T=T_sat_evap)
 T_sat_evap=**t_sat**(R\$;P=P_1)
 P_evap=**pressure**(R\$;T=T_m_evap;x=0,5)
 mu_evap_f=**viscosity**(R\$;T=T_m_evap;x=0)
 mu_evap_g=**viscosity**(R\$;T=T_m_evap;x=1)
 nu_evap_f=**kinematicviscosity**(R\$;T=T_m_evap;x=0)
 nu_evap_g=**kinematicviscosity**(R\$;T=T_m_evap;x=1)
 rho_evap_f=**density**(R\$;T=T_m_evap;x=0)
 rho_evap_g=**density**(R\$;T=T_m_evap;x=1)
 sigma_evap=**surfacentension**(R\$;T=T_m_evap)
 k_evap_refg=**conductivity**(R\$;T=T_m_evap;P=P_4)
 k_evap_refg_fo=**conductivity**(R\$;T=T_m_evap;x=0)
 Pr_evap_f=**prandtl**(R\$;T=T_m_evap;P=P_4)

T_5=275 [K]
 T_m_evap_brine=(T_5+T_6)/2
 c_p_brine=**cp**(EG;T=T_m_w;C=C_EG)
 k_evap_brine=**conductivity**(EG;T=T_m_evap_brine;C=C_EG)
 mu_evap_brine=**viscosity**(EG;T=T_m_evap_brine;C=C_EG)
 rho_evap_brine=**density**(EG;T=T_m_evap_brine;C=C_EG)
 Pr_evap_brine=**prandtl**(EG;T=T_m_evap_brine;C=C_EG)

"Mass balance "

m_dot_1=m_dot_2
 m_dot_2=m_dot_3
 m_dot_3=m_dot_4
 m_dot_4=m_dot_refg

"COP "

COP_carnot=(h_2s-h_3)/(h_2s-h_1)
 "COP of a Carnot HP"

Q_dot_cond=15000 [W]
 "The energy demand for the HP based on the energy calculations of the school"

m_dot_refg=Q_dot_cond/(h_2a-h_3)
 "Mass flow rate of the refrigerant based on heat transfer in the condenser"

File:C:\Users\s351343\Downloads\HP R1234ze(E).EES 19.05.2022 09:56:53 Page 3
 EES Ver. 10.836: #3911: For use only by the Department of Civil Engineering and Energy Technology, HiOA

$W_{\dot{comp}} = m_{\dot{refg}}(h_{2a} - h_1)$
 "The work input in the compressor"

$COP_{HP} = Q_{\dot{cond}} / W_{\dot{comp}}$
 "COP of the HP"

$\eta_{v/\eta_i} = (1 + k_e * (((T_1 - 273[K]) - 18[K]) / 100[K])) * \exp(a * (T_{\text{sat_cond}} / T_{\text{m_evap}}) + b)$
 "Pierre's correlation for isentropic volume and efficiency"

$\eta_v = k_1 * (1 + k_s * (((T_1 - 273[K]) - 18[K]) / 100[K])) * \exp(k_2 * (P_{\text{sat_cond}} / P_{\text{sat_evap}}))$

"Pierre's constants for the chosen refrigerant
"

$k_1 = 1,04$
 $k_2 = -0,07$
 $k_s = 0,15$
 $k_e = -0,1$
 $a = -2,4$
 $b = 2,88$

"Area condenser
"

"Components values
"

$D_{\text{pipe_w}} = 0,028$ [m]
 "Inner diameter for pipes with water - Data sheet "

$D_{\text{pipe_HP}} = 0,003$ [m]
 "Inner diameter for the pipes inside the HP"

$d_{\text{plate}} = 0,00144$ [m]
 "Plate thickness of the condenser - Data sheet"

$\mu_{\text{wall}} = \text{viscosity}(\text{Water}, T = T_{\text{wall}}, x = 0)$
 "The viscosity of the water by the wall in the condenser"

$T_{\text{wall}} = (T_{\text{sat_cond}} + T_{\text{m_w}}) / 2$
 "The temperature of the wall in the condenser"

$\lambda_{\text{cond_wall}} = 15$
 "Thermal conductivity of the condenser with plates of stainless steel - Data sheet "

"Main equations
"

$A_c = Q_{\dot{cond}} / (U_{\text{cond}} * \Delta T_{\text{lm_cond}})$
 "LMTD-method"

$\Delta T_{\text{lm_cond}} = ((T_2 - T_8) - (T_3 - T_9)) / \ln((T_2 - T_8) / (T_3 - T_9))$
 "The logarithmic mean temperature in the condenser"

$U_{\text{cond}} = 1 / ((1/h_{\text{cond_refg}}) + R_{\text{f_refg}} + (d_{\text{plate}} / \lambda_{\text{cond_wall}}) + R_{\text{f_w}} + (1/h_w))$
 "The overall heat transfer in the condenser"

"Nusselt correlation for refrigerant
"

$x = 0,5$
 "Flow quality of the refrigerant in the condenser"

$G_{\text{cond}} = m_{\dot{refg}} / (\pi * D_{\text{pipe_HP}}^2 / 4)$
 "Mass velocity of the refrigerant in the condenser"

$J_{\text{g_cond}} = (x * G_{\text{cond}}) / (g * D_{\text{pipe_HP}} * \rho_{\text{cond_g}} * (\rho_{\text{cond_f}} - \rho_{\text{cond_g}}))^{0,5}$

File:C:\Users\s351343\Downloads\HP R1234ze(E).EES 19.05.2022 09:56:53 Page 4
 EES Ver. 10.836: #3911: For use only by the Department of Civil Engineering and Energy Technology, HiOA

"The dimensionless vaopr velocity"

g=9,81 [m/s^2]

"The gravity of the Earth"

Z_cond=((1/x)-1)^(0,8)*P_r_cond^(0,4)

"Correlation parameter"

P_r_cond=P_cond/P_c

h_cond_refg=h_cond_fo*(1+1,128*x^(0,817)*(rho_cond_f/rho_cond_g)^(0,3635)*(mu_cond_f/mu_cond_g)^(0,2362))*(1-(mu_cond_g/mu_cond_f)^(2,144)*Pr_cond_f^(-0,1))

h_cond_fo=0,023*Re_cond_fo^(0,8)*Pr_cond_f^0,4*k_cond_refg/D_pipe_HP

Re_cond_fo=((G_cond)*D_pipe_HP)/mu_cond_f

"Liquid only Reynolds number of the refrigerant"

"Nusselt correlation for water"

....."

Nus_cond_w=(h_w*D_pipe_w)/k_cond_w

"Average Nusselt number for the water in the condenser"

Nus_cond_w=0,4225*(Re_cond_w)^(0,733)*(Pr_cond_w)^(0,33)*(mu_cond_w/mu_wall)^(0,14)

"The nussel number correlation from Zhang (2020)"

Re_cond_w=(rho_cond_w*v_avg_w*D_pipe_w)/mu_cond_w

"Reynolds number for water in the condenser"

v_avg_w=(m_dot_w/rho_cond_w)/((PI*D_pipe_w^2)/4)

"Average velocity of the water in the condenser"

m_dot_w=(Q_dot_cond)/(cp_w*(T_8-T_9))

"Mass flow rate of the water through the condenser"

"Area evaporator"

....."

"Components values"

....."

d_plate_evap=0,00174 [m]

"Plate thickness of the evaporator, data sheet for H55-C heat pump evaporator, Danfoss"

lambda_evap_wall=15

"Thermal conductivity of the condenser with plates of stainless steel - Data sheet "

D_pipe_brine=0,028 [m]

"Inner diameter for pipes with brine into the evaporator - Data sheet "

D_pipe_o=0,032 [m]

"Outer diameter of the pipe inside the GHX"

"Main equations"

....."

A_evap= Q_dot_evap/(U_evap*DELTAT_lm_evap)

"LMTD-method"

Q_dot_evap=m_dot_refg*(h_1-h_4)

"The useful heat obtained by the evaporator"

DELTAT_lm_evap=((T_6-T_1)-(T_5-T_4))/ln((T_6-T_1)/(T_5-T_4))

File:C:\Users\s351343\Downloads\HP R1234ze(E).EES 19.05.2022 09:56:53 Page 5
 EES Ver. 10.836: #3911: For use only by the Department of Civil Engineering and Energy Technology, HiOA

"The logarithmic mean temperature in the evaporator"

$$U_{\text{evap}} = 1 / \left(\frac{1}{h_{\text{evap_refg}}} + R_{\text{f_refg}} + \frac{d_{\text{plate_evap}}}{\lambda_{\text{evap_wall}}} + R_{\text{f_brine}} + \frac{1}{h_{\text{evap_brine}}} \right)$$
 "The overall heat transfer in the evaporator"

"Nusselt correlation for refrigerator in the evaporator
"

$$J_{\text{g_evap}} = \frac{x \cdot G_{\text{evap}}}{(g \cdot D_{\text{pipe_HP}} \cdot \rho_{\text{evap}} \cdot \rho_{\text{evap_g}} (\rho_{\text{evap_f}} - \rho_{\text{evap_g}}))^{0.5}}$$
 "The dimensionless vapor velocity"

$$G_{\text{evap}} = \frac{\dot{m}_{\text{refg}}}{\pi \cdot D_{\text{pipe_HP}}^2 / 4}$$
 "Mass velocity of the refrigerant in the evaporator"

$$Z_{\text{evap}} = \left(\frac{1}{x} - 1 \right)^{0.8} \cdot P_{\text{r_evap}}^{0.4}$$
 "Correlation parameter"

$$P_{\text{r_evap}} = \frac{P_{\text{evap}}}{P_{\text{c}}}$$

$$h_{\text{evap_refg}} = h_{\text{evap_fo}} \cdot (1 + 1.128 \cdot x^{0.817}) \cdot \left(\frac{\rho_{\text{evap_f}}}{\rho_{\text{evap_g}}} \right)^{0.3635} \cdot \left(\frac{\mu_{\text{evap_f}}}{\mu_{\text{evap_g}}} \right)^{0.2362} \cdot (1 - \mu_{\text{evap_g}} / \mu_{\text{evap_f}})^{2.144} \cdot P_{\text{r_evap_f}}^{-0.1}$$

$$h_{\text{evap_fo}} = 0.023 \cdot \text{Re}_{\text{evap_fo}}^{0.8} \cdot P_{\text{r_evap_f}}^{0.4} \cdot k_{\text{evap_refg_fo}} / D_{\text{pipe_HP}}$$

$$\text{Re}_{\text{evap_fo}} = \frac{(G_{\text{evap}}) \cdot D_{\text{pipe_HP}}}{\mu_{\text{evap_f}}}$$
 "Liquid only Reynolds number of the refrigerant"

"Nusselt correlation for brine in the evaporator
"

$$h_{\text{evap_brine}} = (\text{Nus}_{\text{evap_brine}} \cdot k_{\text{evap_brine}}) / D_{\text{pipe_brine}}$$
 "Average Nusselt number for the brine in the evaporator"

$$\text{Nus}_{\text{evap_brine}} = (0.8761 \cdot (f_{\text{brine}}/8) \cdot (\text{Re}_{\text{evap_brine}} - 147.3) \cdot P_{\text{r_evap_brine}}) / (1 + 10.3 \cdot \sqrt{f_{\text{brine}}/8} \cdot (P_{\text{r_evap_brine}}^{2/3} - 1))$$

"The nusselt number correlation from Sándhez-Escalona et al. (2021) for the brine in the evaporator"

$$f_{\text{brine}} = (1.82 \cdot \log_{10}(\text{Re}_{\text{evap_brine}}) - 1.64)^{-2}$$
 "Filonenko model of the friction factor"

$$\text{Re}_{\text{evap_brine}} = \frac{\rho_{\text{evap_brine}} \cdot v_{\text{avg_brine}} \cdot D_{\text{pipe_brine}}}{\mu_{\text{evap_brine}}}$$
 "Average Reynolds number for the brine in the evaporator"

$$v_{\text{avg_brine}} = \frac{\dot{m}_{\text{dot_brine}} / \rho_{\text{evap_brine}}}{(\pi \cdot D_{\text{pipe_brine}}^2) / 4}$$
 "Average velocity of the water in the condenser"

$$T_6 = 277.1 \text{ [K]}$$
 "Temperatur in to the evaporator from the GHX"

$$\dot{m}_{\text{dot_brine}} = 2 \text{ [kg/s]}$$
 "Mass flow rate of the brine in the evaporator, collected from the GHX model"

" Exergy
 _____ "

"Compressor
"

$$\eta_{\text{II_comp}} = 1 - (X_{\text{dot_des_comp}} / W_{\text{dot_comp}})$$
 "Second order thermal efficiency of the compressor"

$$X_{\text{dot_des_comp}} = T_0 \cdot \dot{m}_{\text{dot_refg}} \cdot (s_2 - s_1)$$
 "Exergy destruction in the compressor"

"Condenser
"

File:C:\Users\s351343\Downloads\HP R1234ze(E).EES 19.05.2022 09:56:53 Page 6
 EES Ver. 10.836: #3911: For use only by the Department of Civil Engineering and Energy Technology, HiOA

$\eta_{II_cond} = 1 - (X_{dot_des_cond}) / (m_{dot_refg} * ((h_{2a} - h_3) - T_{0} * (s_2 - s_3)))$
 "Second order thermal efficiency of the condenser"

$X_{dot_des_cond} = T_0 * (m_{dot_refg} * (s_3 - s_2) + (Q_{dot_cond} / T_{m_w}))$
 "Exergy destruction in the condenser"

"Expansion valve
"

$\eta_{II_exp} = 0$
 "Second order thermal efficiency of the expansion valve"

$X_{dot_des_exp} = m_{dot_refg} * T_0 * (s_4 - s_3)$
 "Exergy destruction in the expansion valve"

"Evaporator
"

$\eta_{II_evap} = 1 - (X_{dot_des_evap}) / (m_{dot_refg} * ((h_4 - h_1) - T_0 * (s_4 - s_1)))$
 "Second order thermal efficiency of the Evaporator"

$X_{dot_des_evap} = T_0 * (m_{dot_refg} * (s_1 - s_4) - (Q_{dot_evap} / T_{m_evap_brine}))$
 "Exergy destruction in the evaporator"

$X_{dot_des_HP} = X_{dot_des_comp} + X_{dot_des_cond} + X_{dot_des_exp} + X_{dot_des_evap}$
 "Total exergy destruction of the HP"

L P-h graphs

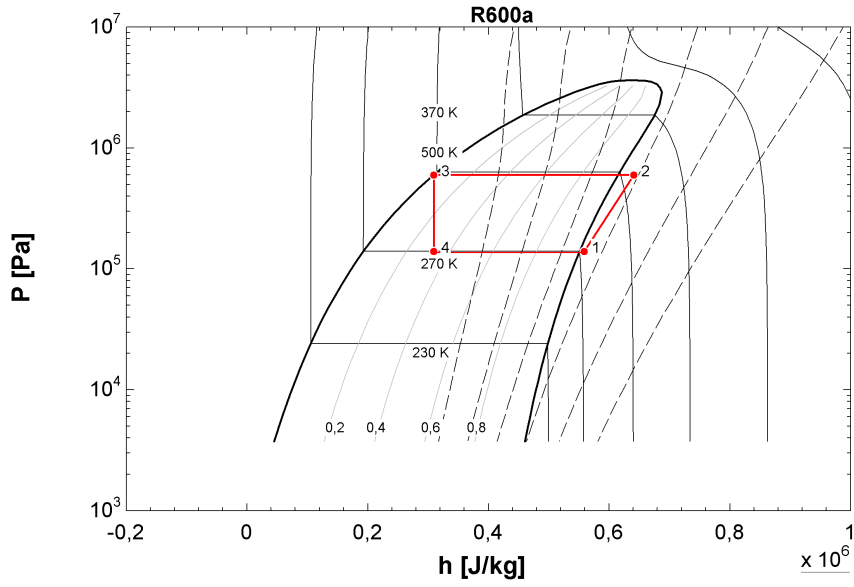


Figure 47: P-h diagram for R600a

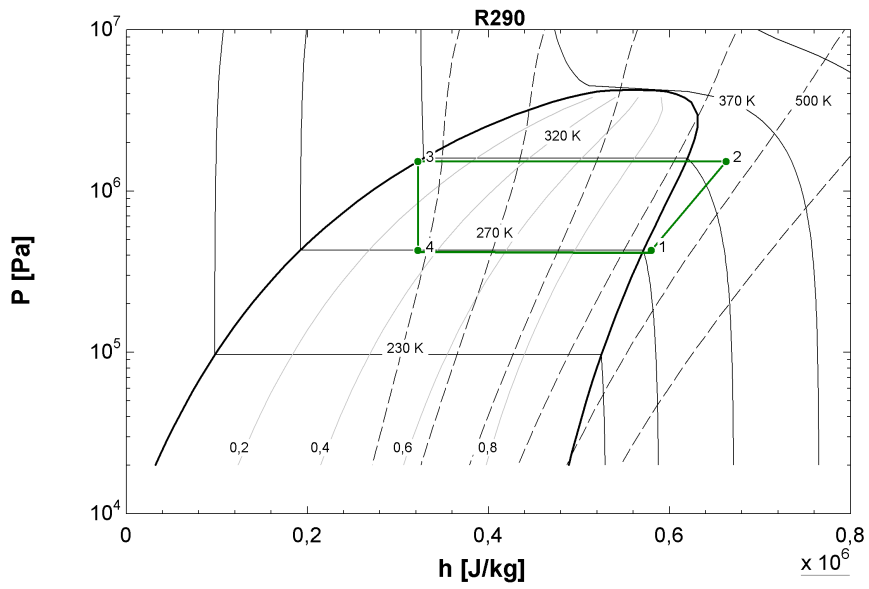


Figure 48: P-h diagram for R290

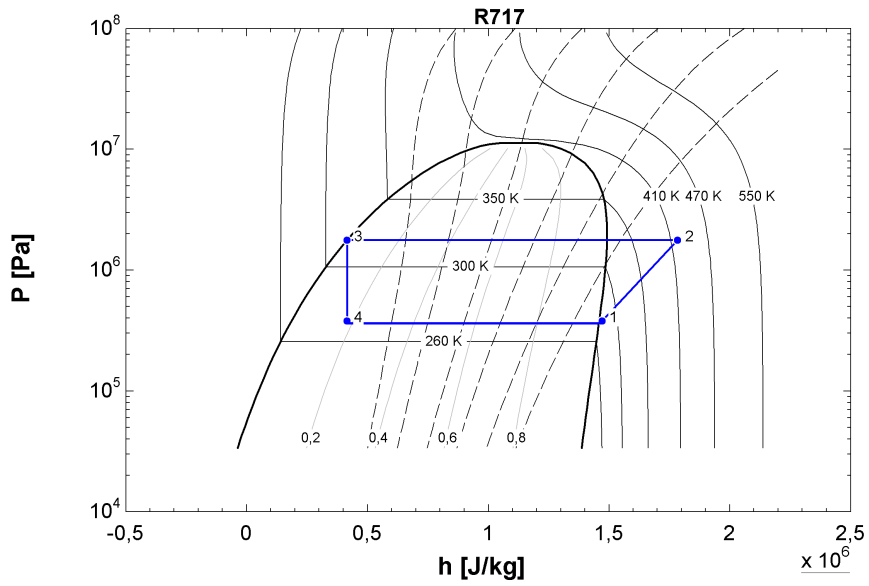


Figure 49: P-h diagram for R717

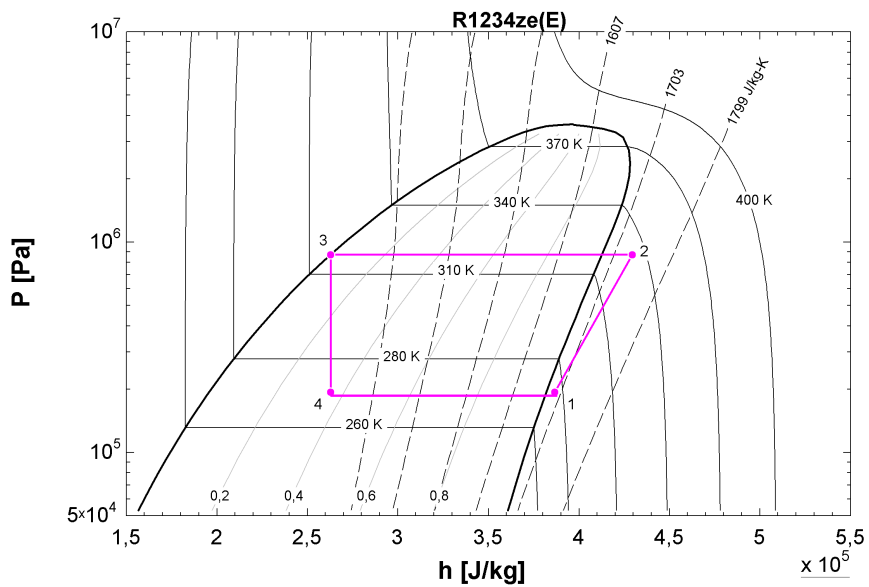


Figure 50: P-h diagram for R1234ze(E)

M EES SC results

File:C:\Users\s351343\Downloads\SC.EES

22.05.2022 14:34:17 Page 1

EES Ver. 10.836: #3911: For use only by the Department of Civil Engineering and Energy Technology, HiOA

SOLUTION

Unit Settings: SI K Pa J mass deg

$A = 2,51 \text{ [m}^2\text{]}$
 $a_1 = 3,653 \text{ [W/m}^2\text{-K]}$
 $A_{aa} = 3,144 \text{ [m}^2\text{]}$
 $A_{tot,SC} = 3,358 \text{ [m}^2\text{]}$
 $CEG = 35 \text{ [%]}$
 $\eta_0 = 0,765 \text{ [-]}$
 $\eta_{SC} = 0,5614 \text{ [-]}$
 $G = 700 \text{ [W/m}^2\text{]}$
 $h_0 = 1707 \text{ [J/kg]}$
 $h_{11} = 109850 \text{ [J/kg]}$
 $h_{13} = 221888 \text{ [J/kg]}$
 $\dot{m}_{11} = 0,02676 \text{ [kg/s]}$
 $\dot{m}_{13} = 0,02676 \text{ [kg/s]}$
 $\dot{m}_{SC} = 0,02 \text{ [kg/s]}$
 $N_{SC} = 1,338 \text{ [-]}$
 $\phi_{SC} = 60 \text{ [deg]}$
 $\dot{Q}_i = 1409 \text{ [W]}$
 $Q_u = 510,6 \text{ [W]}$
 $\tau = 0,8 \text{ [-]}$
 $T_{11} = 313 \text{ [K]}$
 $T_a = 293 \text{ [K]}$
 $T_s = 5778 \text{ [K]}$
 $\dot{X}_{des} = 995,2 \text{ [W]}$
 $\dot{X}_{i,fr} = 65,27 \text{ [W]}$
 $\dot{X}_o = 383,3 \text{ [W]}$

$\alpha = 0,8 \text{ [-]}$
 $a_2 = 0,012 \text{ [W/m}^2\text{-K}^2\text{]}$
 $A_{aa,SC} = 2,35 \text{ [m}^2\text{]}$
 $\beta_{SC} = 44 \text{ [deg]}$
 $C_{p,sun} = 3735 \text{ [J/kg-K]}$
 $\eta_{II,SC} = 0,2422 \text{ [-]}$
 $F_R = 0,8 \text{ [-]}$
 $\gamma_{SC} = 2 \text{ [deg]}$
 $h_{10} = 109850 \text{ [J/kg]}$
 $h_{12} = 221888 \text{ [J/kg]}$
 $\dot{m}_{10} = 0,02676 \text{ [kg/s]}$
 $\dot{m}_{12} = 0,02676 \text{ [kg/s]}$
 $\dot{m}_{coil} = 0,02676 \text{ [kg/s]}$
 $\dot{m}_{solar,f} = 0,02676 \text{ [kg/s]}$
 $P = 250000 \text{ [Pa]}$
 $P_0 = 101000 \text{ [Pa]}$
 $\dot{Q}_{tank} = 2998 \text{ [W]}$
 $R_{f,sun} = 0,000352 \text{ [m}^2\text{-K/W]}$
 $T_0 = 279,3 \text{ [K]}$
 $T_{12} = 343 \text{ [K]}$
 $T_m = 328 \text{ [K]}$
 $U_L = 7 \text{ [W/m}^2\text{-K]}$
 $\dot{X}_i = 1379 \text{ [W]}$
 $\dot{X}_{i,sr} = 1313 \text{ [W]}$
 $\dot{X}_s = 0 \text{ [W]}$

No unit problems were detected.

N EES GHX results

File:C:\Users\s351343\Downloads\GHX-final.EES

16.05.2022 13:11:47 Page 1

EES Ver. 10.836: #3911: For use only by the Department of Civil Engineering and Energy Technology, HiOA

SOLUTION

Unit Settings: SI K Pa J mass deg

AHX = 0,1352 [m²]
 CEG = 35 [%]
 Cp,brine,7 = 3556 [J/kg-K]
 Cp,HX,brine = 3555 [J/kg-K]
 ΔP_{pump} = 230514 [Pa]
 ΔS₁₅ = 425,5 [J/kg-K]
 ΔS₇ = -49,81 [J/kg-K]
 Δv_{,76} = 65,49 [J/kg]
 D_{ed,i} = 0,04525 [m]
 D_{pipe,HX} = 0,01576 [m]
 D_{pipe,o} = 0,04 [m]
 η_{ll,borehole} = 0,6517 [-]
 f_{brine} = 0,02692 [-]
 f_{solar} = 0,05191 [-]
 h₁₄ = 221888 [J/kg]
 h₅ = -27810 [J/kg]
 h₇ = -26339 [J/kg]
 h_{ghx} = 795,5 [W/m²-K]
 k_g = 0,5775 [W/m-K]
 k_{HX,brine} = 0,4294 [W/m-K]
 k_{pipe,GHX} = 0,35 [W/m-K]
 L_{pipe,GHX} = 130 [m]
 μ_{HX,brine} = 0,004603 [kg/m-s]
 ṁ₆ = 2,056 [kg/s]
 ṁ_{brine} = 2,056 [kg/s]
 ṁ_{solar,f} = 0,027 [kg/s]
 N_{USolar} = 25,28 [-]
 N_{borehole} = 4,113 [-]
 P_{RGHX} = 38,44 [-]
 P_{RGHX,solar} = 8,381 [-]
 P_{borehole} = 200000 [Pa]
 P_{solar} = 250000 [Pa]
 Q̇_{GHX} = 2755 [W]
 Q̇_{HX} = 3025 [W]
 Re_{brine} = 17774 [-]
 Re_{solar} = 2054 [-]
 ρ_{HX,brine} = 1052 [kg/m³]
 ρ_w = 1000 [kg/m³]
 R_{f,brine} = 0,000352 [m²-K/W]
 R_{grout} = 0,1833 [m-K/W]
 R_{tot} = 0,2936 [m-K/W]
 T₁₄ = 343 [K]
 T₅ = 275 [K]
 T₇ = 275,4 [K]
 T_g = 282,5 [K]
 T_{m,HX,brine} = 275,2 [K]
 T_s = 283,3 [K]
 V_{avg,brine} = 2,43 [m/s]
 V_{avg,solar} = 0,1348 [m/s]
 Ẋ₁₄ = 20055 [J/kg]
 Ẋ₅ = 84,82 [J/kg]
 Ẋ_{des,borehole} = 294,7 [W]
 Ẋ_i = 817,9 [W]
 z₁ = 0,8761 [-]
 z₃ = 10,3 [-]

cp = 4196 [J/kg-K]
 Cp,brine,6 = 3738 [J/kg-K]
 Cp,brine,m = 3559 [J/kg-K]
 Cp,HX,solar = 3735 [J/kg-K]
 ΔS₁₄ = 767,4 [J/kg-K]
 ΔS₅ = -55,15 [J/kg-K]
 δT_{lm} = 51,38 [K]
 D_b = 0,11 [m]
 D_{ed,o} = 0,05657 [m]
 D_{pipe,i} = 0,032 [m]
 d_{plate} = 0,00198 [m]
 η_{ll,HX} = 0,7051 [-]
 f_{GHX} = 0,02289 [-]
 h₀ = -12491 [J/kg]
 h₁₅ = 109850 [J/kg]
 h₆ = -20418 [J/kg]
 h_{brine} = 3707 [W/m²-K]
 h_{solar} = 759,2 [W/m²-K]
 k_{GHX} = 0,4292 [W/m-K]
 k_{HX,solar} = 0,4733 [W/m-K]
 λ_{HX,wall} = 386 [W/m-K]
 μ_{GHX} = 0,004641 [kg/m-s]
 μ_{HX,solar} = 0,001062 [kg/m-s]
 ṁ₇ = 2,056 [kg/s]
 ṁ_{GHX} = 0,5 [kg/s]
 N_{usbrine} = 276,3 [-]
 v_{GHX} = 59,31 [-]
 N_{tube} = 2 [-]
 P_{RGHX,brine} = 38,12 [-]
 P₀ = 101000 [Pa]
 P_{evap} = 430514 [Pa]
 Q̇_{evap} = 11332 [W]
 Q̇_{ground} = 11332 [W]
 q_{GHX} = 21,19 [W/m]
 Re_{GHX} = 4287 [-]
 ρ_{GHX} = 1052 [kg/m³]
 ρ_{HX,solar} = 1026 [kg/m³]
 R_{brine} = 0,008842 [m-K/W]
 R_{f,solar} = 0,000352 [m²-K/W]
 R_{pipe} = 0,1015 [m-K/W]
 T₀ = 279,3 [K]
 T₁₅ = 313 [K]
 T₆ = 277,1 [K]
 T_F = 254,3 [K]
 T_{m,brine} = 276,2 [K]
 T_{m,HX,solar} = 328 [K]
 U_{HX} = 435,5 [W/m²-K]
 V_{avg,GHX} = 0,5909 [m/s]
 W_{pump} = 450,5 [W]
 Ẋ₁₅ = 3501 [J/kg]
 Ẋ₇ = 63,26 [J/kg]
 Ẋ_{des,HX} = 16576 [J/kg]
 Ẋ_o = 533,1 [W]
 z₂ = 147,3 [-]

No unit problems were detected.

O EES HP results

O.1 R600a HP results

File:C:\Users\s351343\Downloads\HP R600a.EES

16.05.2022 13:12:06 Page 1

EES Ver. 10.836: #3911: For use only by the Department of Civil Engineering and Energy Technology, HiOA

SOLUTION

Unit Settings: SI K Pa J mass deg

```

a = -2,4 [-]
Aevap = 3,268 [m²]
COPcarnot = 5,43 [-]
cpbrine = 3688 [J/kg-K]
Ccond = 8,553 [-]
Cevap = 13,91 [-]
ΔTlm,evap = 3,343 [K]
Dpipe,HP = 0,003 [m]
dplate = 0,00144 [m]
Dpz,evap,f = -12,56 [kg²/m³-s³]
Dpz,f = -7,222 [kg²/m³-s³]
ηj = 0,6856 [-]
ηll,cond = 0,7891 [-]
ηll,exp = 0 [-]
fbrine = 0,0263 [-]
fcond,g = 0,002841 [-]
fevap,g = 0,002721 [-]
Gevap = 6401 [kg/m²-s]
h2a = 641021 [J/kg]
h3 = 309523 [J/kg]
hcond,refg = 7954 [W/m²-K]
hevap,refg = 9668 [W/m²-K]
k1 = 1,04 [-]
kcond,refg = 0,01983 [W/m-K]
ke = -0,1 [-]
kevap,refg = 0,01431 [W/m-K]
λcond,wall = 15 [W/m-K]
μcond,f = 0,0001145 [kg/m-s]
μcond,w = 0,0006548 [kg/m-s]
μevap,f = 0,0002006 [kg/m-s]
μwall = 0,0005976 [kg/m-s]
ṁ2 = 0,04525 [kg/s]
ṁ4 = 0,04525 [kg/s]
ṁrefg = 0,04525 [kg/s]
vcond,f = 2,219E-07 [m²/s] {2,219E-07 [m²/s]}
vcond,refg = 1204 [-]
vevap,brine = 295,2
vevap,g = 0,000001671 [m²/s]
φcond,g = 3,031 [-]
Pfcond,f = 0,8581 [-]
Pfevap,brine = 36,86 [-]
P1 = 139863 [Pa]
P3 = 601750 [Pa]
Pheating = 60000 [Pa]
Psat,evap = 139863 [Pa]
Qevap = 11285 [W]
Recond,f = 83828 [-]
Recond,g = 1,112E+06 [-]
Reevap,brine = 19474 [-]
Reevap,fo = 95736 [-]
ρcond,f = 516,2 [kg/m³]
ρcond,w = 992,2 [kg/m³]
ρevap,f = 581,2 [kg/m³]
Rf,brine = 0,000352 [m²-K/W]
Rf,w = 0,000175 [m²-K/W]
σevap = 0,01285 [N/m]
SUevap,go = 3,318E+06 [-]
s2 = 2409 [J/kg-K]
s3 = 1368 [J/kg-K]
Ac = 0,8489 [m²]
b = 2,88 [-]
COPHP = 4,037 [-]
cpw = 4180 [J/kg-K]
CEG = 35 [%]
ΔTlm,cond = 11,25 [K]
Dpipe,brine = 0,028 [m]
Dpipe,w = 0,028 [m]
dplate,evap = 0,00174 [m]
Dpz,evap,g = -31,06 [kg²/m³-s³]
Dpz,g = -9,562 [kg²/m³-s³]
ηll,comp = 0,7153 [-]
ηll,evap = 0,7343 [-]
ηv = 0,7216 [-]
fcond,f = 0,004765 [-]
fevap,f = 0,00533 [-]
Gcond = 6401 [kg/m²-s]
h1 = 558913 [J/kg]
h2s = 615207 [J/kg]
h4 = 309523 [J/kg]
hevap,brine = 4534 [W/m²-K]
hw = 15679 [W/m²-K]
k2 = -0,07 [-]
kcond,w = 0,6283 [W/m-K]
kevap,brine = 0,4301 [W/m-K]
ks = 0,15 [-]
λevap,wall = 15 [W/m-K]
μcond,g = 0,000008636 [kg/m-s]
μevap,brine = 0,004455 [kg/m-s]
μevap,g = 0,000006951 [kg/m-s]
ṁ1 = 0,04525 [kg/s]
ṁ3 = 0,04525 [kg/s]
ṁbrine = 1,908 [kg/s]
ṁw = 0,1794 [kg/s]
vcond,g = 4,927E-07 [m²/s]
vcond,w = 698,8 [-]
vevap,f = 3,451E-07 [m²/s]
vevap,refg = 2027 [-]
φevap,g = 3,202 [-]
Pfcond,w = 4,356 [-]
Pfevap,f = 0,7853 [-]
P2 = 601750 [Pa]
P4 = 139863 [Pa]
Psat,cond = 681890 [Pa]
Qcond = 15000 [W]
R$ = 'R600a'
Recond,fo = 167655 [-]
Recond,w = 12462 [-]
Reevap,f = 47868 [-]
Reevap,g = 1,381E+06 [-]
ρcond,g = 17,53 [kg/m³]
ρevap,brine = 1052 [kg/m³]
ρevap,g = 4,159 [kg/m³]
Rf,refg = 0,000176 [m²-K/W]
σcond = 0,007128 [N/m]
SUcond,go = 5,026E+06 [-]
s1 = 2329 [J/kg-K]
s2s = 2329 [J/kg-K]
s4 = 1406 [J/kg-K]

```

File:C:\Users\s351343\Downloads\HP R600a.EES 16.05.2022 13:12:06 Page 2
EES Ver. 10.836: #3911: For use only by the Department of Civil Engineering and Energy Technology, HiOA

$T_0 = 294$ [K]	$T_1 = 275$ [K]
$T_2 = 331,2$ [K]	$T_3 = 318$ [K]
$T_4 = 270$ [K]	$T_5 = 275$ [K]
$T_6 = 277,1$ [K]	$T_8 = 323$ [K]
$T_9 = 303$ [K]	$T_{m, \text{evap}} = 272,5$ [K]
$T_{m, \text{evap, brine}} = 276,1$ [K]	$T_{m, w} = 313$ [K]
$T_{\text{sat, cond}} = 323$ [K]	$T_{\text{wall}} = 318$ [K]
$U_{\text{cond}} = 1571$ [W/m ² -K]	$U_{\text{evap}} = 1033$ [W/m ² -K]
$V_{\text{avg, brine}} = 2,946$ [m/s]	$V_{\text{avg, w}} = 0,2937$ [m/s]
$\dot{W}_{\text{comp}} = 3715$ [W]	$x = 0,5$ [-]
$x_3 = 0$ [-]	$X_{\text{cond}} = 0,8691$ [-]
$\dot{X}_{\text{des, comp}} = 1058$ [W]	$\dot{X}_{\text{des, cond}} = 243,3$ [W]
$\dot{X}_{\text{des, evap}} = 265,5$ [W]	$\dot{X}_{\text{des, exp}} = 504,4$ [W]
$\dot{X}_{\text{des, HP}} = 2071$ [W]	$X_{\text{evap}} = 0,636$ [-]
$X_{\text{tt, cond}} = 0,2386$ [-]	$X_{\text{tt, evap}} = 0,1184$ [-]

No unit problems were detected.

O.2 R290 HP results

File:C:\Users\s351343\Downloads\HP R290-ny.EES

16.05.2022 13:12:36 Page 1

EES Ver. 10.836: #3911: For use only by the Department of Civil Engineering and Energy Technology, HiOA

SOLUTION

Unit Settings: SI K Pa J mass deg

```

a = -2,4 [-]
Aevap = 3,503 [m²]
COPcarnot = 5,228 [-]
cpbrine = 3558 [J/kg-K]
Ccond = 6,227 [-]
Cevap = 10,4
ΔTlm,evap = 3,132 [K]
Dpipe,HP = 0,003 [m]
dplate = 0,00144 [m]
Dpz,evap,f = -7,727 [kg²/m³-s³]
Dpz,f = -4,7 [kg²/m³-s³]
ηi = 0,7306 [-]
ηll,cond = 0,7678 [-]
ηll,exp = 0 [-]
fbrine = 0,02602 [-]
fcond,g = 0,00294
fevap,g = 0,002799 [-]
Gevap = 6217 [kg/m²-s]
h2a = 663408 [J/kg]
h3 = 322073 [J/kg]
hcond,refg = 9515 [W/m²-K]
hevap,refg = 8951 [W/m²-K]
k1 = 1,04 [-]
kcond,refg = 0,02279 [W/m-K]
ke = -0,1 [-]
kevap,refg = 0,01568 [W/m-K]
λcond,wall = 15 [W/m-K]
μcond,f = 0,00007447 [kg/m-s]
μcond,w = 0,0006548 [kg/m-s]
μevap,f = 0,0001294 [kg/m-s]
μw = 0,0005976 [kg/m-s]
ṁ2 = 0,04395 [kg/s]
ṁ4 = 0,04395 [kg/s]
ṁrefg = 0,04395 [kg/s]
NuScond,w = 698,8 [-]
NuSevap,refg = 1713
νcond,g = 2,579E-07 [m²/s]
νevap,f = 2,442E-07 [m²/s]
φcond,g = 2,841 [-]
Pr = 1
Prevap,brine = 37,08 [-]
P1 = 430514 [Pa]
P3 = 1,529E+06 [Pa]
Pheating = 60000 [Pa]
Psat,evap = 430514 [Pa]
Q̇evap = 11332 [W]
Recond,f = 125229 [-]
Recond,g = 938331 [-]
Reevap,brine = 20295 [-]
Reevap,fo = 144184 [-]
ρcond,f = 448,8 [kg/m³]
ρcond,w = 992,2 [kg/m³]
ρevap,f = 529,6 [kg/m³]
Rf,brine = 0,000352 [m²-K/W]
Rf,w = 0,000175 [m²-K/W]
σevap = 0,01004 [N/m]
SUevap,go = 5,068E+06 [-]
s2 = 2475 [J/kg-K]
s3 = 1406 [J/kg-K]
Ac = 0,6219 [m²]
b = 2,88 [-]
COPHP = 4,089 [-]
cpw = 4180 [J/kg-K]
CEG = 35 [%]
ΔTlm,cond = 14,85 [K]
Dpipe,brine = 0,028 [m]
Dpipe,w = 0,028 [m]
dplate,evap = 0,00174 [m]
Dpz,evap,g = -13,78 [kg²/m³-s³]
Dpz,g = -4,884 [kg²/m³-s³]
ηll,comp = 0,7619 [-]
ηll,evap = 0,7408 [-]
ηv = 0,7689 [-]
fcond,f = 0,004398
fevap,f = 0,004911 [-]
Gcond = 6217 [kg/m²-s]
h1 = 579930 [J/kg]
h2s = 640921 [J/kg]
h4 = 322073 [J/kg]
hevap,brine = 4707 [W/m²-K]
hw = 15679 [W/m²-K]
k2 = -0,07 [-]
kcond,w = 0,6283 [W/m-K]
kevap,brine = 0,43 [W/m-K]
ks = 0,15 [-]
λevap,wall = 15 [W/m-K]
μcond,g = 0,00009938 [kg/m-s]
μevap,brine = 0,004481 [kg/m-s]
μevap,g = 0,00007772 [kg/m-s]
ṁ1 = 0,04395 [kg/s]
ṁ3 = 0,04395 [kg/s]
ṁbrine = 2 [kg/s]
ṁw = 0,1794 [kg/s]
NuSevap,brine = 306,6 [-]
νcond,f = 1,659E-07 [m²/s] {1,659E-07 [m²/s]}
νcond,refg = 1253 [-]
νevap,g = 7,646E-07 [m²/s]
φevap,g = 3,058 [-]
Prcond,w = 4,356 [-]
Prevap,f = 0,8664 [-]
P2 = 1,529E+06 [Pa]
P4 = 430514 [Pa]
Psat,cond = 1,708E+06 [Pa]
Q̇cond = 15000 [J/s]
R$ = 'R290'
Recond,fo = 250458 [-]
Recond,w = 12462 [-]
Reevap,f = 72092 [-]
Reevap,g = 1,200E+06 [-]
ρcond,g = 38,53 [kg/m³]
ρevap,brine = 1052 [kg/m³]
ρevap,g = 10,16 [kg/m³]
Rf,refg = 0,000176 [m²-K/W]
σcond = 0,004095 [N/m]
SUcond,go = 4,792E+06 [-]
s1 = 2407 [J/kg-K]
s2s = 2407 [J/kg-K]
s4 = 1453 [J/kg-K]

```

File:C:\Users\s351343\Downloads\HP R290-ny.EES

16.05.2022 13:12:36 Page 2

EES Ver. 10.836: #3911: For use only by the Department of Civil Engineering and Energy Technology, HiOA

$T_0 = 294$ [K]	$T_1 = 275$ [K]
$T_2 = 337,7$ [K]	$T_3 = 318$ [K]
$T_4 = 270$ [K]	$T_5 = 275$ [K]
$T_6 = 276,8$ [K]	$T_8 = 323$ [K]
$T_9 = 303$ [K]	$T_{m, \text{evap}} = 272,5$ [K]
$T_{m, \text{evap, brine}} = 275,9$ [K]	$T_{m, w} = 313$ [K]
$T_{\text{sat, cond}} = 323$ [K]	$T_{\text{wall}} = 318$ [K]
$U_{\text{cond}} = 1624$ [W/m ² -K]	$U_{\text{evap}} = 1033$ [W/m ² -K]
$V_{\text{avg, brine}} = 3,088$ [m/s]	$V_{\text{avg, w}} = 0,2937$ [m/s]
$\dot{W}_{\text{comp}} = 3668$ [W]	$x = 0,5$ [-]
$x_3 = 0$ [-]	$X_{\text{cond}} = 0,981$
$\dot{X}_{\text{des, comp}} = 873,3$ [W]	$\dot{X}_{\text{des, cond}} = 275,3$ [W]
$\dot{X}_{\text{des, evap}} = 260,1$ [W]	$\dot{X}_{\text{des, exp}} = 605,8$ [W]
$\dot{X}_{\text{des, HP}} = 2015$ [W]	$X_{\text{evap}} = 0,7487$ [-]
$X_{\text{tt, cond}} = 0,3584$ [-]	$X_{\text{tt, evap}} = 0,1835$ [-]

No unit problems were detected.

O.3 R717 HP results

File:C:\Users\351343\Downloads\HP R717.EES

16.05.2022 13:12:22 Page 1

EES Ver. 10.836: #3911: For use only by the Department of Civil Engineering and Energy Technology, HiOA

SOLUTION

Unit Settings: SI K Pa J mass deg

```

a = -1,69 [-]
Aevap = 3,379 [m2]
COPcarnot = 5,556 [-]
cpbrine = 3559 [J/kg-K]
CEG = 35 [%]
ΔTlm,cond = 43,77 [K]
Dpipe,brine = 0,028 [m]
Dpipe,w = 0,028 [m]
dplate,evap = 0,00174 [m]
ηll,comp = 0,8216 [-]
ηll,evap = 0,7329 [-]
ηv = 0,7298 [-]
g = 9,81 [m/s2]
Gevap = 54,67 [kg/m2-s]
h2a = 1,779E+06 [J/kg]
h3 = 414718 [J/kg]
hcond,fo = 1193 [W/m2-K]
hevap,brine = 4722 [W/m2-K]
hevap,refg = 8589 [W/m2-K]
Jg,cond = 1,488 [-]
k1 = 1,02 [-]
kcond,refg = 0,02964 [W/m-K]
kcond,w = 0,6283 [W/m-K]
kevap,brine = 0,4301 [W/m-K]
kevap,refg,fo = 0,5614 [W/m-K]
λcond,wall = 15 [W/m-K]
μcond,f = 0,0001039 [kg/m-s]
μcond,w = 0,0006548 [kg/m-s]
μevap,f = 0,0001714 [kg/m-s]
μwall = 0,0005976 [kg/m-s]
ṁ2 = 0,01099 [kg/s]
ṁ4 = 0,01099 [kg/s]
ṁrefg = 0,01099 [kg/s]
vcond,f = 1,845E-07 [m2/s] {1,845E-07 [m2/s]}
vcond,w = 698,8 [-]
vevap,f = 2,680E-07 [m2/s]
Pfcond,f = 1,251 [-]
Pfevap,brine = 36,86 [-]
P1 = 381213 [Pa]
P3 = 1,775E+06 [Pa]
Pc = 1,133E+07 [Pa]
Pevap = 419208 [Pa]
Pr,cond = 0,5058 [-]
Psat,cond = 2,026E+06 [Pa]
Q̇cond = 15000 [J/s]
R$ = 'R717'
Recond,w = 12462 [-]
Revap,fo = 1276 [-]
ρcond,g = 15,72 [kg/m3]
ρevap,brine = 1052 [kg/m3]
ρevap,g = 3,379 [kg/m3]
Rf,refg = 0,000176 [m2-K/W]
σcond = 0,01492 [N/m]
s1 = 5710 [J/kg-K]
s2s = 5710 [J/kg-K]
s4 = 1796 [J/kg-K]
T1 = 275 [K]
T3 = 318 [K]
T5 = 275 [K]
Acond = 0,2448 [m2]
b = 1,97 [-]
COPHP = 4,438 [-]
cpw = 4180 [J/kg-K]
CPG = 50 [%]
ΔTlm,evap = 3,343 [K]
Dpipe,HP = 0,004 [m]
dplate = 0,00144 [m]
ηi = 0,7545 [-]
ηll,cond = 0,607 [-]
ηll,exp = 0 [-]
fbrine = 0,02598 [-]
Gcond = 54,67 [kg/m2-s]
h1 = 1,472E+06 [J/kg]
h2s = 1,704E+06 [J/kg]
h4 = 414718 [J/kg]
hcond,refg = 4914 [W/m2-K]
hevap,fo = 990,2 [W/m2-K]
hw = 15679 [W/m2-K]
Jg,evap = 2,976 [-]
k2 = -0,063 [-]
kcond,refg,fo = 0,4163 [W/m-K]
ke = 0 [-]
kevap,refg = 0,02325 [W/m-K]
ks = 0 [-]
λevap,wall = 15 [W/m-K]
μcond,g = 0,00001067 [kg/m-s]
μevap,brine = 0,004455 [kg/m-s]
μevap,g = 0,000009036 [kg/m-s]
ṁ1 = 0,01099 [kg/s]
ṁ3 = 0,01099 [kg/s]
ṁbrine = 2 [kg/s]
ṁw = 0,1794 [kg/s]
vcond,g = 6,787E-07 [m2/s]
vevap,brine = 307,4
vevap,g = 0,000002674 [m2/s]
Pfcond,w = 4,356 [-]
Pfevap,f = 1,013 [-]
P2 = 1,775E+06 [Pa]
P4 = 381213 [Pa]
Pcond = 5,732E+06 [Pa]
Pheating = 60000 [Pa]
Pr,evap = 0,03699 [-]
Psat,evap = 381213 [Pa]
Q̇evap = 11620 [W]
Recond,fo = 2105 [-]
Revap,brine = 20413 [-]
ρcond,f = 563,1 [kg/m3]
ρcond,w = 992,2 [kg/m3]
ρevap,f = 639,6 [kg/m3]
Rf,brine = 0,000352 [m2-K/W]
Rf,w = 0,000175 [m2-K/W]
σevap = 0,02645 [N/m]
s2 = 5897 [J/kg-K]
s3 = 1720 [J/kg-K]
T0 = 294 [K]
T2 = 419,5 [K]
T4 = 270 [K]
T6 = 277,1 [K]

```

File:C:\Users\s351343\Downloads\HP R717.EES

16.05.2022 13:12:22 Page 2

EES Ver. 10.836: #3911: For use only by the Department of Civil Engineering and Energy Technology, HiOA

$T_8 = 323$ [K]	$T_9 = 303$ [K]
$T_{m,cond} = 368,7$ [K]	$T_{m,evap} = 272,5$ [K]
$T_{m,evap,brine} = 276,1$ [K]	$T_{m,w} = 313$ [K]
$T_{sat,cond} = 323$ [K]	$T_{wall} = 318$ [K]
$U_{cond} = 1400$ [W/m ² -K]	$U_{evap} = 1029$ [W/m ² -K]
$v_{avg,brine} = 3,088$ [m/s]	$v_{avg,w} = 0,2937$ [m/s]
$\dot{W}_{comp} = 3380$ [W]	$x = 0,5$ [-]
$x_3 = 0$ [-]	$X_{des,HP} = 1714$ [W]
$\dot{X}_{des,comp} = 602,9$ [W]	$\dot{X}_{des,cond} = 589,6$ [W]
$\dot{X}_{des,evap} = 275,4$ [W]	$\dot{X}_{des,exp} = 246,2$ [W]
$Z_{cond} = 0,7613$	$Z_{evap} = 0,2674$

No unit problems were detected.

O.4 R1234ze(E) HP results

File:C:\Users\ls351343\Downloads\HP R1234ze(E).EES

16.05.2022 13:13:00 Page 1

EES Ver. 10.836: #3911: For use only by the Department of Civil Engineering and Energy Technology, HiOA

SOLUTION

Unit Settings: SI K Pa J mass deg

```

a = -2,4 [-]
Aevap = 2,907 [m²]
COPearnot = 5,301 [-]
cpw = 4180 [J/kg-K]
Cp,brine = 3688 [J/kg-K]
ΔTlm,evap = 3,343 [K]
Dpipe,HP = 0,003 [m]
Dpipe,w = 0,028 [m]
dplate,evap = 0,00174 [m]
ηll,comp = 0,7065 [-]
ηll,evap = 0,7424 [-]
ηv = 0,7096 [-]
g = 9,81 [m/s²]
Gevap = 12748 [kg/m²-s]
h2a = 429256 [J/kg]
h3 = 262792 [J/kg]
hcond,fo = 11199 [W/m²-K]
hevap,brine = 4722 [W/m²-K]
hevap,refg = 64101 [W/m²-K]
Jg,cond = 158 [-]
k1 = 1,04 [-]
kcond,refg = 0,01565 [W/m-K]
kcond,w = 0,6283 [W/m-K]
kevap,brine = 0,4301 [W/m-K]
kevap,refg,fo = 0,08469 [W/m-K]
λcond,wall = 15 [W/m-K]
μcond,f = 0,0001393 [kg/m-s]
μcond,w = 0,0006548 [kg/m-s]
μevap,f = 0,0002654 [kg/m-s]
μwall = 0,0005976 [kg/m-s]
ṁ2 = 0,09011 [kg/s]
ṁ4 = 0,09011 [kg/s]
ṁrefg = 0,09011 [kg/s]
NUScond,w = 698,8 [-]
νcond,f = 1,297E-07 [m²/s] {1,297E-07 [m²/s]}
νevap,f = 2,136E-07 [m²/s]
Prcond,f = 0,9573 [-]
Prevap,brine = 36,86 [-]
P1 = 194321 [Pa]
P3 = 873161 [Pa]
Pc = 3,632E+06 [Pa]
Pevap = 213244 [Pa]
Prcond = 0,2905 [-]
Psat,cond = 993585 [Pa]
Q̇cond = 15000 [W]
R$ = 'R1234ze(E)'
Recond,w = 12462 [-]
Reevap,fo = 144081 [-]
ρcond,g = 54,28 [kg/m³]
ρevap,brine = 1052 [kg/m³]
ρevap,g = 11,65 [kg/m³]
Rf,refg = 0,000176 [m²-K/W]
σcond = 0,00568 [N/m]
s1 = 1690 [J/kg-K]
s2s = 1690 [J/kg-K]
s4 = 1232 [J/kg-K]
T1 = 275 [K]
T3 = 318 [K]
T5 = 275 [K]
Ac = 0,659 [m²]
b = 2,88 [-]
COPHP = 3,9 [-]
CEG = 35 [%]
ΔTlm,cond = 12,19 [K]
Dpipe,brine = 0,028 [m]
Dpipe,o = 0,032 [m]
dplate = 0,00144 [m]
ηi = 0,6743 [-]
ηll,cond = 0,7833 [-]
ηll,exp = 0 [-]
fbrine = 0,02598 [-]
Gcond = 12748 [kg/m²-s]
h1 = 386577 [J/kg]
h2s = 415355 [J/kg]
h4 = 262792 [J/kg]
hcond,refg = 40628 [W/m²-K]
hevap,fo = 8042 [W/m²-K]
hw = 15679 [W/m²-K]
Jg,evap = 310,2 [-]
k2 = -0,07 [-]
kcond,refg,fo = 0,06625 [W/m-K]
ke = -0,1 [-]
kevap,refg = 0,01153 [W/m-K]
ks = 0,15 [-]
λevap,wall = 15 [W/m-K]
μcond,g = 0,00001379 [kg/m-s]
μevap,brine = 0,004455 [kg/m-s]
μevap,g = 0,00001069 [kg/m-s]
ṁ1 = 0,09011 [kg/s]
ṁ3 = 0,09011 [kg/s]
ṁbrine = 2 [kg/s]
ṁw = 0,1794 [kg/s]
NUSevap,brine = 307,4 [-]
νcond,g = 2,540E-07 [m²/s]
νevap,g = 9,170E-07 [m²/s]
Prcond,w = 4,356 [-]
Prevap,f = 0,8224 [-]
P2 = 873161 [Pa]
P4 = 194321 [Pa]
Pcond = 1,055E+06 [Pa]
Pheating = 60000 [Pa]
Prevap = 0,05871 [-]
Psat,evap = 194321 [Pa]
Q̇evap = 11154 [W]
Recond,fo = 274625 [-]
Reevap,brine = 20413 [-]
ρcond,f = 1073 [kg/m³]
ρcond,w = 992,2 [kg/m³]
ρevap,f = 1243 [kg/m³]
Rf,brine = 0,000352 [m²-K/W]
Rf,w = 0,000175 [m²-K/W]
σevap = 0,01248 [N/m]
s2 = 1733 [J/kg-K]
s3 = 1211 [J/kg-K]
T0 = 294 [K]
T2 = 332,7 [K]
T4 = 270 [K]
T6 = 277,1 [K]

```

File:C:\Users\s351343\Downloads\HP R1234ze(E).EES 16.05.2022 13:13:00 Page 2
EES Ver. 10.836: #3911: For use only by the Department of Civil Engineering and Energy Technology, HiOA

$T_8 = 323$ [K]	$T_9 = 303$ [K]
$T_{m,cond} = 325,4$ [K]	$T_{m,evap} = 272,5$ [K]
$T_{m,evap,brine} = 276,1$ [K]	$T_{m,w} = 313$ [K]
$T_{sat,cond} = 323$ [K]	$T_{sat,evap} = 270$ [K]
$T_{wall} = 318$ [K]	$U_{cond} = 1868$ [W/m ² -K]
$U_{evap} = 1148$ [W/m ² -K]	$V_{avg,brine} = 3,088$ [m/s]
$V_{avg,w} = 0,2937$ [m/s]	$\dot{W}_{comp} = 3846$ [W]
$x = 0,5$ [-]	$x_3 = 0$ [-]
$\dot{X}_{des,comp} = 1129$ [W]	$\dot{X}_{des,cond} = 251,9$ [W]
$\dot{X}_{des,evap} = 251,7$ [W]	$\dot{X}_{des,exp} = 577,6$ [W]
$\dot{X}_{des,HP} = 2210$ [W]	$Z_{cond} = 0,6099$ [-]
$Z_{evap} = 0,3217$ [-]	


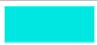
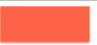


No unit problems were detected.

P IDA ICE plant 1

Table 25: Used energy for plant 1 in IDA ICE - Table collected from IDA ICE.

Used energy

kWh (sensible and latent)

Month	Zone heating	Zone cooling	AHU heating	AHU cooling	Dom. hot water
					
1	1488.0	0.0	0.0	0.0	456.8
2	1344.0	0.0	0.0	0.0	411.8
3	1488.0	0.0	0.0	0.0	455.2
4	1440.0	0.0	0.0	0.0	440.6
5	1488.0	0.0	0.0	0.0	455.0
6	1440.0	0.0	0.0	0.0	441.6
7	1438.0	0.0	0.0	0.0	457.3
8	1377.0	0.0	0.0	0.0	456.9
9	1440.0	0.0	0.0	0.0	440.5
10	1488.0	0.0	0.0	0.0	456.3
11	1440.0	0.0	0.0	0.0	442.0
12	1488.0	0.0	0.0	0.0	457.1
Total	17359.0	0.0	0.0	0.0	5371.1

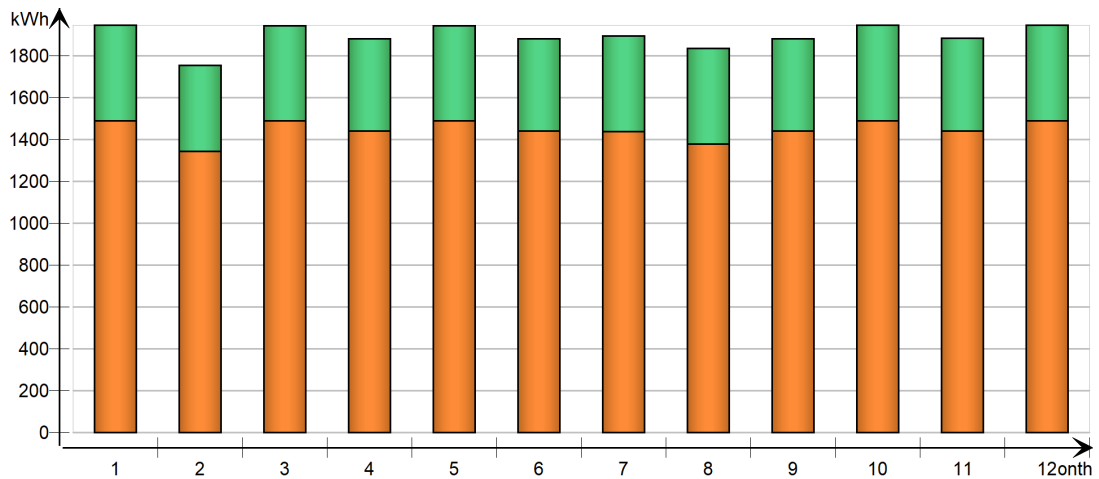


Figure 51: Used energy for plant 1 in IDA ICE - Diagram collected from IDA ICE.

Table 26: Utilized free heat for plant 1 in IDA ICE - Table collected from IDA ICE.

Utilized free energy

kWh (sensible and latent)

Month	AHU heat recovery	AHU cold recovery	Plant heat recovery	Plant cold recovery	Solar heat	Ground heat	Ground cold	Ambient heat	Ambient cold
1	0.0	0.0	-0.0	-2.5	25.9	5315.0	0.0		
2	0.0	0.0	-0.0	-2.3	63.8	4728.0	0.0		
3	0.0	0.0	-0.0	-2.5	161.7	5186.0	0.0		
4	0.0	0.0	-0.0	-3.0	167.7	4860.0	0.0		
5	0.0	0.0	-0.0	-416.9	271.4	3191.0	-246.3		
6	0.0	0.0	-0.0	-684.4	205.2	2484.0	-387.8		
7	0.0	0.0	-0.0	-976.0	237.3	1579.0	-678.3		
8	0.0	0.0	-0.0	-828.8	190.9	2061.0	-556.3		
9	0.0	0.0	-0.0	-25.8	131.9	4102.0	-1.6		
10	0.0	0.0	-0.0	-1.7	93.0	5057.0	0.0		
11	0.0	0.0	-0.0	-2.5	32.0	4970.0	0.0		
12	0.0	0.0	-0.0	-2.4	8.1	5113.0	0.0		
Total	0.0	0.0	-0.0	-2948.6	1589.0	48646.0	-1870.3		

Table 27: Energy required from the top heater in plant 1 when the mass flow rate in the solar system is set to $2e^{-8}$ kg/s - Table collected from IDA ICE.





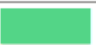
	Variables
	QREQ, W
January	39809.7
February	34955.9
March	28331.0
April	18528.3
May	4985.7
June	1533.4
July	377.4
August	924.3
September	4948.8
October	14025.0
November	23233.0
December	31515.3
mean	16834.2
mean*8760.0 h	1.474679295E8
min	377.4
max	39809.7

Q IDA ICE plant 2

Table 28: Used energy for plant 2 in IDA ICE - Table collected from IDA ICE.

Used energy

kWh (sensible and latent)

Month	Zone heating	Zone cooling	AHU heating	AHU cooling	Dom. hot water
					
1	1488.0	0.0	0.0	0.0	453.6
2	1344.0	0.0	0.0	0.0	409.7
3	1488.0	0.0	0.0	0.0	453.4
4	1440.0	0.0	0.0	0.0	437.6
5	1488.0	0.0	0.0	0.0	446.2
6	1440.0	0.0	0.0	0.0	432.7
7	1407.0	0.0	0.0	0.0	450.4
8	1349.0	0.0	0.0	0.0	449.4
9	1440.0	0.0	0.0	0.0	432.4
10	1488.0	0.0	0.0	0.0	451.5
11	1440.0	0.0	0.0	0.0	438.3
12	1488.0	0.0	0.0	0.0	454.6
Total	17300.0	0.0	0.0	0.0	5309.8

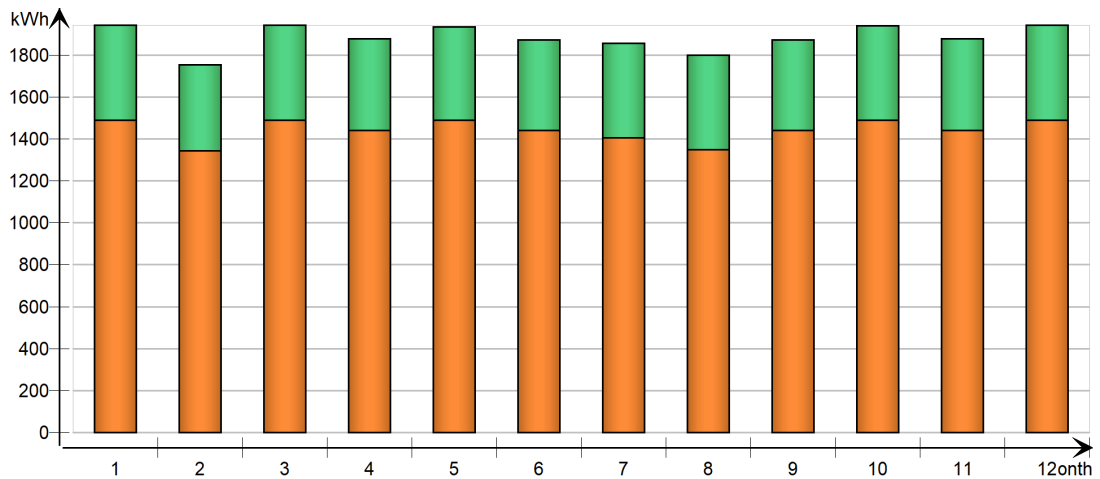


Figure 52: Used energy for plant 2 in IDA ICE - Diagram collected from IDA ICE.

Table 29: Utilized free heat for plant 2 in IDA ICE - Table collected from IDA ICE.

Utilized free energy

kWh (sensible and latent)

Month	AHU heat recovery	AHU cold recovery	Plant heat recovery	Plant cold recovery	Solar heat	Ground heat	Ground cold	Ambient heat	Ambient cold
1	0.0	0.0	-0.0	-0.3	181.5	5301.0	0.0		
2	0.0	0.0	-0.0	-0.2	293.6	4405.0	0.0		
3	0.0	0.0	-0.0	-0.3	431.5	3092.0	0.0		
4	0.0	0.0	-0.0	-0.3	472.2	2753.0	0.0		
5	0.0	0.0	-0.0	-225.8	616.5	996.3	-118.6		
6	0.0	0.0	-0.0	-367.2	584.2	728.3	-153.6		
7	0.0	0.0	-0.0	-633.8	615.6	517.6	-310.0		
8	0.0	0.0	-0.0	-552.2	547.9	877.3	-292.8		
9	0.0	0.0	-0.0	-21.0	449.7	1950.0	-4.1		
10	0.0	0.0	-0.0	-0.3	405.3	3791.0	0.0		
11	0.0	0.0	-0.0	-0.2	292.7	5020.0	0.0		
12	0.0	0.0	-0.0	-0.2	194.1	5182.0	0.0		
Total	0.0	0.0	-0.0	-1801.8	5084.8	34613.5	-879.1		

Table 30: Energy required from the top heater in plant 2 - Table collected from IDA ICE.

	Variables
	QREQ, W
January	42173.9
February	41273.4
March	36546.9
April	27174.4
May	11464.2
June	6554.3
July	3291.6
August	4749.1
September	12581.2
October	21839.2
November	27482.8
December	32809.8
mean	22213.5
mean*8760.0 h	1.945905636E8
min	3291.6
max	42173.9